QUADRIPOLE MAPPING NEAR THE FLY RANCH GEOTHERMAL PROSPECT, NORTHWEST NEVADA

1975

M.S.

By

Drew Morris

T-1699

A Thesis submitted to the Faculty and the Board of Trustees of the Colorado School of Mines in partial fulfillment of the requirements for the degree of Master of Science in Geophysics.

Signed: Drew Morris
Drew Morris

Golden, Colorado

Date: May 2, 1975

Approved: G. V. Keller
G. V. Keller
Thesis Advisor

G. V. Keller
G. V. Keller
Head of Department

Golden, Colorado

Date: May 2, 1975

T-1699

ABSTRACT

The quadripole mapping method is a surface based direct current exploration technique to investigate the subsurface resistivity structure. Two orthogonal bipole sources (four current electrodes) are used instead of conventional single source methods. The electric field intensity and azimuth due to each bipole source is measured and by adding the two electric field vectors in various combinations, the apparent resistivity and conductance can be calculated as a function of the direction of the resultant electric field vector at each of the receiver stations. The result is a resistivity ellipse for which only three parameters are needed to define it. The ellipticity, defined as the square root of the ratio of the maximum resistivity to the minimum, the bearing of one of the principal axes and the average of the maximum and minimum resistivities, are the three most useful parameters to use when interpreting the field data. This technique was applied to several types of the theoretical models in order to understand and better interpret the field data.

The quadripole mapping method was used in the vicinity of Hualapai Flat, a basin in northwest Nevada, to study the subsurface geology and evaluate the geothermal prospect in Hualapai, the Fly Ranch hot springs. Some theoretical models were found that could match the field data and these were

used in determining the basement configuration under Hualapai. No large resistivity anomaly is associated with the hot springs, but if high temperatures are present in the alluvium, then a geothermal reservior of sufficient extent to be economically feasible for utilization may exist.

CONTENTS

ILLUSTRATIONS

TABLE OF SYMBOLS

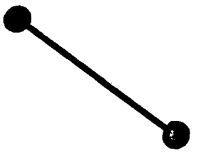

BIPOLE SOURCE

SURFACE TRACE OF CONTACT

BEARING OF ρ_{min}

RECEIVER STATION

THERMAL SPRINGS

COLD SPRINGS

ALL RESISTIVITES IN OHM-METERS

ACKNOWEDGEMENTS

I wish to express my gratitude to Professor George Keller for his interest and guidance as thesis advisor.

To C. Y. Lee, Ken Carlson, Ofiafate Ofrey, Augusto Pires and Takashi Ohya, my appreciation for their care in collecting the field data and Bob Crewdson and Bob Furgerson for their insights and discussions on the quadripole method and the interpretation of the field data.

I thank the National Science Foundation for sponsoring the field work and supporting and author as a research assistant under Grant GI 43866.

INTRODUCTION

In the past decade, geothermal energy has moved from the stage of a scientific curiosity to become a viable economical method for the generation of electrical energy. Geophysical exploration must develop to meet this expansion and innovative technological or interpretive methods need to be developed.

Direct current resistivity investigations have become the primary surface-based exploration technique for the detection and delineation of geothermal reserviors. Because of the ability of DC techniques to locate zones of anomalously low resistivities, dipole mapping or roving dipole exploration systems are becoming popular with the geophysical contractors. Because the field methods involve the measurement of apparent resistivities, instead of the true resistivities, conductive anomalies may not be due to the existence of a subsurface zone of low resistivity, but instead be a consequence of complex patterns of current flow, a "false" anomaly. Because drilling of these false anomalies is wasteful, techniques that can identify these anomalies are of scientific and commercial importance. The technique described in this report utilizes two bipole sources, more or less at right angles. By measuring the electric field

intensity at the receiver station due to each source, it is possible to identify and eliminate false anomalies. Because the field technique involves the use of two bipole sources or four current electrodes, the method is called "quadripole mapping".

The purpose of the study described here is to explain the field results generated by the quadripole method by comparing the data with theoretical models. Risk (1970) was the first to describe the technique to measuring the total electric field in dipole mapping, while the theory of dipole mapping and its limitations are well described by Keller (1966a), Alpin (1966), Furgerson (1970), Furgerson and Keller (1974), and Keller and others (1975). However, quadripole mapping is a recent innovation and the literature is scanty. Vedrintsev (1966) has discussed the effect of the azimith of sounding traverses across areas of complex basement structure on resistivity patterns. Other work and results of field programs are reported in thesis reports at the Colorado School of Mines (Tasci, 1975, and Furgerson, 1975).

The theoretical models used are two horizontal layers, one vertical contact (a fault) and two vertical parallel contacts (a dike). Various formulas for the components of the electric field intensity for these cases are given by Furgerson and Keller (1974), Alpin (1966) and Furgerson

(1970), while expressions for the electric potential are given by Van Nostrand and Cook (1966) and Vedrintsev (1966). Expressions for the electric potential for hemispheriodal bodies in an otherwise uniform halfspace are found in Van Nostrand and Cook (1966) and Bibby and Risk (1973). The electric potential and components of the electric field for the case of the dipping layer can be found in Lee (1974).

When resistivity surveys are carried out in regions where there is an electrically resistive basement at depth, then it can be assumed that the current is confined to an upper conducting layer, rather than a halfspace. For this case, the theoretical models of the single vertical contact (a fault) and two, parallel vertical contacts (a dike) are modified by placing this insulating basement at a depth but the analytic expressions for the electric field components can be derived. A list of the models used in this study is included in figure 1.

The field work included in this thesis was done under the guidance of Drs. G. V. Keller and Takashi Ohya in May and June 1974, as part of a study of the nature of geothermal systems in a Basin and Range setting funded by the National Science Foundation.

TYPES OF THEORETICAL MODELS

2 HORIZONTAL LAYERS

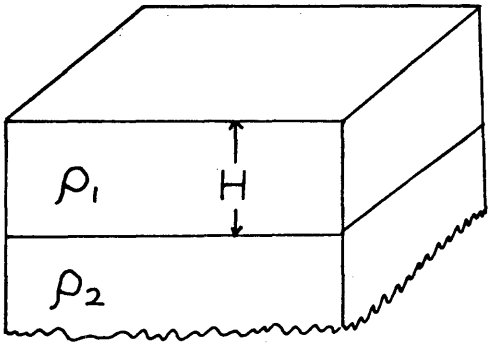

VERTICAL DIKE

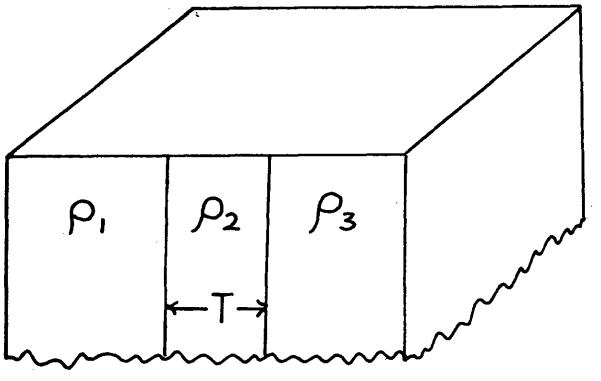

VERTICAL DIKE OVER INSULATING BASEMENT

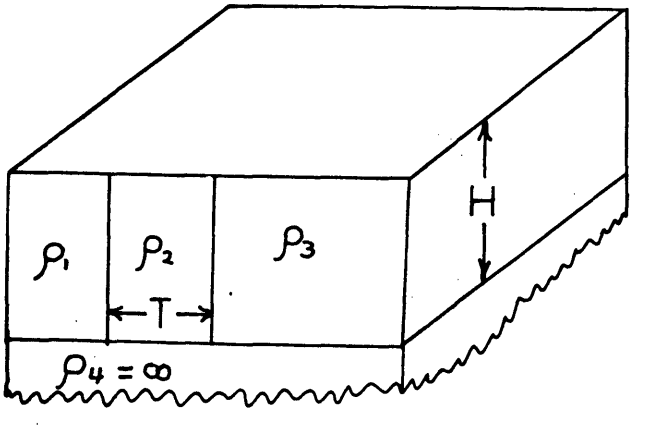

Figure 1. Geometry of theoretical models used in this study.

THEORY OF QUADRIPOLE MAPPING

With conventional single source techniques, the magnitude and azimuth of the electric field vector are the only two sets of field data with which interpretations are made, the former being used with a geometric factor to find the apparent resistivity or conductance. Generally, only the magnitude is used because field work has shown that the azimuth of the electric field vectors do not vary much from the case of a homogeneous halfspace (Jordan, 1974). The bearings of electric field vectors taken in the field do not allow easy differentiation between models, even though differences up to 50^{o} are present in the theoretical cases. As examples, the azimuths of the electric field vectors for the cases of a halfspace and a resistive dike are shown in figures 2A and 2B.

The electric field vector patterns are shown in figure 2A, while the difference in the bearings is shown in figure 2B. It should be noted that on the source side of the first contact, the magnitude of the bearing differences changes from positive to negative. This indicates that there is a region where the electric field vectors for a dike (or fault) will diverge away from the normal (halfspace) case as the current flow attempts to avoid the more resistive medium. This region of divergence will have, as a result, a low electric field magnitude. Thus when calculating the

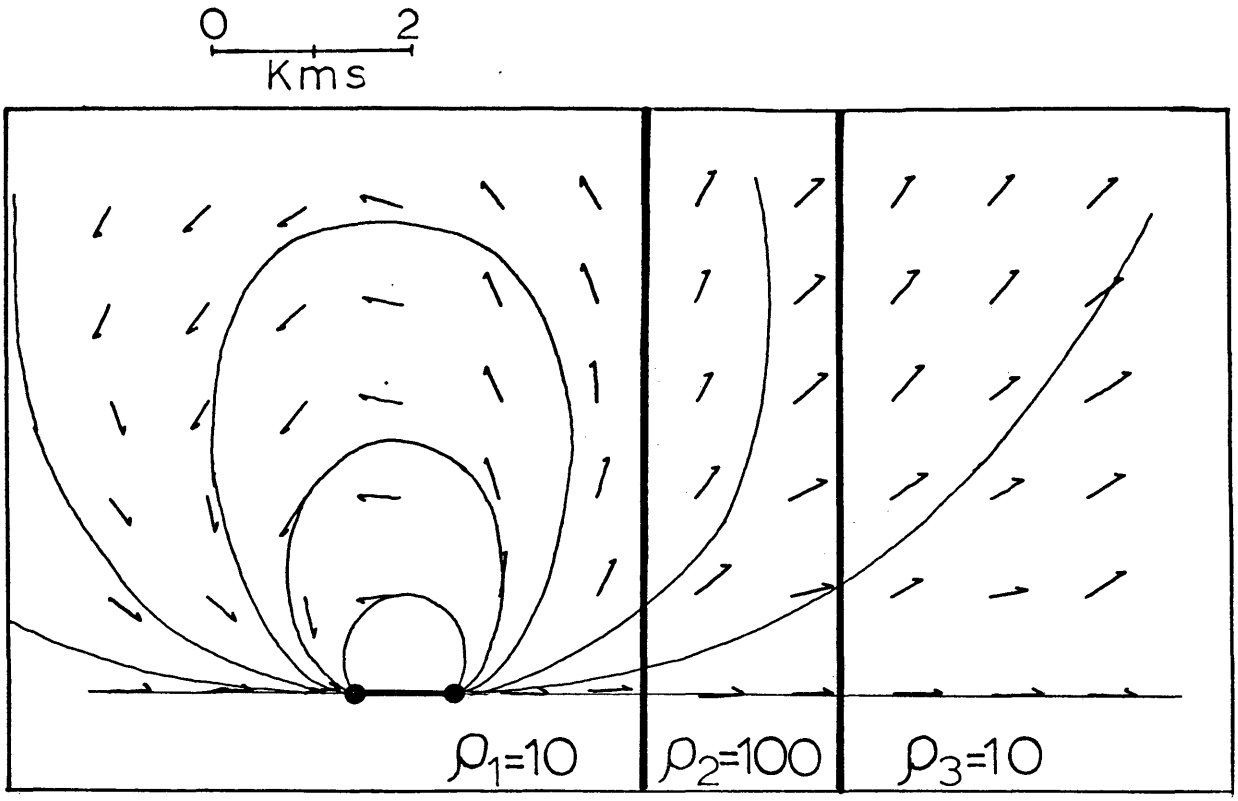

Figure 2A. Electric field directions for two models. Continous curves are for a halfspace, arrows are for a dike model.

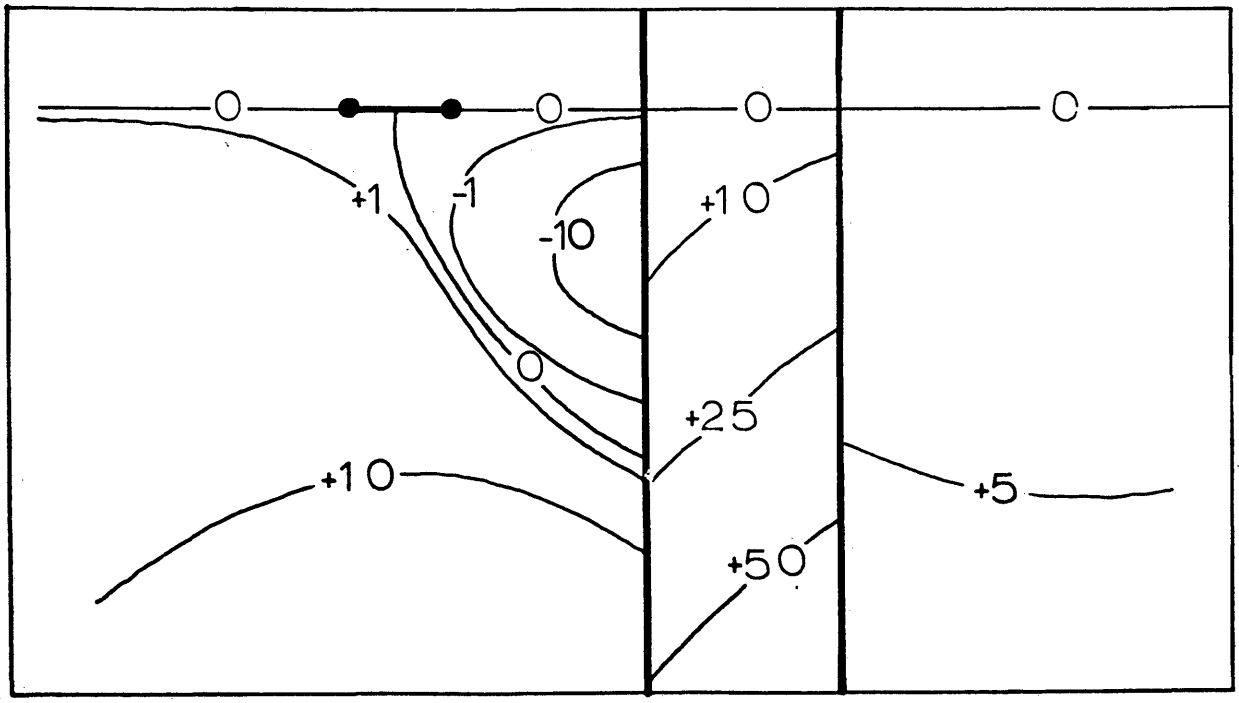

Figure 2B. Difference in electric field bearings for cases of a halfspace and a dike. Values are in degrees and were found by subtracting the bearing for the dike case from the bearing of the halfspace model.

apparent resistivity for stations located in this region, low values should result. Complicated current flow patterns resulting in false anomalies are formed near other resistive masses, such as faults, dikes, and hemispheres. Figure 3A shows the calculations for the case of a resistive dike with resistivity 50 Ω-m bordered on the left by a medium of resistivity 1 Ω-m and on the right by a medium of 10 Ω-m. The source is oriented parallel to the dike and 2.25 km from the near contact. Located next to the near boundary on the source side, resistivity lows appear in the regions of complex current flow caused by lateral variations in resistivity. However, if the source is rotated 90° (figure 3B), false lows still occur but either in a different position along the first boundary or with less resistivity contrast. In present field practice, multiple coverage is provided by using a second source whose location might also create another false anomaly in a location near one generated by the first source. The quadripole mapping method uses a second source at or near right angles to the first source but at the same location. At any receiver station, the two sources should generate two electric field vectors with different magnitudes and azimuths, because the electric field is a function of source orientation. Depending on such factors as the distance and azimuth of the receiver station from the source, the length of the source and lateral and vertical changes in resistivity, apparent resistivity maps will change

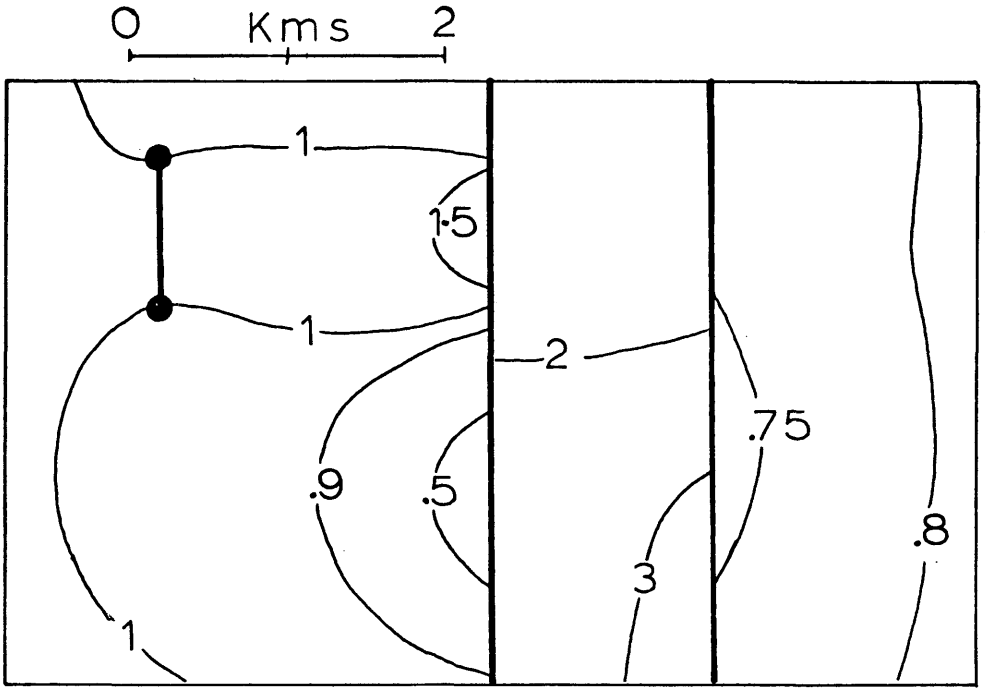

Figure 3A. Calculated apparent resistivities for a bipole source pointed parallel to a dike.

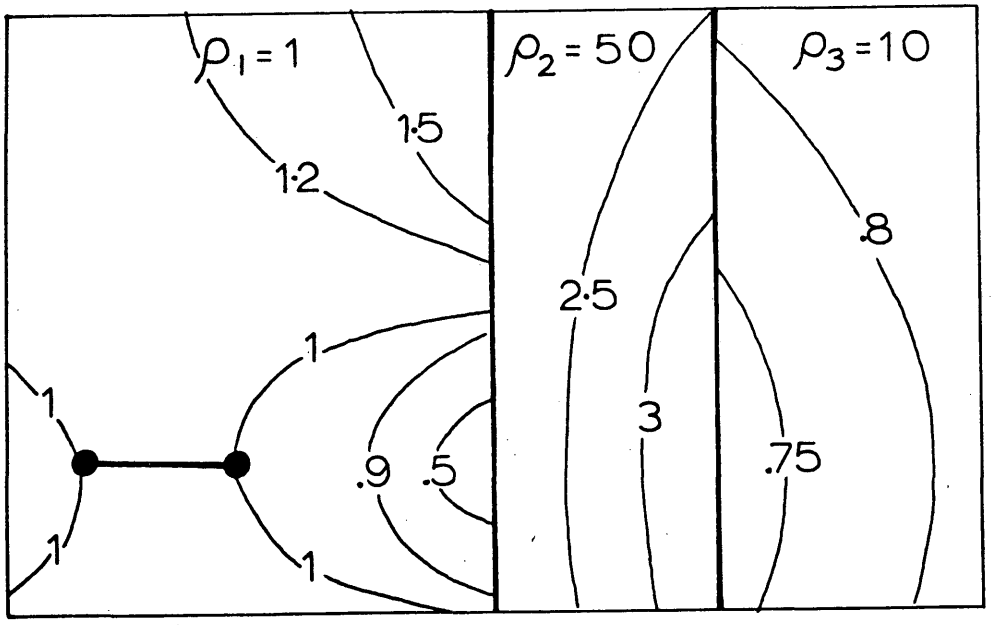

Figure 3B. Calculated apparent resistivities for a bipole source pointed perpendicular to a dike.

as different sources are used, but interpretation should not be changed (Stanley and others, 1973).

With the quadripole method, we can combine the single source electric field vectors to give a resultant which will have some third azimuth, by taking various ratios of the two measured field vectors. If this is done and a new geometric factor is used involving the four source electrodes, the apparent resistivity and conductance can be calculated as a function of the bearing of the resultant vector. One way to do this is to set up two sources in the field by powering them with different amounts of current; in doing so, we can create a multiple of resultant vectors which will have various bearings and magnitudes. If the two sources are powered simultaneously by currents I_1 and I_2, at each receiver station we will measure the vector sum of the two single source electric vectors. However, the earth is linear in its electrical behavior, and so by powering each source separately at a fixed current and measuring the magnitude and azimuth of the electric field vector at the receiver stations, we can add the two vectors in the office on the computer, saving large amounts of money and crew time. By taking various combinations of the two electric fields, we can make the resultant rotate through 360° and be pointed in any direction of interest.

If the current to a source bipole is varied, the magnitude but not the azimuth of the electric field vector will be changed. Hence by changing the two currents by scaling factors alpha (α) and beta (β), we can change the two single source electric field magnitudes and polarity, which will change the resultant vector. Inasmuch as the bearing and magnitude of the resultant will depend upon the sign and ratio of alpha and beta, we can specify the two scalars to give a resultant in the desired direction.

The derivation for the formulas used in the quadripole method is straight forward. The two sources and their four source electrodes are shown in figure 4. At a receiver station, the contribution to the potential, U, by one electrode in a uniform, isotropic halfspace is given by:

$$U_i = \frac{\rho I}{2\pi R_i}$$

where ρ is the resistivity of the halfspace, I is the current to the source electrode and R_i is the distance from the receiver station at (x,y) to the i^{th} source electrode at (x_i, y_i). Inasmuch as the electric field intensity is the gradient of the electric potential, its components in Cartesian coordinates will be:

$$E_{ix} = -\frac{\partial U_i}{\partial R_i}\frac{\partial R_i}{\partial x} = \frac{\rho I}{2\pi R_i^2}\frac{\partial R_i}{\partial x}$$

$$E_{iy} = -\frac{\partial U_i}{\partial R_i}\frac{\partial R_i}{\partial y} = \frac{\rho I}{2\pi R_i^2}\cdot\frac{\partial R_i}{\partial y}$$

GENERAL QUADRIPOLE ARRAY

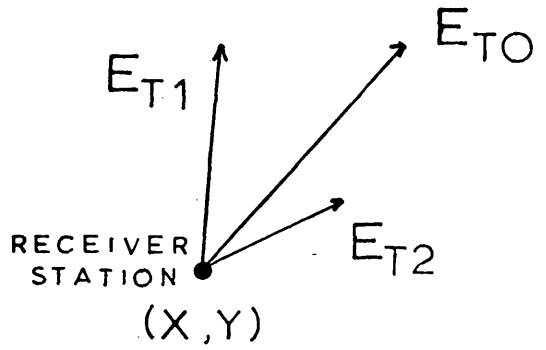

$$\vec{E_{TO}} = \alpha\vec{E_{T1}} + \beta\vec{E_{T2}}$$

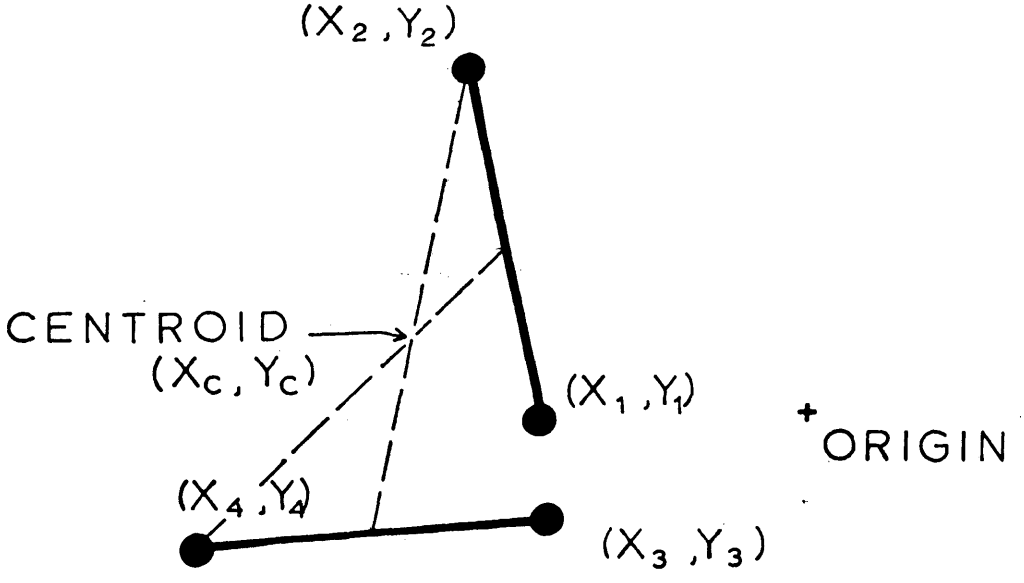

Figure 4. Two bipole sources and their electric field vectors at a receiver station. The resultant, E_{TO}, is the vector sum of the individual electric field vectors.

Because $\frac{\partial R_i}{\partial x}$ and $\frac{\partial R_i}{\partial y}$ represent the cosines between the radial from the receiver station to the electrode, the equations become:

$$E_{ix} = \frac{\rho I}{2\pi R_i^2}\frac{(X-X_i)}{R_i} = \frac{\rho I\,(X-X_i)}{2\pi R_i^3}$$

$$E_{iy} = \frac{\rho I}{2\pi R_i^2}\frac{(Y-Y_i)}{R_i} = \frac{\rho I\,(Y-Y_i)}{2\pi R_i^3}$$

Summing the x and y components for the electric fields from each of the four electrodes gives:

$$E_x = \frac{\rho}{2\pi}\left\{I_1\frac{(x-x_1)}{R_1^3} - I_1\frac{(x-x_2)}{R_2^3} + I_2\frac{(x-x_3)}{R_3^3} - I_2\frac{(x-x_4)}{R_4^3}\right\}$$

$$E_y = \frac{\rho}{2\pi}\left\{I_1\frac{(y-y_1)}{R_1^3} - I_2\frac{(y-y_2)}{R_2^3} + I_3\frac{(y-y_3)}{R_3^3} - I_2\frac{(y-y_4)}{R_4^3}\right\}$$

Squaring the two components and adding gives:

$$E_t^2 = E_x^2 + E_y^2 = \frac{\rho^2}{(2\pi)^2}\left\{\left[I_1\left(\frac{x-x_1}{R_1^3} - \frac{x-x_2}{R_2^3}\right) + I_2\left(\frac{x-x_3}{R_3^3} - \frac{x-x_4}{R_4^3}\right)\right]^2 + \left[I_1\left(\frac{y-y_1}{R_1^3} - \frac{y-y_2}{R_2^3}\right) + I_2\left(\frac{y-y_3}{R_3^3} - \frac{y-y_4}{R_4^3}\right)\right]^2\right\}$$

Letting

$$GM1 = \frac{x-x_1}{R_1^3} - \frac{x-x_2}{R_2^3} \qquad GM2 = \frac{x-x_3}{R_3^3} - \frac{x-x_4}{R_4^3}$$

$$GN1 = \frac{y-y_1}{R_1^3} - \frac{y-y_2}{R_2^3} \qquad GN2 = \frac{y-y_3}{R_3^3} - \frac{y-y_4}{R_4^3}$$

we make the substitutions, take the square root and rearrange as follows:

$$\rho_a = 2\pi E_t\left\{(I_1 GM1 + I_2 GM2)^2 + (I_1 GN1 + I_2 GN2)^2\right\}^{-1/2}$$

In order to rotate, we must make the following substitutions:

$$I_1 \longrightarrow \alpha I_1 \qquad I_2 \longrightarrow \beta I_2$$

$$E_{x1} \longrightarrow \alpha E_{x1} \qquad E_{x2} \longrightarrow \beta E_{x2}$$

$$E_{y1} \longrightarrow \alpha E_{y1} \qquad E_{y2} \longrightarrow \beta E_{y2}$$

where E_{x1} and E_{y1} are the x (east-west) and y (north-south) components of the first measured electric field vector and E_{x2} and E_{y2} are the components for the second field vector.

For the resultant vector E_{TO} to have a specific orientation θ, α and β must be determined. It is evident that:

$$E_{TO} \sin\theta = \alpha E_{x1} + \beta E_{x2}$$

$$E_{TO} \cos\theta = \alpha E_{y1} + \beta E_{y2}$$

However, there are three variables (α, β and E_{TO}) and two equations. This indeterminancy is resolved by keeping E_{TO} of constant magnitude by defining it in terms of the measured field components. Solving the above two equations using Cramer's Rule gives:

$$\alpha = \frac{\begin{vmatrix} E_{TO}\sin\theta & E_{x2} \\ E_{TO}\cos\theta & E_{y2} \end{vmatrix}}{\begin{vmatrix} E_{x1} & E_{x2} \\ E_{y1} & E_{y2} \end{vmatrix}} = \frac{E_{TO}}{DET}(E_{y2}\sin\theta - E_{x2}\cos\theta)$$

$$\beta = \frac{\begin{vmatrix} E_{x1} & E_{TO}\sin\theta \\ E_{y1} & E_{TO}\cos\theta \end{vmatrix}}{\begin{vmatrix} E_{x1} & E_{x2} \\ E_{y1} & E_{y2} \end{vmatrix}} = \frac{E_{TO}}{DET}\left(E_{x1}\cos\theta - E_{y1}\sin\theta\right)$$

where E_{TO} is the vector of constant magnitude that will be rotated and DET is the determinant of the matrix of coefficients. The determinant will be zero only when the two measured electric field vectors are parallel or antiparallel, cases which cannot be rotated anyway. In order to keep the values of α and β under 100, E_{TO} was defined as:

$$E_{TO} = \left\{\left(E_{x1} + E_{x2}\right)^2 + \left(E_{y1} + E_{y2}\right)^2\right\}^{1/2}$$

By specifying the bearing (θ) of the rotating vector E_{TO}, α, and β can be uniquely determined. The formula for the apparent resistivity as a function of θ is then:

$$\rho_a(\theta) = 2\pi E_{TO}\left\{\left(\alpha I_1 GM_1 + \beta I_2 GM_2\right)^2 + \left(\alpha I_1 GN_1 + \beta I_2 GN_2\right)^2\right\}^{-1/2}$$

Instead of assuming that the current is distribute uniformly over a hemisphere as was done for the case of apparent resistivity, we can assume that there is an insulating basement at depth that will make the current be distributed cylindrically in the conductive layer above the basement. Therefore, if the overlying conductor has a resistivity and thickness H, then the electric field components will be:

$$E_{ix} = \frac{\rho I}{2\pi H R_i} \frac{\partial R_i}{\partial x} = \frac{\rho I (x - x_i)}{2\pi H R_i^2}$$

$$E_{iy} = \frac{\rho I}{2\pi H R_i} \frac{\partial R_i}{\partial y} = \frac{\rho I (y - y_i)}{2\pi H R_i^2}$$

The sum of the components for the four source electrodes is

$$E_x = \sum E_{ix} = \frac{\rho}{2\pi H} \left\{ I_1 \left(\frac{x - x_1}{R_1^2} - \frac{x - x_2}{R_2^2} \right) + I_2 \left(\frac{x - x_3}{R_3^2} - \frac{x - x_4}{R_4^2} \right) \right\}$$

$$E_y = \sum E_{iy} = \frac{\rho}{2\pi H} \left\{ I_1 \left(\frac{y - y_1}{R_1^2} - \frac{y - y_2}{R_2^2} \right) + I_2 \left(\frac{y - y_3}{R_3^2} - \frac{y - y_4}{R_4^2} \right) \right.$$

Squaring both components and adding and then taking the square root gives:

$$E_T = \frac{\rho}{2\pi H} \left\{ \left[I_1 \left(\frac{x - x_1}{R_1^2} - \frac{x - x_2}{R_2^2} \right) + I_2 \left(\frac{x - x_3}{R_3^2} - \frac{x - x_4}{R_4^2} \right) \right]^2 + \right.$$

$$\left. \left[I_1 \left(\frac{y - y_1}{R_1^2} - \frac{y - y_2}{R_2^2} \right) + I_2 \left(\frac{y - y_3}{R_3^2} - \frac{y - y_4}{R_4^2} \right) \right] \right\}^{1/2}$$

Defining:

$$GS1 = \frac{x - x_1}{R_1^2} - \frac{x - x_2}{R_2^2} \qquad GS2 = \frac{x - x_3}{R_3^2} - \frac{x - x_4}{R_4^2}$$

$$GT1 = \frac{y - y_1}{R_1^2} - \frac{y - y_2}{R_2^2} \qquad GT2 = \frac{y - y_3}{R_3^2} - \frac{y - y_4}{R_4^2}$$

and making these subtituations and after rearranging will give:

$$H/\rho = \frac{1}{2\pi E_T}\left\{\left[I_1 GS1 + I_2 GS2\right]^2 + \left[I_1 GT1 + I_2 GT2\right]^2\right\}^{1/2}$$

The ratio of H to ρ is defined as the conductance (S_a) of the overlying conducting layer. After making the substitutions for the scaling factors, α and β, the expression for the apparent conductance as a function of the azimuth θ, is:

$$S_a(\theta) = \frac{1}{2\pi E_{TO}}\left\{\left[\alpha I_1 GS1 + \beta I_2 GS2\right]^2 + \left[\alpha I_1 GT1 + \beta I_2 GT2\right]^2\right\}$$

where α, β and E_{TO} are defined as before for apparent resistivity.

QUADRIPOLE RESISTIVITY PARAMETERS

When the values for the apparent resistivity are calculated for values of θ ranging from 0° to 360°, an ellipse will be generated. Figure 5 shows a typical resistivity ellipse and the parameters used to describe it. Only three parameters are needed to uniquely define the ellipse; they are the ellipticity, the bearing of one of the principal axes and the average of the maximum and minimum resistivities.

Ellipticity and Structural Anisotropy

The ellipticity of an ellipse is usually defined as the ratio of the maximum value to the minimum, but in electrical geophysics, the square root of the ratio is used to describe the coefficient of anisotropy (Keller and Frischknecht, 1966). So for reasons of convention, the square root of the ratio, instead of the ratio is used in defining the resistivity ellipse. For the apparent conductance, the ellipse will be dependent upon the trigonometric functions of θ to the fourth power instead of the second. The conductance ellipse can be defined by the same parameters as the resistivity ellipse, but will have different values.

Ellipticities do not depend upon the medium being anisotropic; instead the values of ellipticity are affected by

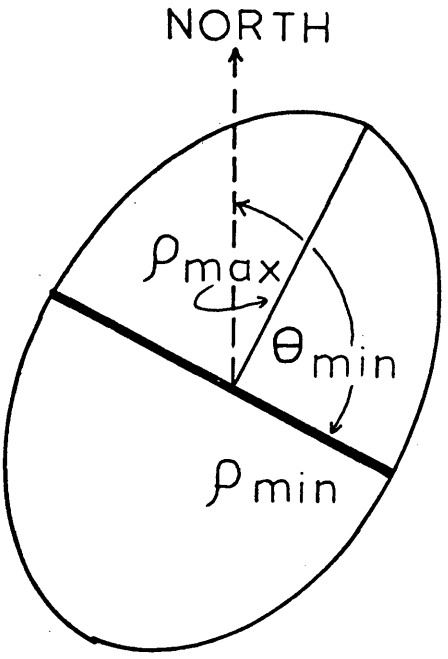

PARAMETERS OF RESISTIVITY ELLIPSES

$$\text{ELLIPTICITY} = \sqrt{\frac{\rho_{max}}{\rho_{min}}}$$

AVERAGE RESISTIVITY $\rho_{ave} =$

$$(\rho_{max} + \rho_{min})/2$$

BEARING OF MINOR AXIS, θ_{min},

MEASURED CLOCKWISE

Figure 5. Typical resistivity ellipse and quadripole parameters used to define it.

the presence of anomalous resistive and conductive bodies and the resulting lateral and vertical resistivity changes.

Figure 6 is the result of the quadripole method using the two sources in figures 3A and 3B. By combining these two orthogonal sources into a four source electrode array, the ellipticities were calculated. In the first medium, the ellipticities will have values near one at the receiver stations close to the sources and will increase as the receiver stations approach the first contact. Past the first contact, the ellipticities decreased by 60% or more, but start to increase again near the second contact. Past the second contact, the ellipticities decrease and approach a value of one. The ellipticities decrease after passing the first contact because close to this boundary, the model appears to be a single fault contact. It has been shown (Furgerson and Keller, 1974) that if both bipole sources are located in the same medium, the same apparent resistivity will be measured everywhere in the second medium. Since the same apparent resistivity is measured regardless of source orientation and hence the bearing of the electric field vector, the ellipticity will be one. Depending on the width of the dike, the receiver stations just inside the dike will not be affected by the second contact and the ellipticities will be near unity. As the receiver stations approach the second contact,

BEARING OF ρ_{min} AND ELLIPTICITIES FOR A RESISTIVE DIKE

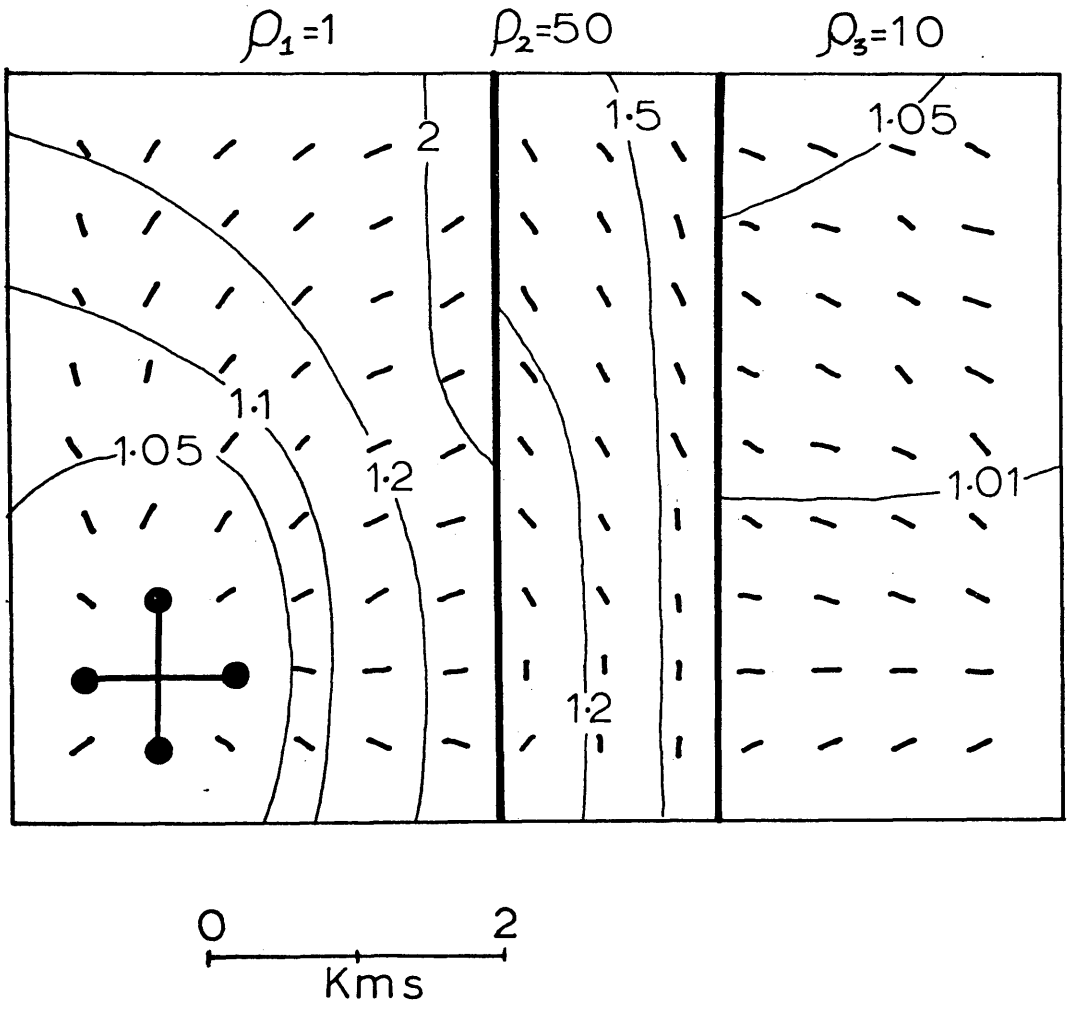

Figure 6. Calculated ellipticities and bearing of ρ_{min} for orthogonal sources shown in figures 3A and 3B. Model is a dike without insulating basement.

the similarity to a fault model breaks down and the ellipticities will once again increase.

The ellipticities for the conductance ellipses will show a similar behavior, but will have lower limits of $\sqrt{2}$ or 1.41. It has been shown (Alpin, 1966) that the magnitude of the electric field for a dipole source located in a halfspace depends on the azimuth of the radial to the receiver station. If the station is in line (polar) with the dipole source, then the magnitude will be twice the value measured when the receiver station is broadside (equatorial) to the dipole source. The geometric factor for the apparent resistivity depends upon the azimuth of the radial to the source, but the geometric factor for the apparent conductance does not. Hence the apparent resistivity will always be the same in halfspace, while the apparent conductance will be not be independent of the dipole source bearing and could differ by a factor of two. It should be noted that these limits are true only for the case of dipole, not bipole sources. In this report the source is always treated as a bipole so the results from a dipole are a limiting case.

In addition to lateral variations in resistivity, there can be vertical change. With the case of a resistive basement at depth underlying a conducting layer of thickness H, a second class of models will be generated. Instead of having

the equipotential surfaces from each source electrode in the form of hemispheres, they will be cylindrical, with a height equal to the thickness of the conducting layer. Taking the previous model of the resistive dike, an insulating basement was added at a depth of .5 km, changing the values of the ellipticities as shown in figure 7. The resistivity ellipticities increase when approaching the near side of the dike, but do not decrease to values near one after passing the contact, remaining close to 1.2 . This is because the magnitude of the electric field is independent of the azimuth of the radial to the dipole source (Alpin, 1966). Therefore, the ratio of apparent resistivities will be 2:1 and the conductance ratio will be one. If the interpreter is certain that a receiver station is not near a lateral resistivity contrast, then comparison of the conductance and resistivity ellipticities can give some indication whether an insulating basement is present. Various theoretical models were studied by varying the resistivity, source offset, depth to insulating basement (if any), and these generalizations were usually true. Whereas plotting the bearings of the electric field vectors from the field data and the case of an isotropic uniform halfspace will show little difference even near resistivity contrasts, plots of ellipticities will more easily locate these contrasts. From the theoretical model studies, several rules of thumb were found for the two classes

BEARING OF ρ_{min} AND ELLIPTICITIES FOR A RESISTIVE DIKE OVER INSULATING BASEMENT

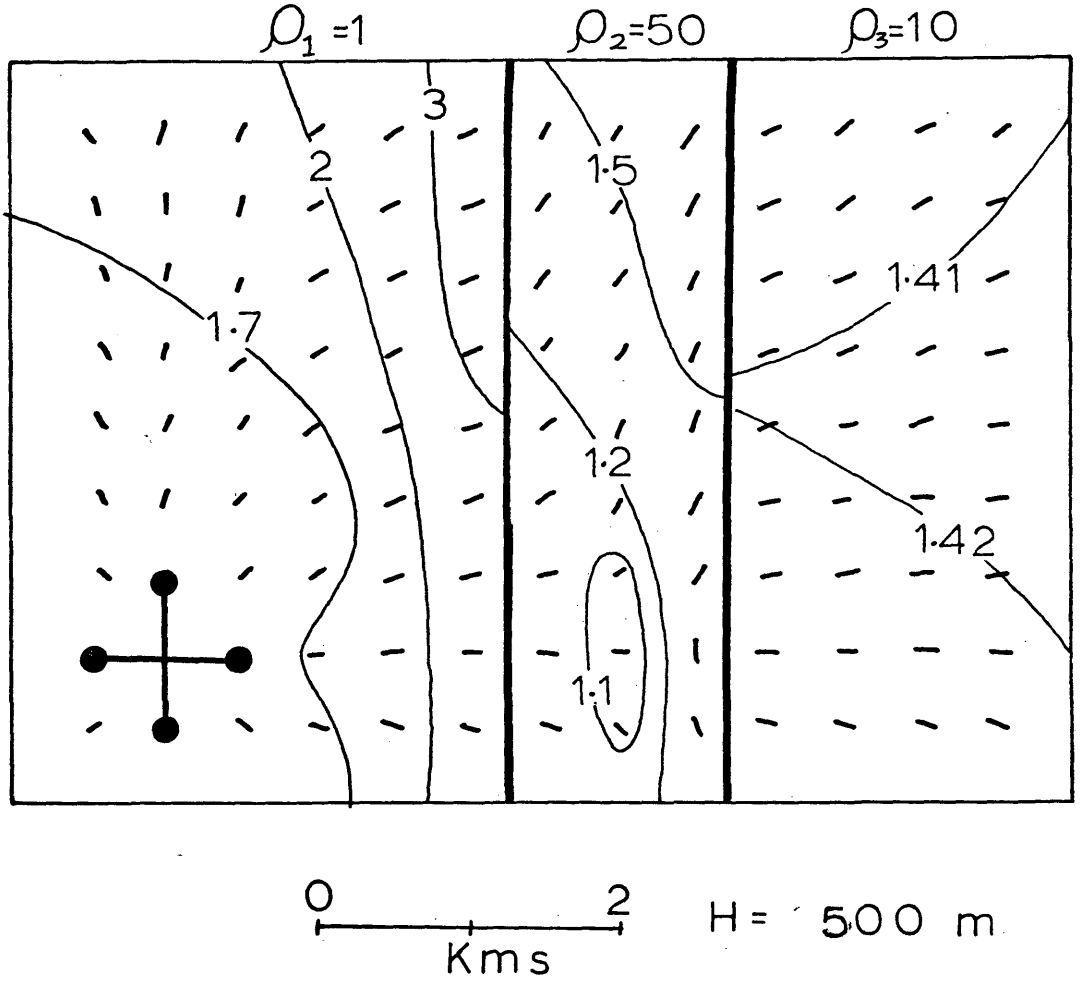

Figure 7. Calculated ellipticities and bearing of ρ_{min} for orthogonal sources shown in figure 3A and 3B. Model is a dike with insulating basement at a depth of 500 meters.

of cases, those without resistive basement and those with:

A) Models without resistive basement

1) resistivity ellipticities will tend to approach unity if the receiver station is well away from lateral resistivity contrasts.

2) conductance ellipticities will have values greater than 1.3 and will approach a limit of 1.41 when distant from the sources and lateral contrasts.

b) Models with resistive basement

1) away from vertical contacts, conductance ellipticities will be lower than the resistivity ellipticities.

2) At great distances, the model of a conductor over an insulator will become similar to a half-space and the resistivity ellipticities will have a limit of unity, the conductance ellipticities approaching $\sqrt{2}$.

Orientation of Resistivity Ellipses

The bearing of one of the principal axes is an important indicator for the presence of lateral changes in resistivity. Using the previous model of a resistive dike without an insulating basement, the bearings of the minimum value, , are plotted along with the resistivity ellipticities in figures 6 and 7. In the first medium, the one containing the

sources, the bearings of ρ_{min} tend to point toward the centroid of the sources until the reciever station approaches the dike. Near the contact, the bearings of ρ_{min} become perpendicular to the strike of the dike. With a resistive dike (or any resistive mass), the electric field vectors will diverge and deflect away from the more resistive regions, near the first boundary. The preferred bearing will then be parallel to the strike of the dike which indicates that the bearing of ρ_{min} is at right angles to the preferred direction, although it is possible to steer the resultant electric vector in any direction. For the case of a conductive dike, which will attract current, the bearings will be parallel to the strike of the dike indicating that the preferred direction will be normal to the dike. From the model studies of cases without a resistive basement, it appears that ρ_{min} will be pointed parallel to conductive bodies and perpendicular to resistive bodies. Studies of models with only vertical changes in resistivity (two horizontal layers) show that the bearing of ρ_{min} will point toward the centroid of the sources in the absence of lateral charges in resistivity. The direction of ρ_{min} is not a parameter that will help define a unique geoelectric structure. When it is used in conjunction with ellipticities, a sensible interpretation can be made that will differentiate between lateral and vertical resistivity

contrasts.

The Average Resistivity

The third quadripole parameter that is useful is the average resistivity, ρ_{ave} , defined as the arithmetic average of the maximum and minimum resistivities of each ellipse. Although this is not the average radius (resistivity) of ellipse, it does have important and useful properties, especially in delineating the locations of lateral changes in resistivity. Figure 8 is a plot of the values of ρ_{ave} for the source arrangement and model parameters in figure 6. When plotting ρ_{ave} , two improvements are realized which will aid the interpretation. The first is that the false anomalies that were present in figures 3A and 3B disappear and the value of ρ_{ave} in the medium containing the sources is always within 10% of the actual resistivity. The second is that the resistivity contrasts are more sharp and there is little possibility of contouring across the contacts of the dike as was possible in figure 3B. The average resistivities in the dike are near 2 Ω-m, only 4% of the actual resistivity, 50 Ω-m. On the far side of the dike, the average resistivities are less than 1 Ω-m , the true resistivity being 10 Ω-m . The use of average resistivity is not always a helpful step, but it can find the true resistivity of the medium containing

AVERAGE RESISTIVITY FOR A RESISTIVE DIKE

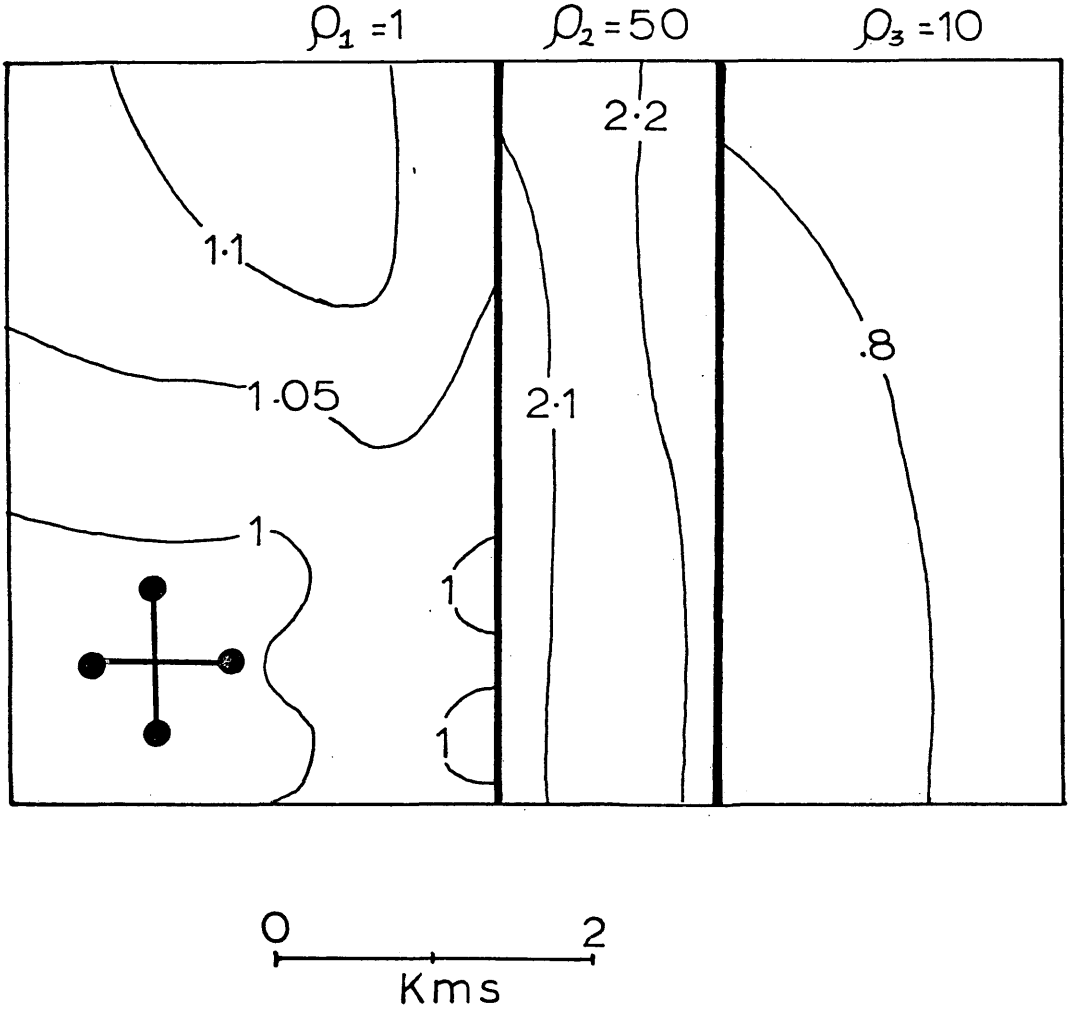

Figure 8. Calculated average resistivities for a dike without insulating basement identical to figure 6.

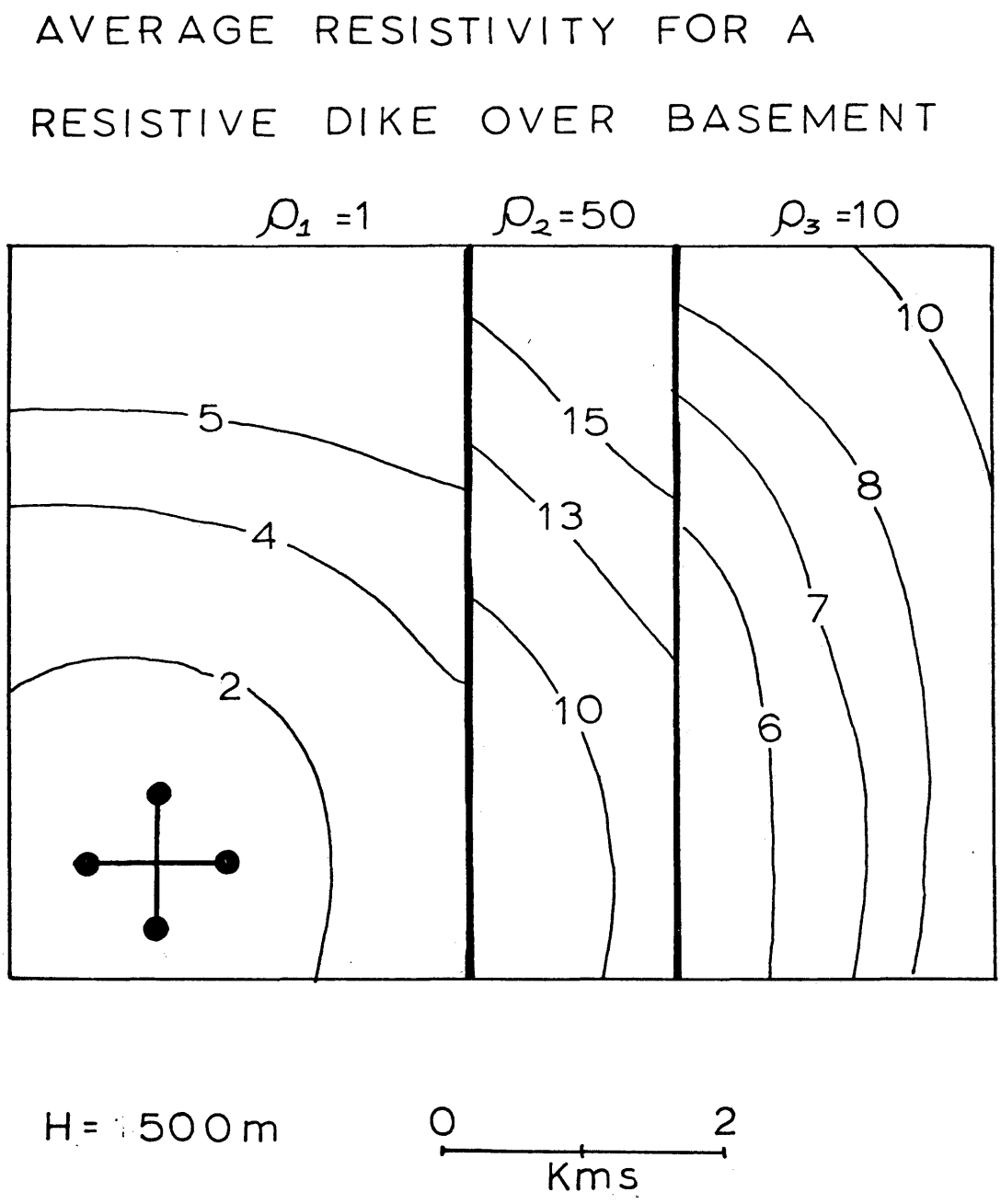

Figure 9. Calculated average resistivities for a dike model identical to one in figure 7. Insulating basement at a depth of 500 meters.

the sources and remove the false anomalies that were present along the near contact. If resistive basement is added, then the effects of lateral and vertical changes of resistivity will be seen (figure 9). Without insulating basement, there is no trend of increasing apparent resistivity with larger separation from the source, regardless of the azimuth of the traverse except when crossing a resistivity contrast. However, this is not true with the presence of an insulating basement. For traverses in any medium that do not cross lateral boundaries, the average resistivity will increase, when plotted on log-log paper, along a line rising at an angle of 45°. This is due to the presence of the non-conducting basement, so it is possible to confuse lateral charges in resistivity with vertical changes unless a large enough area is covered or vertical soundings are made. Unfortunately even with the improvements made by the quadripole mapping method, we are still unable to reach the goal of the electrical geophysicist, the ability of surface DC techniques to measure <u>actual</u> resistivities instead of appearent or average resistivities.

RESULTS OF FIELD SURVEY

Hualapai Flat was chosen as the site to evaluate the potential of the quadripole mapping technique. It is located at the junction of Humboldt, Pershing, and Washoe counties in northwest Nevada, some 140 km north of Reno (figure 10). It is a topographically enclosed basin on the west side of the Black Rock Desert about 35 kilometers north of Gerlach, bordered on the south and west by the Granite Range and on the north and northeast by the Calico Mountains. A low bedrock ridge (to be referred to in this report as the Steamboat ridge) separates Hualapai Flat along the east from the Black Rock Desert.

Regional Setting and Bedrock Geology

Hualapai Flat is located in the Basin and Range tectonic province and is situated on the border between a ridge on the west, the Granite Range and a basin on the east, the Black Rock Desert. Genozoic block faulting has been the primary cause for the distinctive physiographic character of the province. However, Bonham (1969) states that high angle block faulting and tilting has occurred since the Pleistocene and fault scarps are seen in the alluvium in the area. In the area of this study, the bedrock geology con-

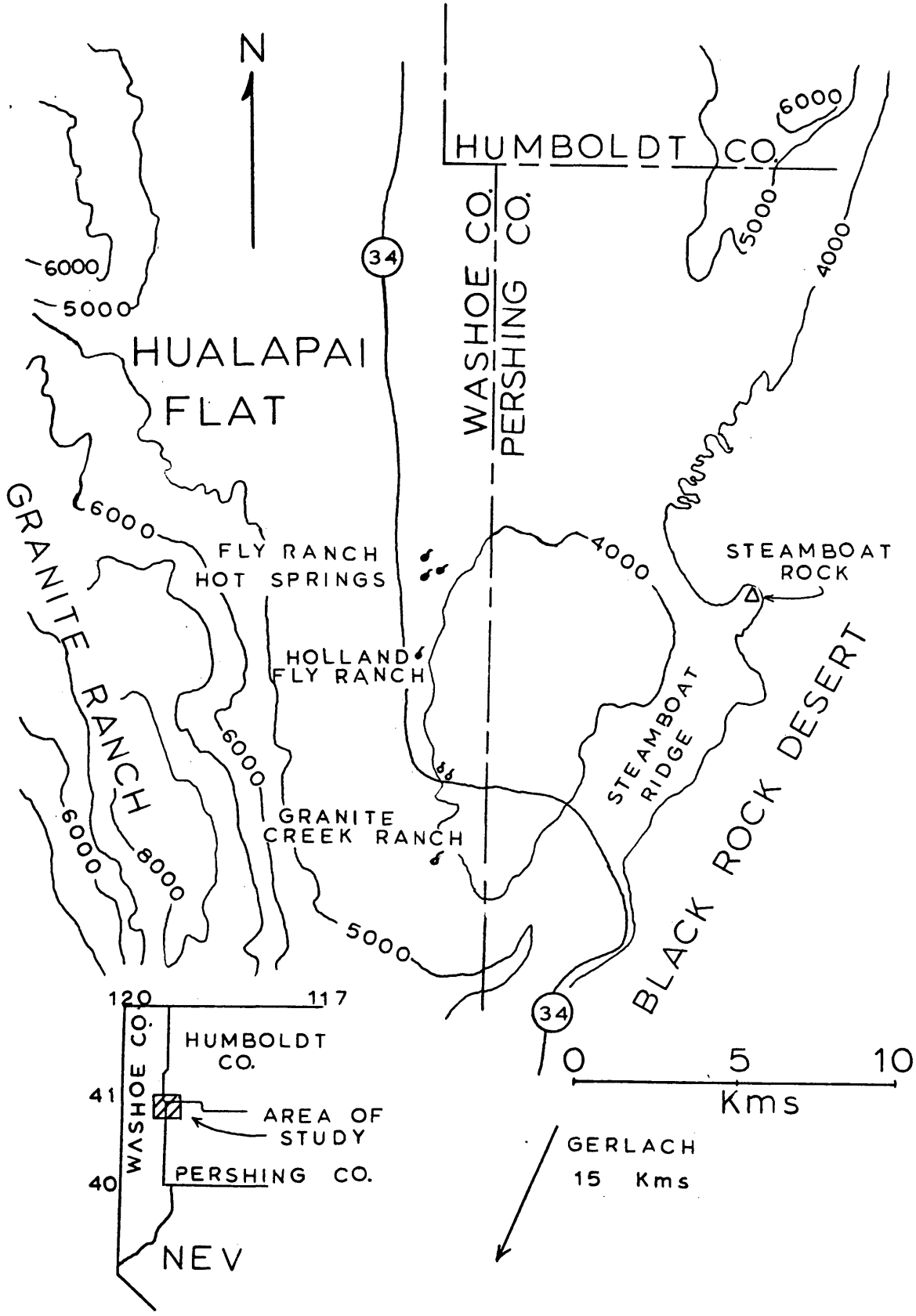

Figure 10. Regional setting and cultural features of Hualapai Flat.

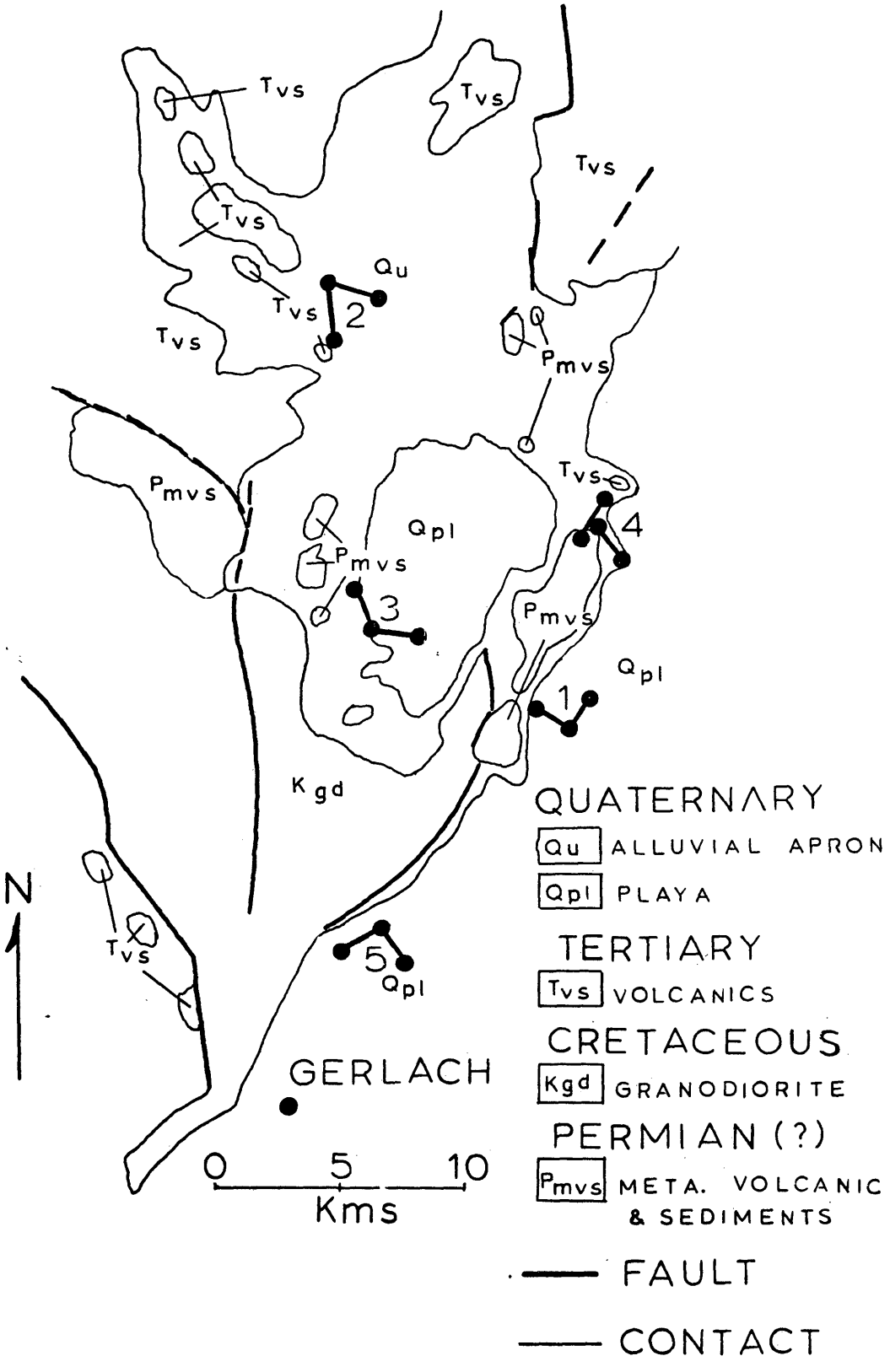

Figure 11. Surficial and bedrock geology map of Hualapai Flat with locations of sources shown.

sists of three main units, Permain or older (Pmvs) metasediments and metavolcanics, mostly on the east and west of Hualapai, Cretaceous granodiorite (Kgd) making up the Granite Range, and Tertiary (Tvs) volcanics and sediments to the north of Hualapai. Figure 11 is a bedrock geology map of the area taken from the work of Bonham (1969) and Tatlock (1969) with supportive information from Crewdson (1975) along with the location of the three pairs of bipole sources that will be discussed.

Surficial Geology

The unconsolidated sediments that make up the alluvium are divided between the alluvial and the playa (Harrill, 1969). The alluvial apron consists principally of alluvial fans at the edges of the basin and a thin veneer of sediments that rest against the ridges that surround Hualapai Flat. The playa is located in the southern end of Hualapai and has little topographic relief. The altitude of the Hualapai playa is about 4000 feet, as is the surface of the Black Rock Desert.

Configuration of the Basement Surface Under Hualapai Flat

Little is known about the depths to basement and its lithology in Hualapai Flat. McGinnis and Dudley (1964) on the basis of a refraction and reflection study found that at

the northeast portion of the flat near Steamboat rock, the depth to basement was 310 feet which put the elevation of the basement surface at 3700 feet. They suggested that the basement most likely consisted of Tertiary basalt flows but could not demonstrate this. Just southeast of the Calico Mountains at the north edge of the Hualapai playa, the reflection survey indicated that the bedrock surface is at 3250 feet elevation with 750 feet of overlying alluvium. Water wells on the northwest side of Hualapai Flat near Humboldt county encountered consolidated sediments/bedrock at depths of 450 feet with a resulting basement elevation of 3650 feet. Toward the south near the Fly Ranch hot springs this "basement" surface rises to an altitude of 3800 feet. Harrill (1969) concluded that the maximum thickness of alluvium is 1000 feet but the electrical data to be presented here indicates that it may be much deeper in places. The well data and previous geophysical results are shown in figure 37.

Resistivity Parameters for Model Studies

When attempting to model a particular area, much trial and error can be avoided by choosing proper values for the resistivities of the geoelectric structure to be studied. The resistivity of the playa in the Black Rock Desert was taken to be 1 Ω-m, on the basis of the results of the receiver

stations close to source 1B. The playa in Hualapai was taken to be the same simply on the basis of lithologic similarity. However, in the theoretical models used, it is necessary to use a single resistivity for the unconsolidated sediments of Hualapai, the playa and the alluvial fans. From the receiver stations near the second pair of sources, apparent resistivities of 5 Ω-m were measured, and this value is used for the resistivity of the alluvium in Hualapai. For rocks like the Cretaceous granodiorite of the Granite Range, Keller (1966b) has reported the range of resistivities for Mesozoic intrusives as ranging from 500 to 2000 Ω-m . The lower value of 500 Ω-m was used although the value had little effect in the modelling. For the Tertiary volcanics and sediments and the Permian metavolcanics, the actual resistivity was first taken to be 100 Ω-m . Model resutts indicated that lower values should be used so the final value for the resistivity used was 35 Ω-m . Because this report evaluates the geothermal potential of the Fly Ranch hot springs using the quadripole method, the results from the fourth and fifth pair of sources are not included because their area of coverage does not provide information on this subject. The values for the average resistivity from these two sources are contoured with the results from the first three pair of sources in figure 39, but are not listed with the processed field data in Appendix A.

Interpretation of the First Pair of Sources

The locations of the receiver stations and position of the sources are shown along with the geology in figure 12. The theoretical model chosen to represent the area was that of a resistive dike (Steamboat ridge) bordered by two conductive media (Black Rock Desert and Hualapai Flat). This model is a gross simplification of the geologic complexity present, but some correlation between the best theoretical model and the field data was found.

A theoretical dike has two vertical, parallel contacts which is probably not the case for the Steamboat ridge. The topographic depression northwest of source 1A and other eroded gullies create embayments between the Black Rock Desert and the ridge. Both boundaries between the ridge and the two conductive media are not straight and the separation between Hualapai and the Black Rock Desert is not linear. In spite of these variations, modelling the levee as a dike appeared to explain the field results.

In trying various combinations of resistivities, dike thicknesses and offset from the sources, depth to resistive basement (if any), and strike of the dike, only one type of model was found to match the field results. It required that the front contact of the dike pass through source 1A, leaving one electrode in the resistive dike and the other in the

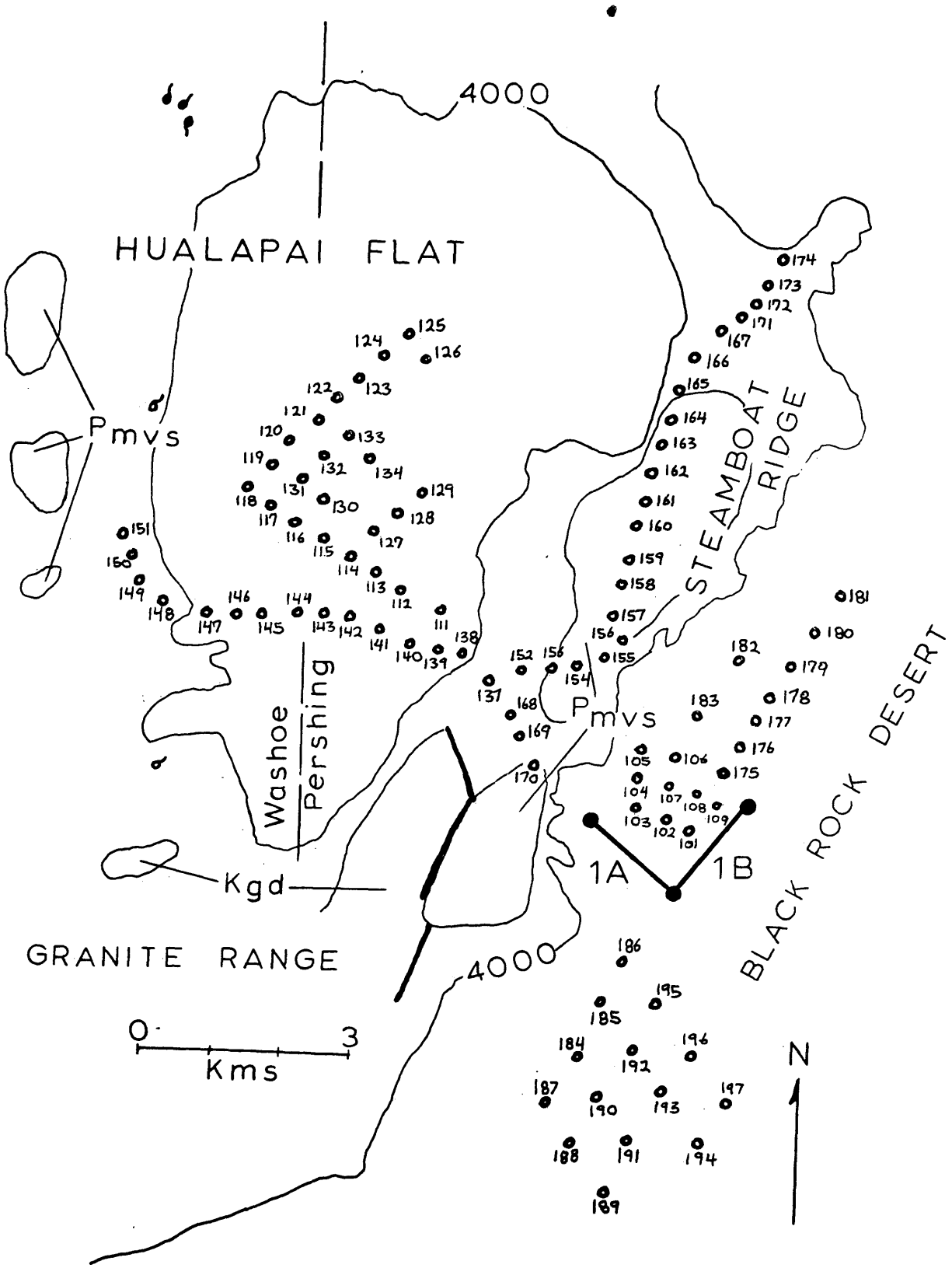

Figure 12. Location of sources 1A and 1B and receiver stations.

conductive Black Rock Desert. An insulating basement at a depth of 500 meters was added to provide better correlation with the field data and to represent the granite or granodiorite that is presumed to underlie the entire area. The final resistivities chosen were 1 Ω-m for the Black Rock Desert, 5 Ω-m for Hualapai Flat, and 35 Ω-m for the Permian metavolcanics that make up the Steamboat ridge.

The apparent resistivities calculated for source 1A are shown in figure 13 with the presumed position of the dike superimposed. The apparent resistivities in the Black Rock Desert are 10 Ω-m or less and increase as the receiver stations approach the ridge. The electrical basement under the Black Rock Desert dips to the east, otherwise the effects of the resistive basement would make the resistivities increase with separation from the source, which is not seen in the map of apparent resistivities. The prominent feature on figure 13 is the conductive anomaly with a northwest trend located in the most saline, conductive part of Hualapai Flat. The anomaly has a low resistivity of 25 Ω-m which is 25% of the values measured along the back of the ridge. However, this anomaly is probably a false anomaly and does not reflect any actual changes in the subsurface resistivity structure. Figure 14 is the single source theoretical resistivity map which best matches the data from source 1A. On the far side of the dike, a false anomaly, with values less than 30

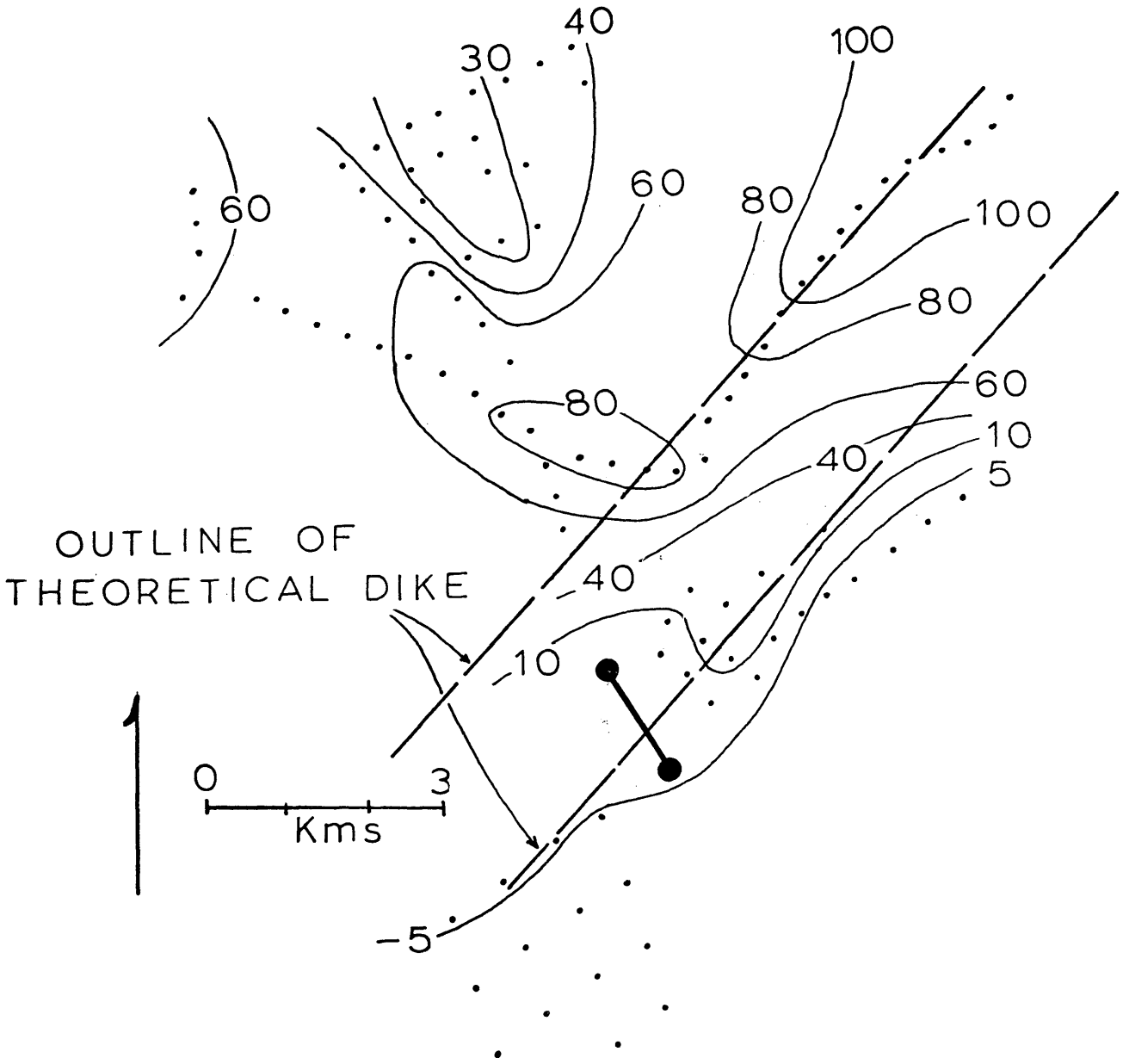

Figure 13. Apparent resistivities for source 1A, values in ohm-meters. Position of theoretical dike shown.

ρ_a FOR MODEL OF SOURCE 1A

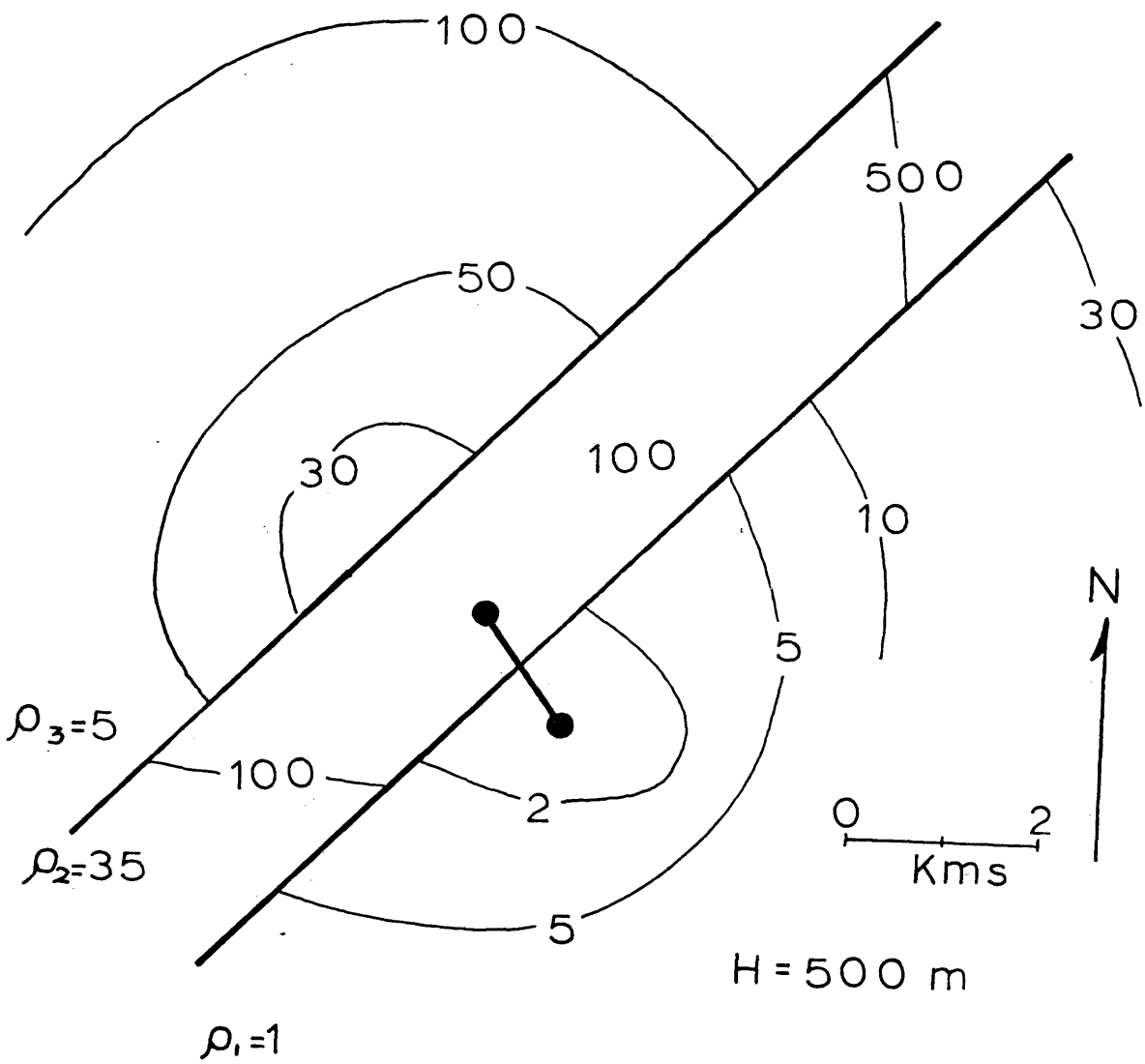

Figure 14. Calculated apparent resistivities for theoretical dike model.

appears. Within three kilometers of the anomaly, the background resistivity is over 60 Ω-m , or twice the value in the anomaly. This 50% change is only half that found in the field data, but the difference could be due to simplifying assumptions made in the theoretical model. In addition the thicknesses of alluvium in Hualapai might increase to the northwest, a factor which can account for the difference. The receiver stations in the Black Rock Desert had resistivities greater than 3 Ω-m , in agreement with the theoretical model.

The apparent resistivities from source 1B are shown in figure 15. Inamuch as this source is located entirely in the conductive Black Rock Desert, most of the current should remain in the saline playa of the Black Rock Desert and the resistivities measured should be lower than for source 1A. The reciever stations in the Black Rock Desert show little indication of the presence of basement and have lower resistivities than found by source 1A. The resistivities in Hualapai Flat were so low that signals could not be distinguished from telluric noise and because of this, it is impossible to tell whether the conductive anomaly would have remained after rotation of the source. The results show that the resistivities tend to get lower toward the center of Hualapai Flat, which could be due to a resistivity change of thickening of alluvium. The theoretical apparent resis-

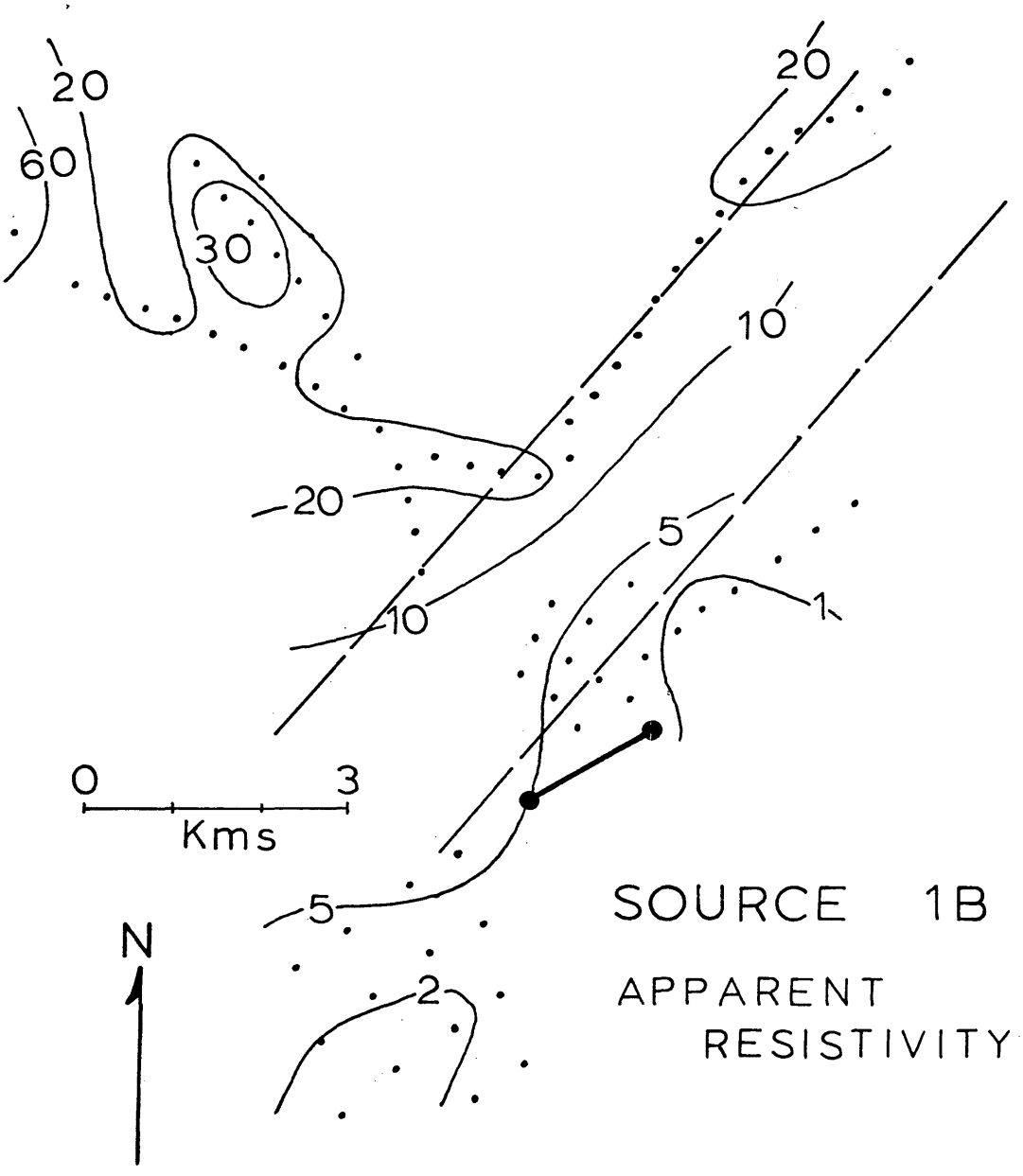

Figure 15. Apparent resistivities for source 1B. Theoretical dike superimposed.

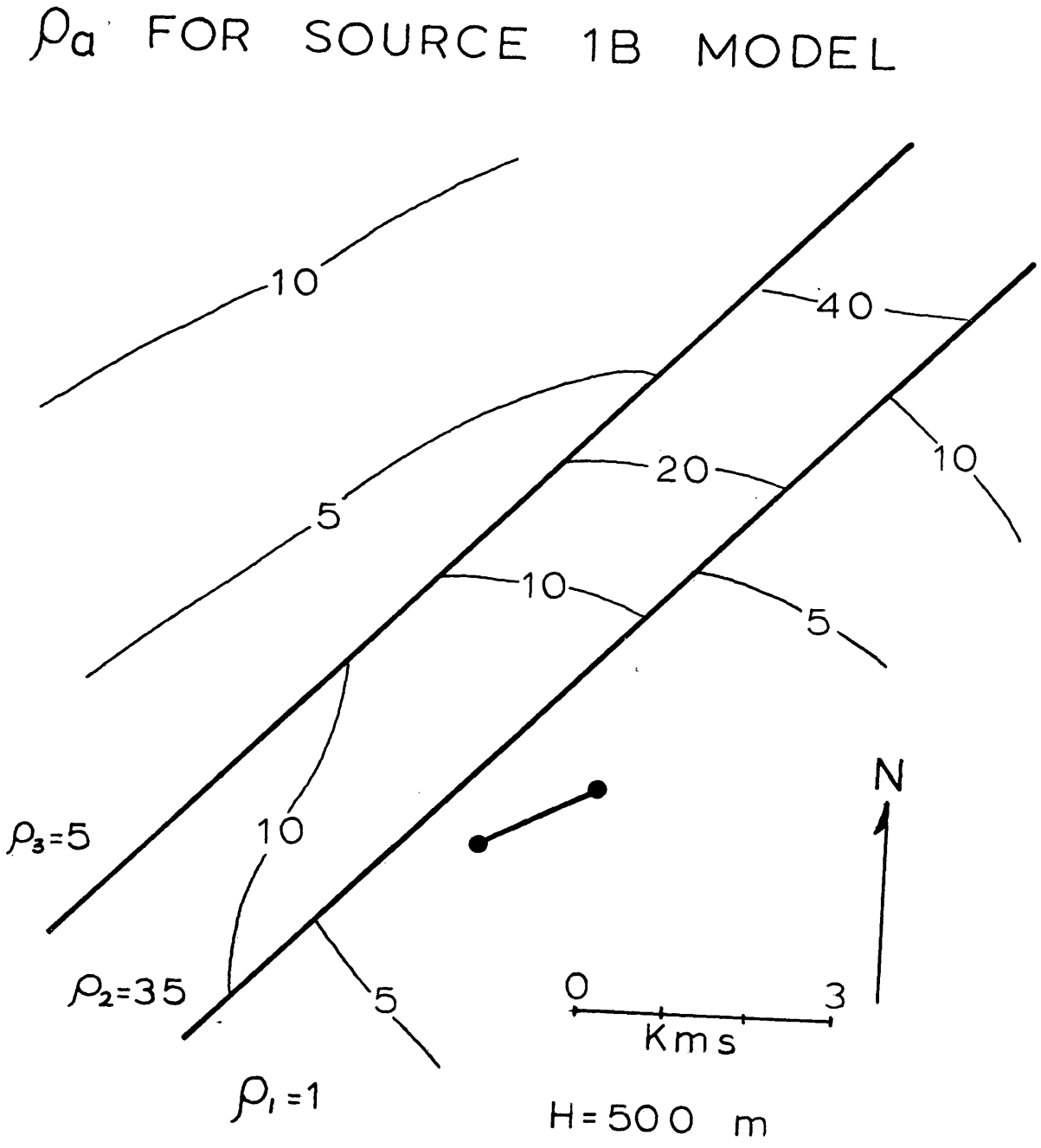

Figure 16. Calculated apparent resistivities for theoretical dike model.

tivities for source 1B are shown in figure 16. After rotation of the source, the resistivities in all three media decreased substantially in the theoretical model as they did in the field because the current tends to remain in the more conductive Black Rock Desert. In Hualapai, the resistivities decreased about 50% while the theoretical values decreased 80%. This discrepancy reflects the difficulty in modelling a geologic region by the simple geoelectric structure used in this study.

The ellipticities and bearing of ρ_{min} both could be duplicated by the approximate theoretical model. Along the back side of the Steamboat ridge, the bearing of ρ_{min} is normal to the strike of the dike as can be seen in figure 17. The stations (111-118, 137-148) in Hualapai Flat had their ρ_{min} bearings parallel to the dike and had lower ellipticity values than the stations (152-173) along the west contact of the ridge. The stations in the Black Rock Desert to the southwest of the sources had the lowest ellipticities and their bearings of ρ_{min} pointed toward the centroid of the sources when more than a kilometer from the ridge.

The ellipticities and ρ_{min} bearing generated by the theoretical model (figure 18) were in agreement with the field results. The stations in Hualapai had their minor axes pointed parallel to the strike of the ridge, as do the theoretical calculations. The string of stations along the

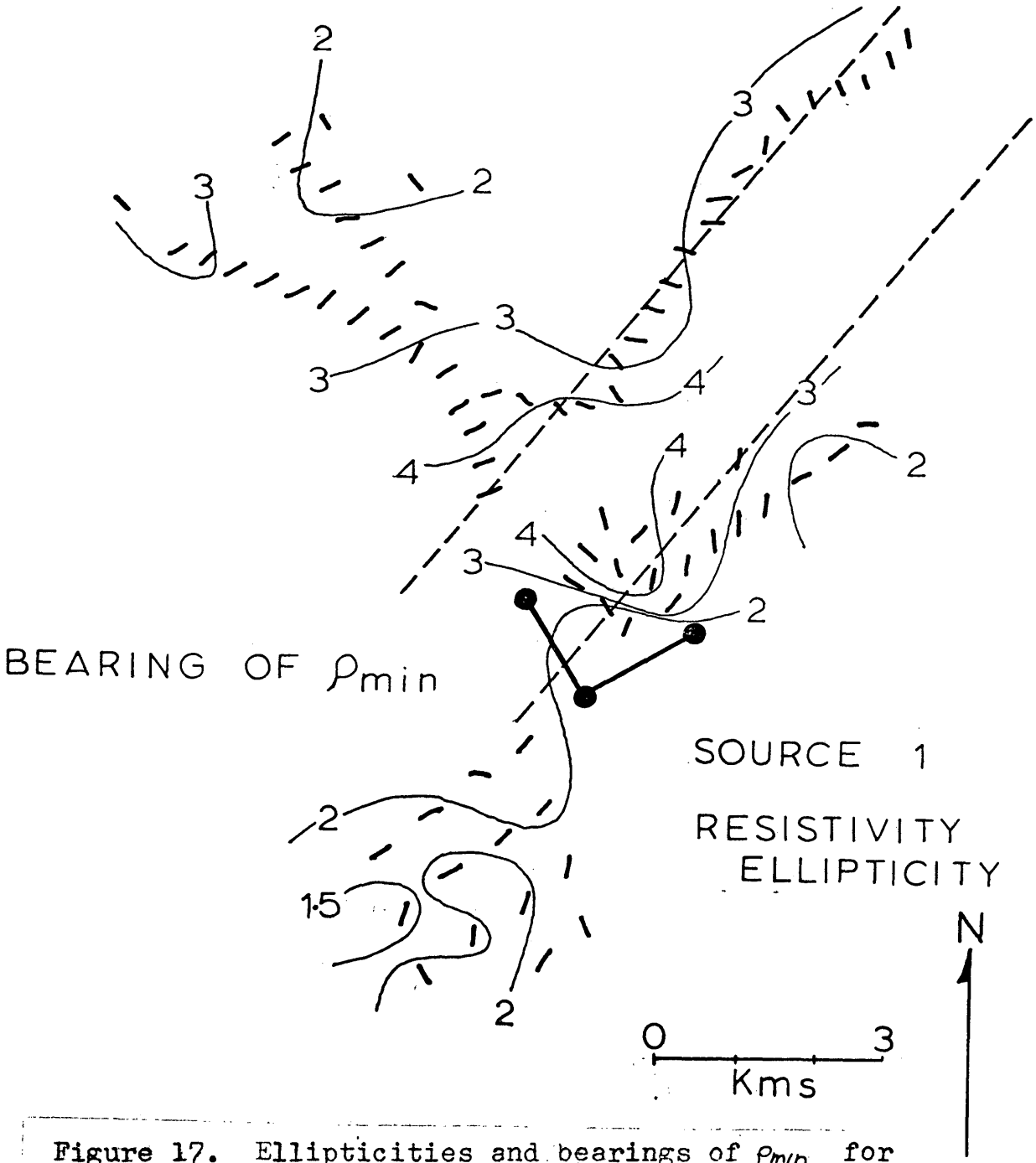

Figure 17. Ellipticities and bearings of ρ_{min} for sources 1A and 1B.

ELLIPTICITIES and θ_{min} FOR SOURCE ONE MODEL

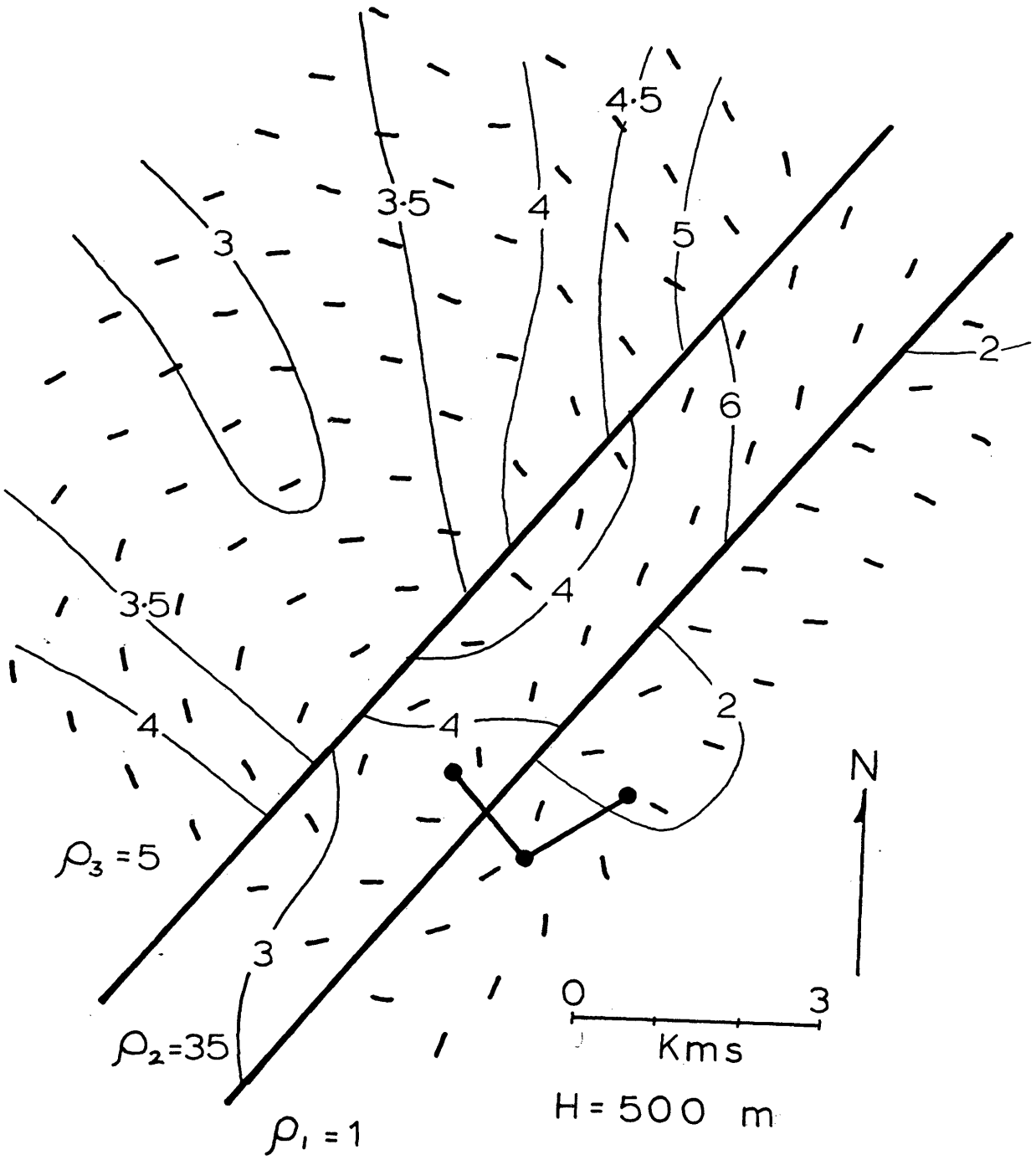

Figure 18. Calculated ellipticities and bearings of ρ_{min} for theoretical dike model.

back of the levee had their ρ_{min} bearings perpendicular to the dike, again in agreement with the field results. For the stations in the model that are located in the medium representing the Black Rock Desert, the minor axes were aligned toward the centroid of the sources, as did most of the stations actually observed in the Black Rock Desert. Only two stations (118 and 128) suggest that there is a resistivity anomaly in Hualapai Flat for these, the directions of are nearly 90° different from the other values in Hualapai and were in an ellipticity low, which could be due to the existence of a conductive feature. However the anomaly in the middle of Hualapai was not observed from the third pair of sources in the southwest corner of Hualapai, suggesting it is a false anomaly.

Comparison of the average resistivity (ρ_{ave}) values from the field data (figure 19) and the theoretical results (figure 20) show some agreement. The values of ρ_{ave} are still affected by false anomalies as seen by the 20 Ω-m contours on the back side of the dike in the model. This appears to be the explanation for the 30 Ω-m (2 stations, 128 and 131) low in Hualapai and both maps agree that the average resistivity will increase along the back side of the dike.

The prime causes for the discrepancies between the theoretical model and the field results is the use of simple models and their inadequacy to properly describe regions of

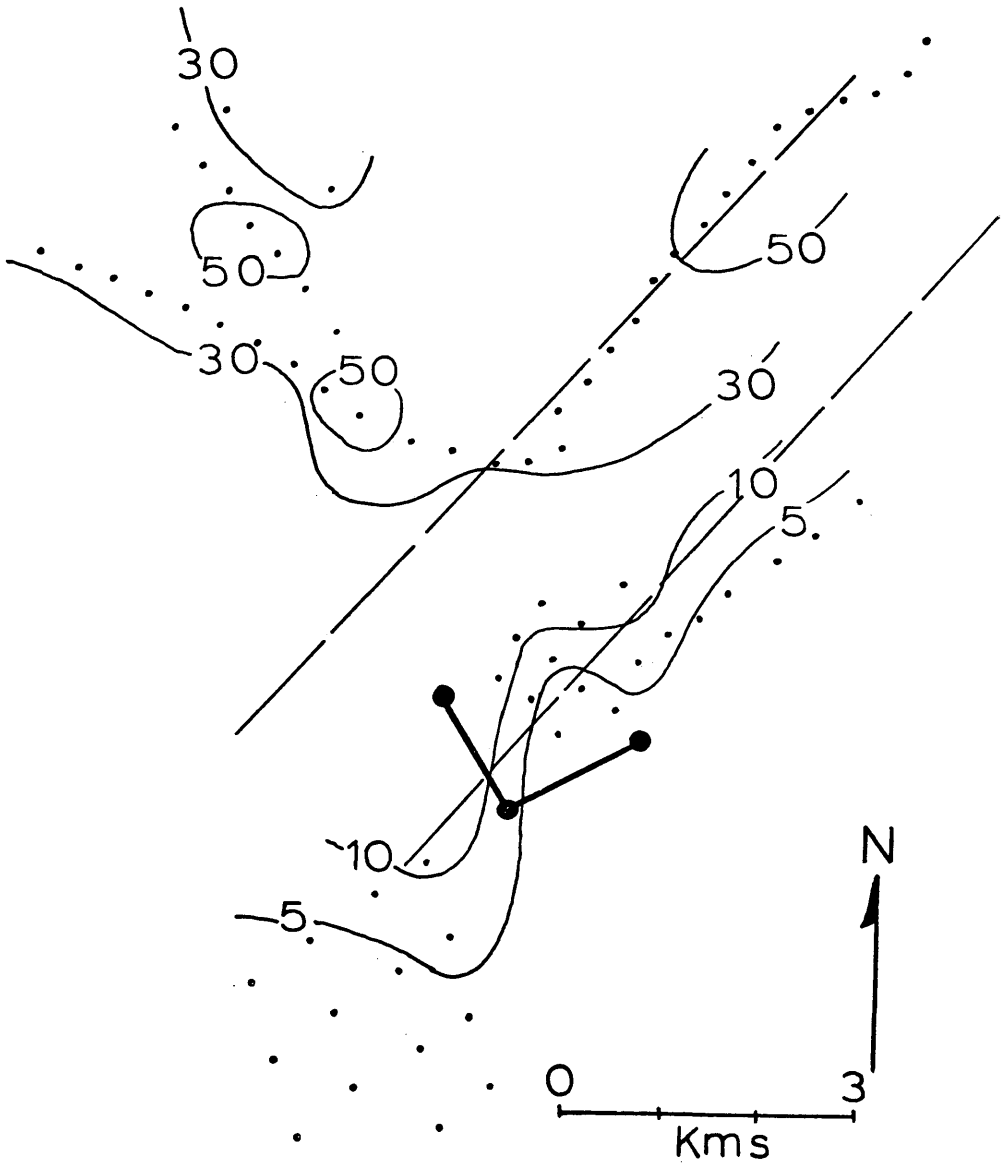

Figure 19. Average resistivities for sources 1A and 1B.

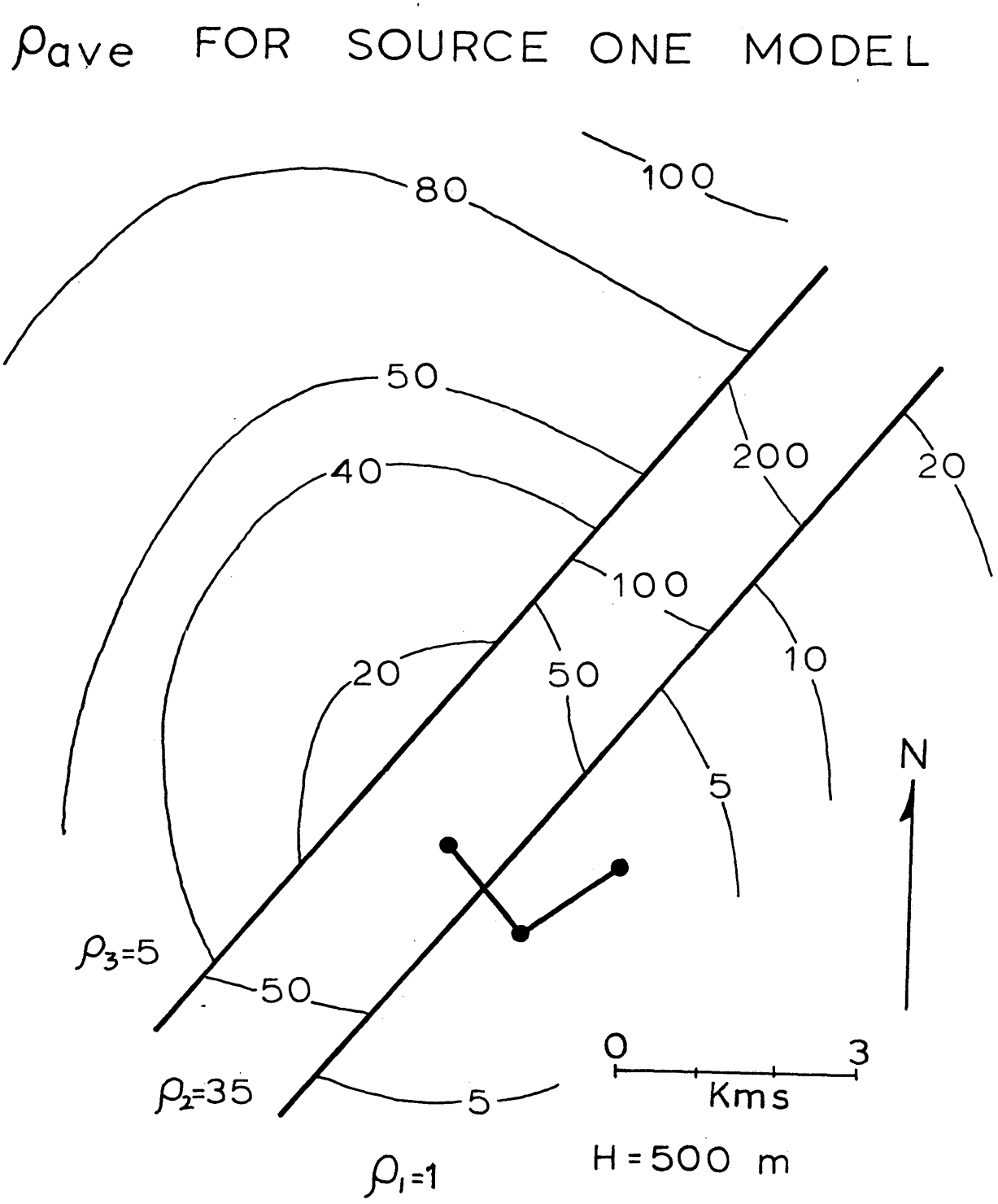

Figure 20. Calculated average resistivities for dike model.

geologic complexity. As will be seen later, the basement is not a horizontal surface but dips to the northwest probably in a series of faulted blocks. Moreover, the value for the depth to resistive basement will affect the resistivity results. A depth of 500 meters was used to model the data in the Black Rock Desert and was taken on the basis of time domain electromagnetic (TDEM) soundings by Ofrey (1975). The depth to basement in Hualapai Flat is probably not as great near the ridge and is closer to 300 m. Because the theoretical model requires a constant depth to insulating basement, actual variations will result in discrepancies between the model and the field. If a different value were chosen, the resistivities in Hualapai might have been in better agreement with theoretical results, but still showed large differences elsewhere. Although not shown, the apparent conductance maps from source 1A suggest that the basement in the southeast corner of Hualapai is less than 300 meters from the surface.

Attempts to vary six parameters and reach agreement with quadripole results can be ill-fated, but the theoretical results compare favorably. The most important result from the model studies is that the anomaly in Hualapai could be a false anomaly and might not represent a conductive (geothermal) feature.

Interpretation of Second Pair of Sources

The second pair of sources (2A and 2B) to be discussed here was located in the northwest corner of Hualapai Flat (figure 21), with most of the area of interest being covered by alluvium with little topographic relief. The model chosen to represent the site consisted of two horizontal layers, with an upper layer of thickness H and resistivity ρ_1, overlying a halfspace of resistivity ρ_2. The apparent resistivities measured at the receiver stations close to the sources were around 5 Ω-m, and this was chosen to be the resistivity of the upper layer in the model. The two remaining variables, ρ_2 and H were found by plotting the average resistivity (ρ_{ave}) as a function of receiver station separation from the centroid of the source (R_c) for several traverses (figure 22). Although there is scatter in the data, the results from stations 201-210, 231 and 232 (solid circles) indicate that the basement has a very great resistivity inasmuch as the line (L_1) through these points has a slope of 1 (Alpin, 1966). For the case of an insulating ($\rho_2 = \infty$) basement, the line with slope of 1 is a S (conductance) line which can determine the ratio of H to ρ_1. Depending on the geometric array used to measure the apparent or average resistivity, the ratio of spacing to apparent resistivity for any point on this line is equal to the true conductance times

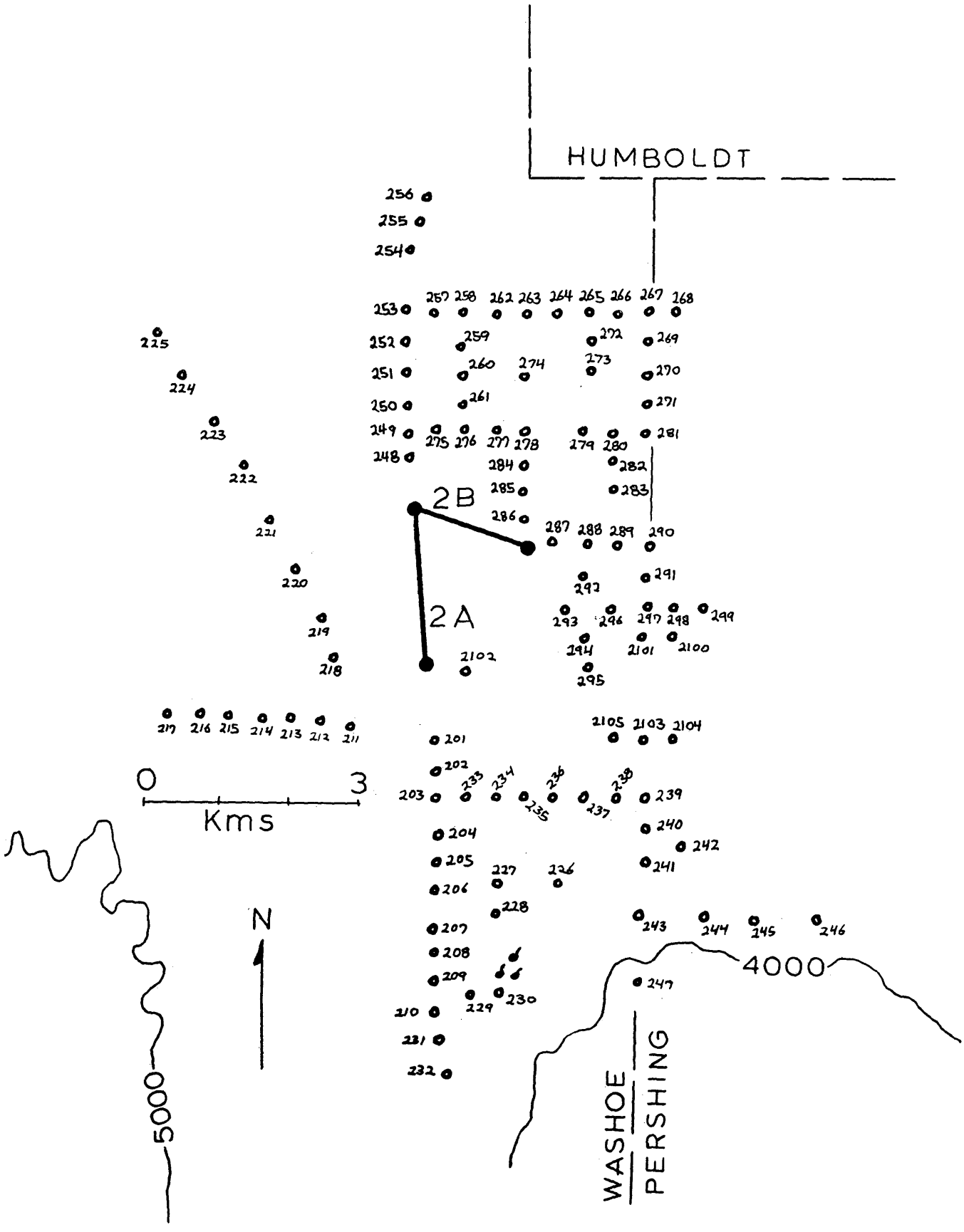

Figure 21. Location of sources 2A and 2B and receiver stations.

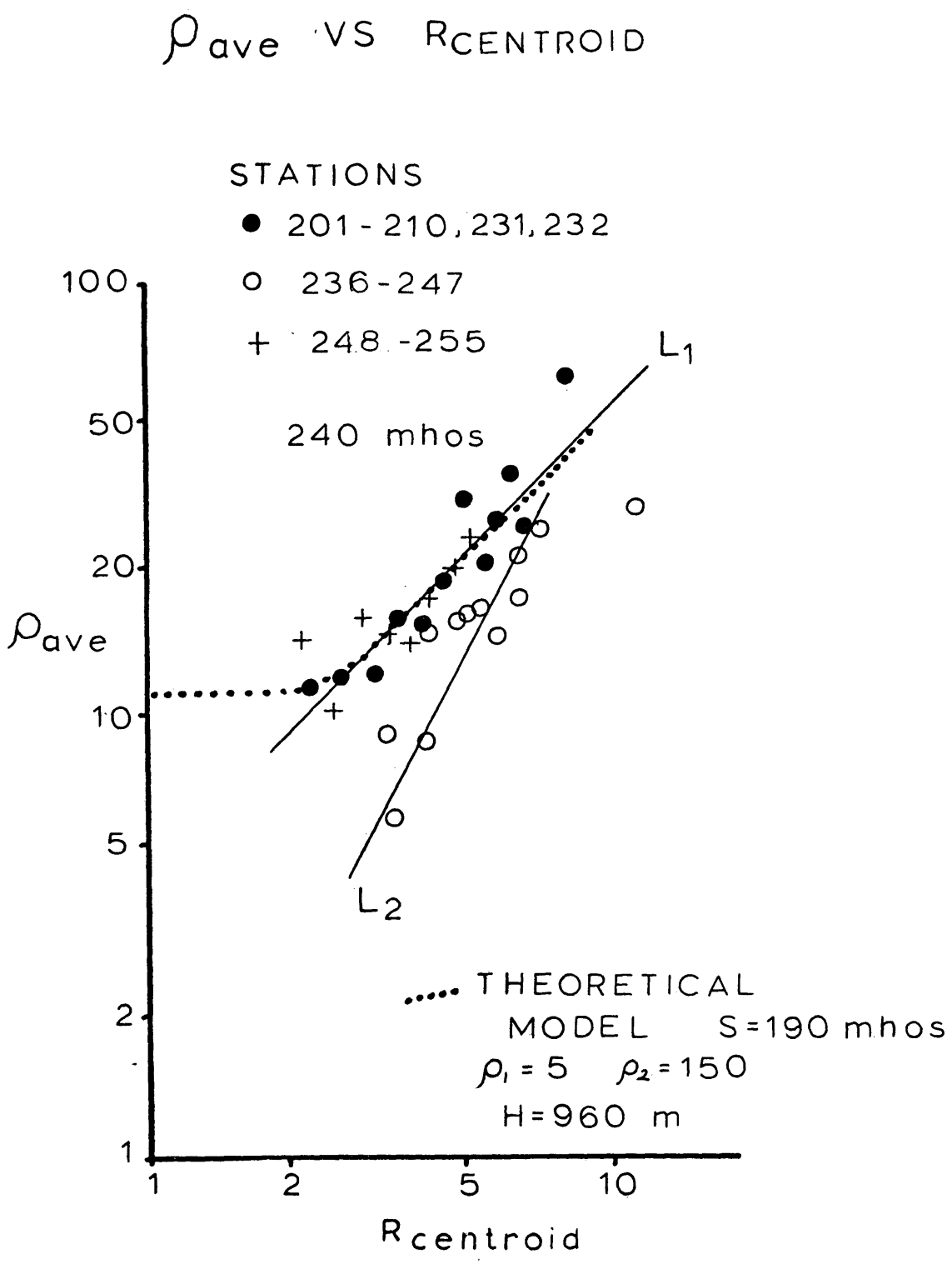

Figure 22. Plot of average resistivity from field data versus distance from centroid of sources.

a constant. The conductance is found by picking any point on the S line and finding the ratio of R_c to the average resistivity. For L_1 the ratio was 240 mhos, but without any information on the resistivity or thickness of the overlying conductor, it would be impossible to go any further. The assumption is made that the apparent resistivities measured at the receiver stations close to the source represent the true resistivity of the section and that this resistivity is constant to basement. The value of ρ_1 chosen was 5 which gives the result:

$$S_{TRUE} = H/\rho_1 = K \cdot S_{MEASURED} = K \cdot 240$$

$$H = K \cdot 240 \cdot \rho_1 = K \cdot 1200$$

Several models with a single layer over a basement of infinite resistivity were run, and the results indicate that the constant K varies somewhat but that a value of .8 would give reasonable results. Using this value, the thickness of the upper layer is 960 meters or about 3000 feet. To confirm this, the plot of this theoretical model was added to the field data (dotted line). This line coincides with the line L_1 and lies to the left of the rest of the field data from the other receiver stations. Stations 248-255 (crosses)

located on a north-south traverse north of the sources, were close to the line L_1 and the theoretical results (dotted line).

However, if stations 236-247 (open circles) are used, a line (L_2) with slope greater than 1 can be drawn. This indicates the presence of a dipping layer, or in this case that the basement comes closer to the surface near the stations to the southeast of the surface. Unfortunately, the presence of a dipping layer makes it impossible to distinguish between the case of horizontal basement with infinite resistivity from the case of a dipping basement with finite resistivity. For the theoretical model mentioned above, by adding a dip to the basement, the theoretical (dotted) line could have a slope of 1, without the requirement of infinite resistivity in the basement. It should be noted that most of the values for ρ_{ave} lie to the left of L_1 which indicate that those stations were located in an area either where the alluvium is thicker or the resistivity of the alluvium is lower. Since these stations are located near the Fly Ranch hot springs, the latter explanation seems more likely.

The apparent resistivities for source 2A are shown in figure 23 and the results from the theoretical model are in figure 24. The ellipse patterns in figure 23 is characteristic of those for two layer models that do not have lateral changes in resistivity. The 6 Ω-m resistivity low in figure

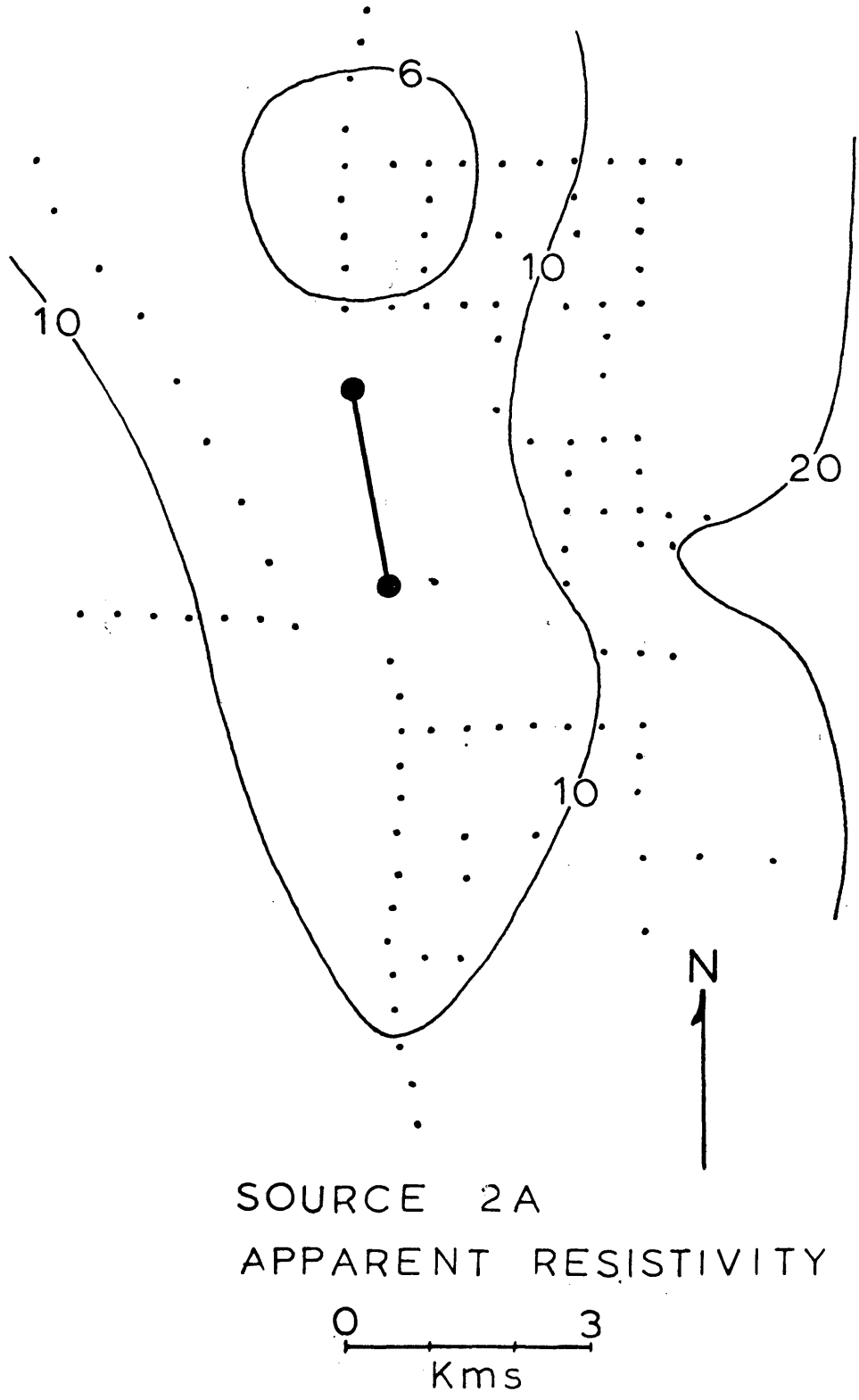

Figure 23. Apparent resistivities from source 2A. Values in ohm-meters.

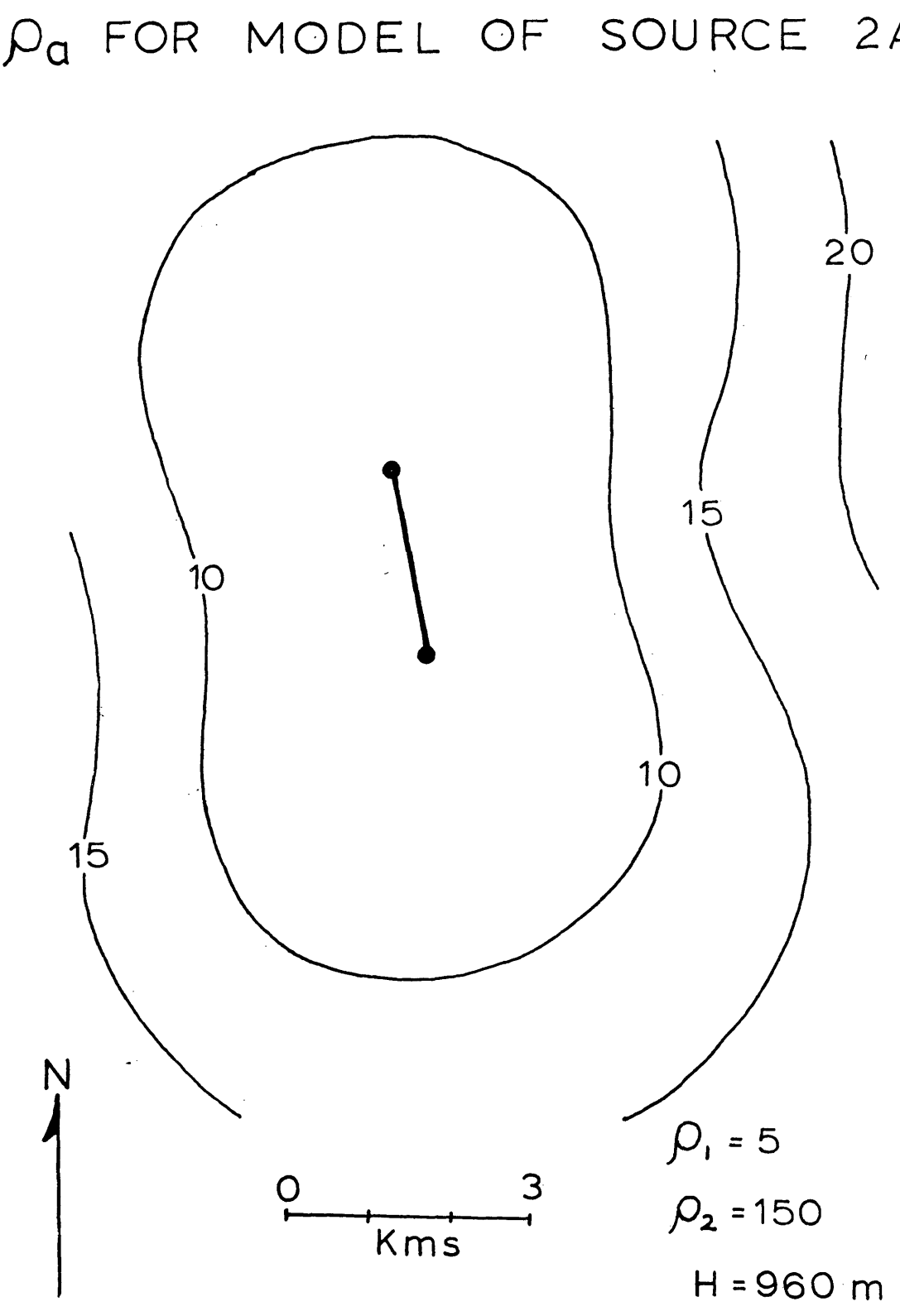

Figure 24. Calculated apparent resistivities for theoretical two layer model.

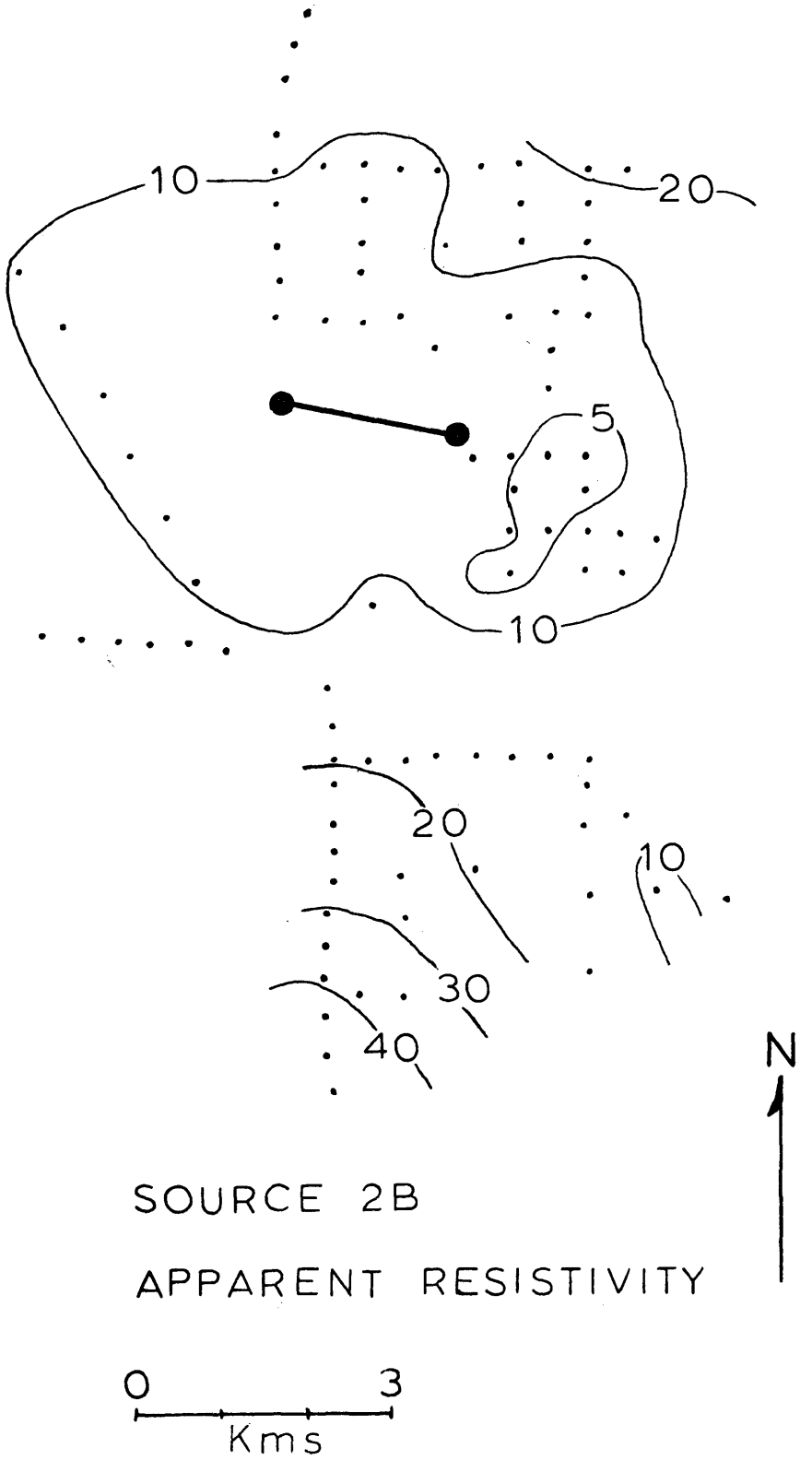

Figure 25. Apparent resistivities from source 2B. Values in ohm-meters.

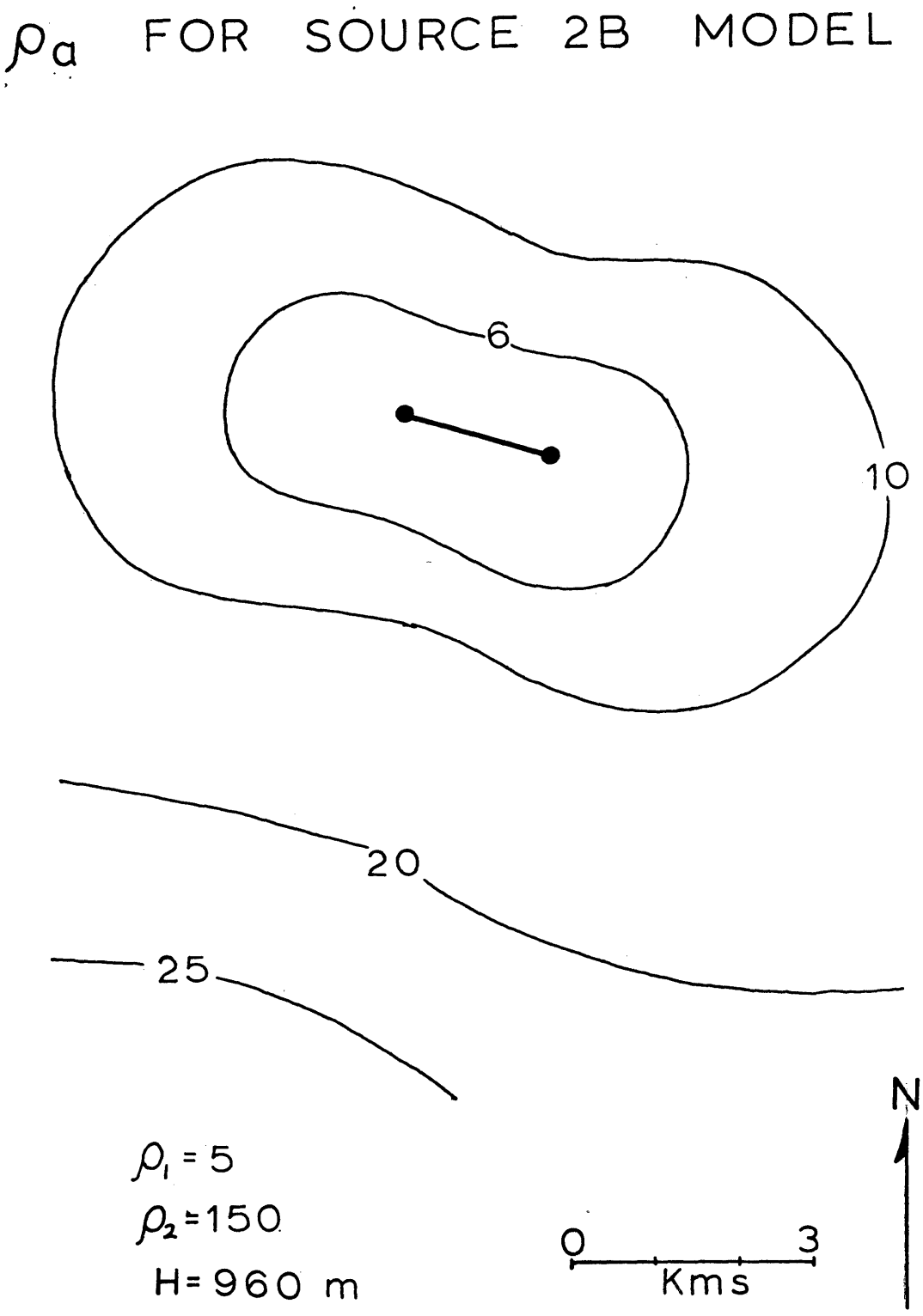

Figure 26. Calculated apparent resistivities for theoretical two layer model.

23 north of the source is a false anomaly caused by the proximity of the receiver stations to the source, being a function of the ratio of source length to the thickness of the upper layer. The absence of a similar anomaly to the south could be due to changes in the depth to basement (an increase) or variations in water salinity in the near surface rocks caused by irrigation and watering in the neighboring farms. Likewise, the results from source 2B (figure 25) and the theoretical model (figure 26) form elliptical patterns and another false anomaly appears to the east of source 2B. When the source is rotated, this anomaly did not appear, indicative that it is a false anomaly.

In figure 27, ρ_{ave} from the quadripole results is shown and the results from the model are shown in figure 28. The model indicates that they should form an egg-shaped pattern with the 20 Ω-m contour about three source lengths from the source centroid. To the south of the sources, this contour is only two south lengths from the centroid, suggesting that the alluvium thins to the south.

The resistivity ellipticities and bearing of ρ_{min} are shown in figure 29. The directions of the minor axes are toward the centroid of the sources, indicating that there are no lateral variations in resistivity, only vertical changes. Unfortunately, the bearing of ρ_{min} cannot be used to distinguish between a flat-lying basement and a circular

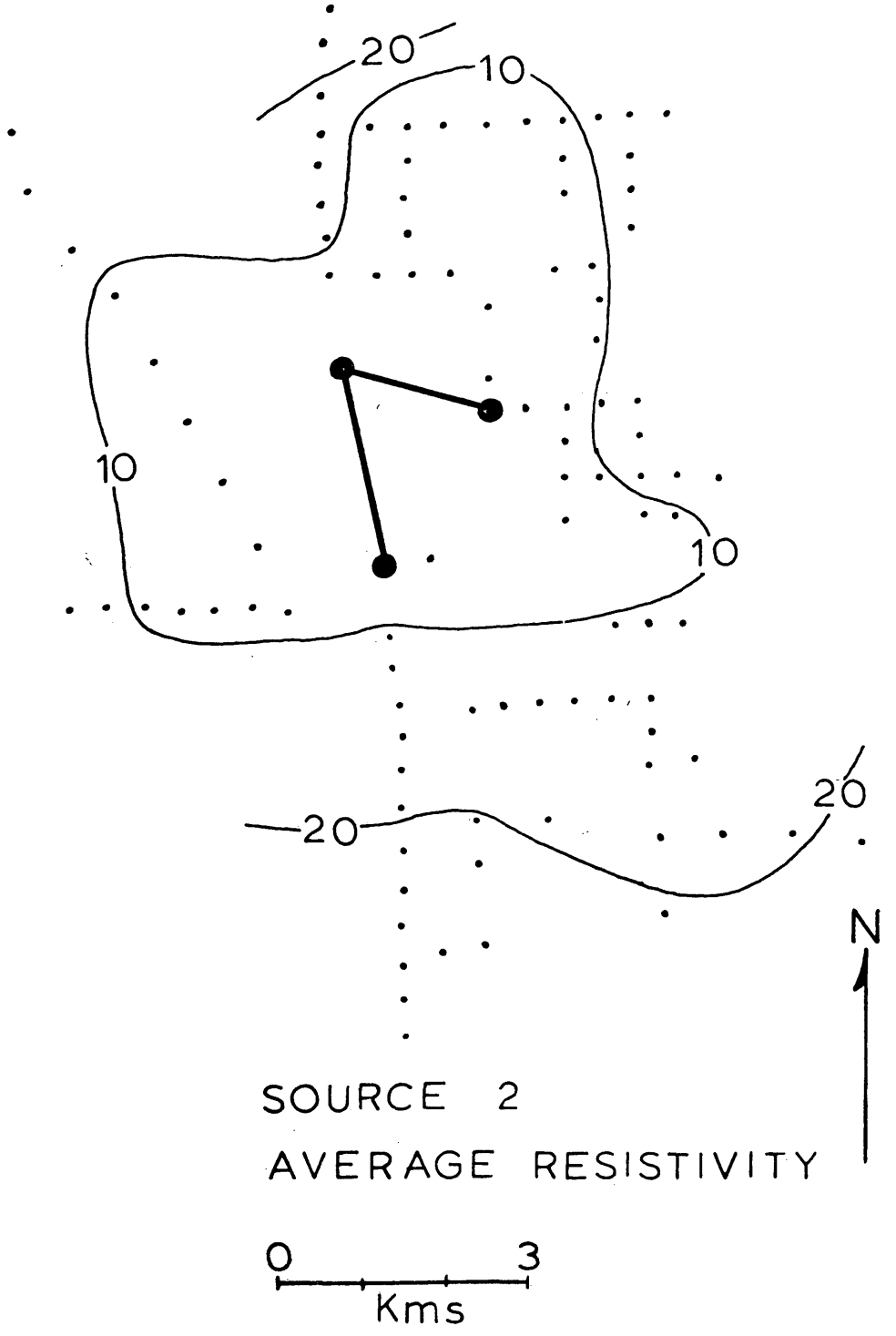

Figure 27. Average resistivities from field results for sources 2A and 2B. Values in ohm-meters.

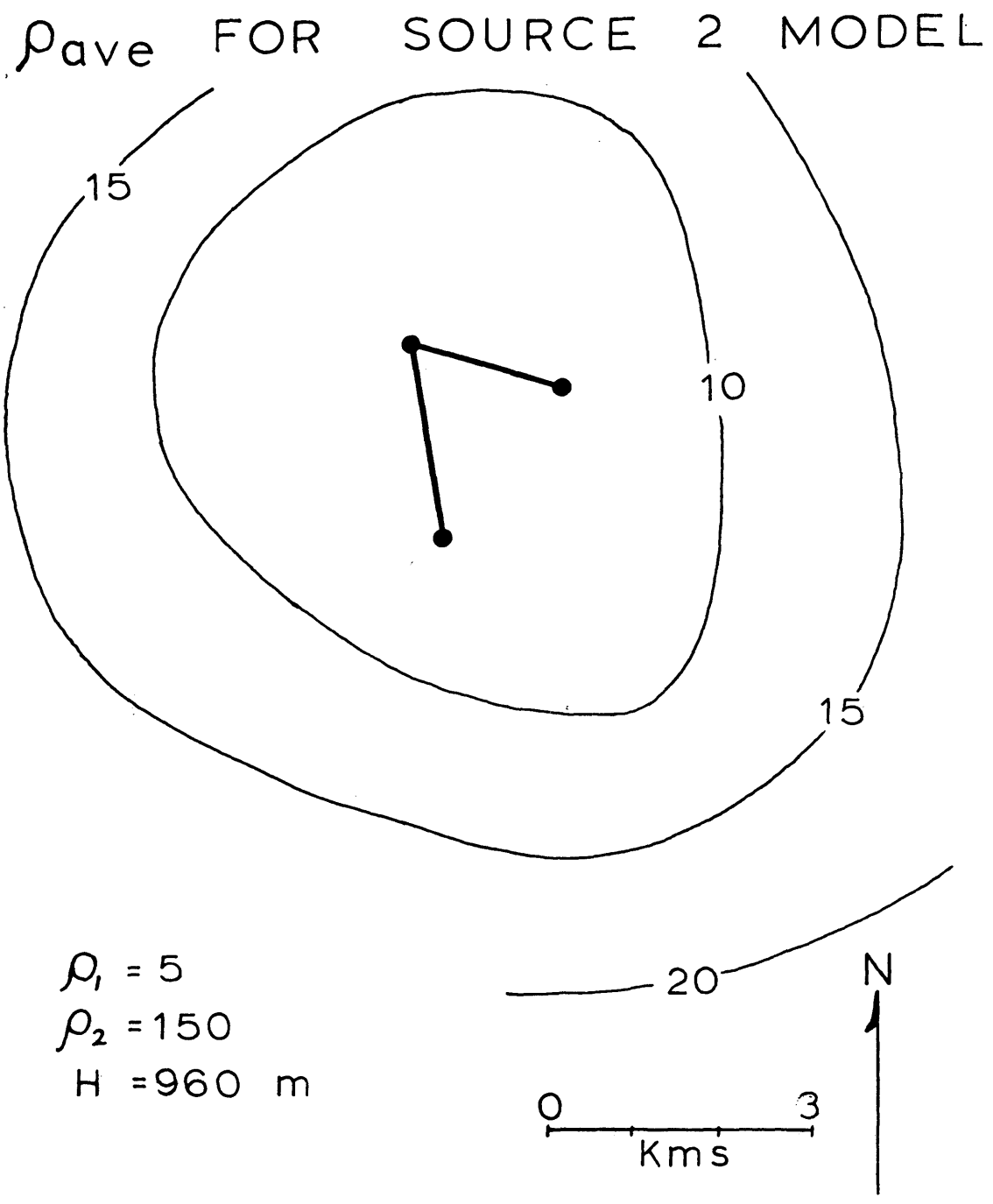

Figure 28. Calculated average resistivities for theoretical two layer model.

depression centered under the sources. The theoretical results confirm that the bearing of ρ_{min} will point toward the centroid of the sources but the ellipticity patterns are different (figure 30). For the model of the two layer case, ellipticity highs should form off the ends of the sources and should decrease with distance. However, the field results did not support the model results and do not show any tendency to roll over with increasing separation from the sources. Figure 31 is a plot of resistivity ellipticity versus separation from the centroid of a pair of sources in an array identical to the second pair. The upper layer resistivity is 5 Ω-m, the basement has a resistivity of 150 Ω-m, and the thickness of the upper layer (H) is varied. None of these models duplicated the ellipticities measured in the field, either in magnitude or position of the peak. The field ellipticities do not peak but increase asymtotically to a limit of about 2.5, behavior which was not observed in any of the models. A possible explanation is that the sources were placed over a large depression in the basement surface that has a diameter greater than five kilometers, but until vertical soundings, Schlumberger or TDEM are carried out, it is impossible on the basis of quadripole results to decide. The 'basement' at 450 feet depth reported by drillers could be a thin consolidated sediment/basalt flow which appears to divide the alluvium into two zones.

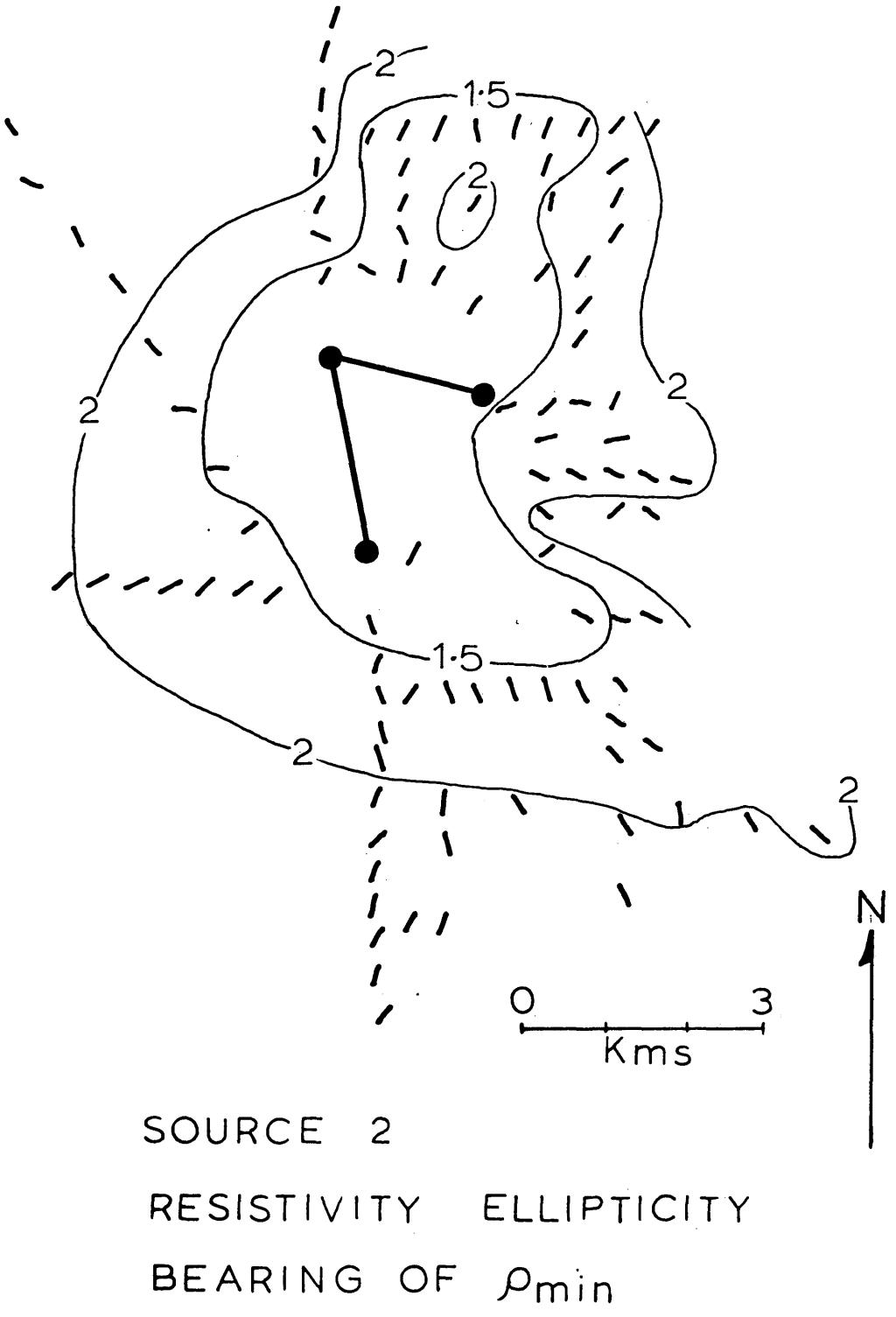

Figure 29. Ellipticities and bearing of ρ_{min} for sources 2A and 2B.

ELLIPTICITIES and θ_{min} for SOURCE 2 MODEL

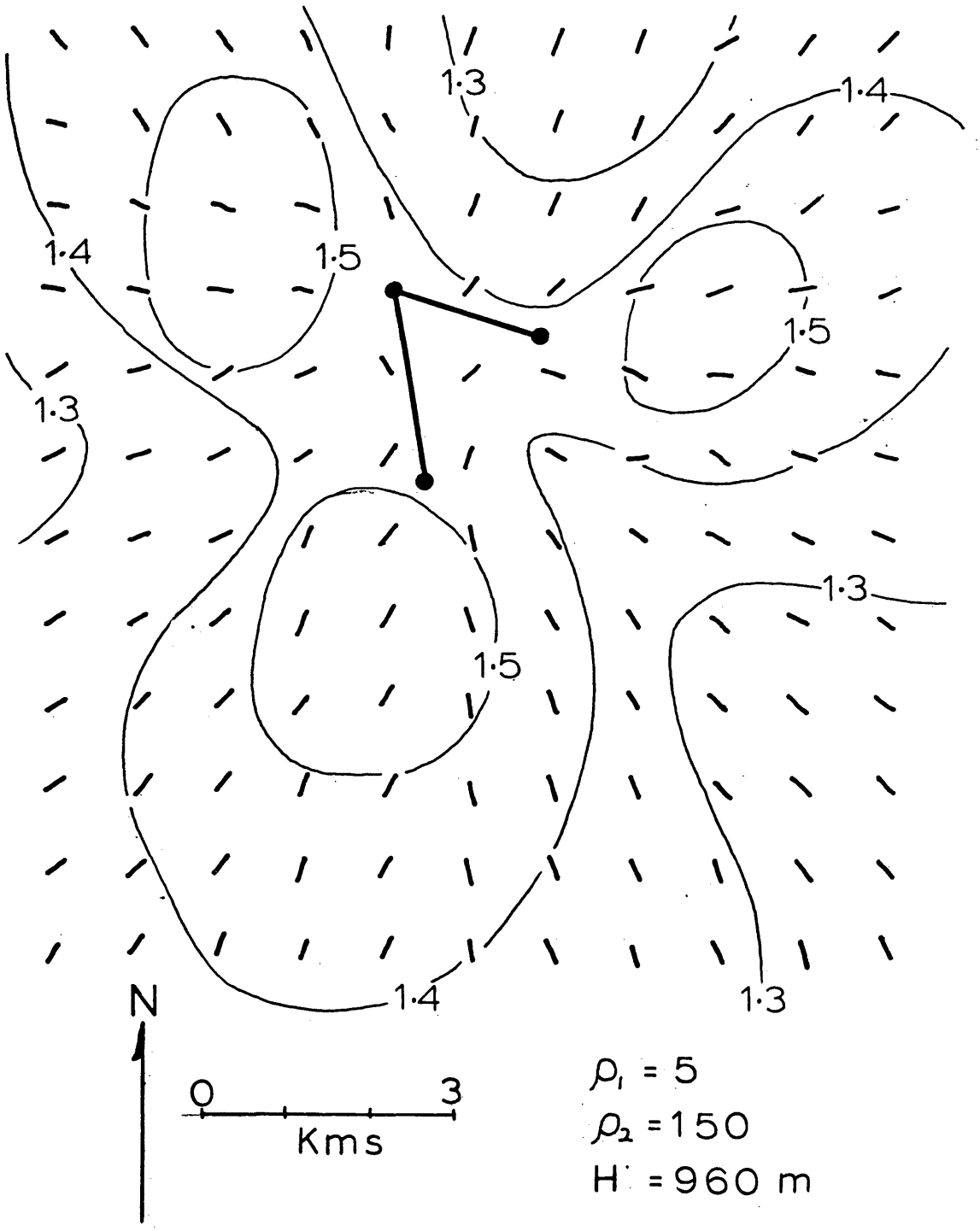

Figure 30. Calculated ellipticities and bearings of ρ_{min} for theoretical two layer model.

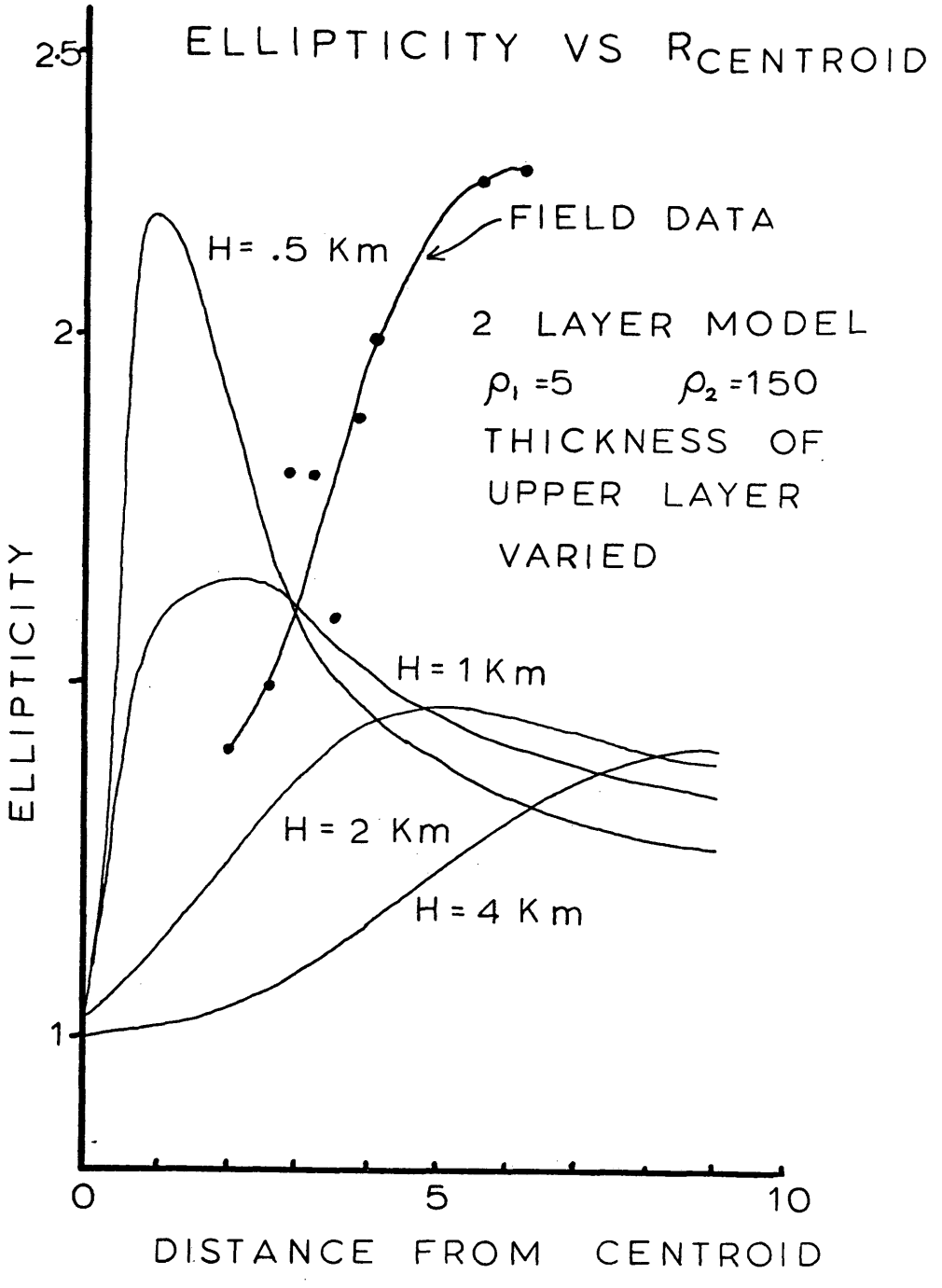

Figure 31. Ellipticity versus receiver separation from centroid for field results and theoretical models.

Interpretation of the Third Pair of Sources

The third pair of sources (3A and 3B) was located in the southwest corner of Hualapai Flat (figure 32). Attempts to model Hualapai Flat as a conductive region bounded by two resistive regions, the Granite Range and the Steamboat ridge, were failures. The geologic structure, known and inferred, is too complex to be represented by simple models, resulting in little correspondence with the results of the survey. In spite of the failure to model this section of Hualapai, it was still possible to interpret the quadripole results and explain the difficulties in modelling.

The source 3A apparent resistivities are shown in figure 33. No longer is there a prominent conductive anomaly, with a northwest trend in the Hualapai playa as there was from source 1A. Only five stations (313-317) had resistivities less than 30 Ω-m , but they were located in the position of the anomaly found from source 1A. The 100 high north of the source (stations 371-374) is located near a prominent outcrop of Permian metavolcanics and is caused by thinning of the alluvium and the presence of this more resistive outcrop. Beyond this outcrop, the resistivities drop rapidly to below 50 Ω-m (stations 356-361) in proximity to the Fly Ranch hot springs, and possibly caused by thickening of alluvium. The high resistivities (30 Ω-m) measured near the source indicate that the depth to basement is small,

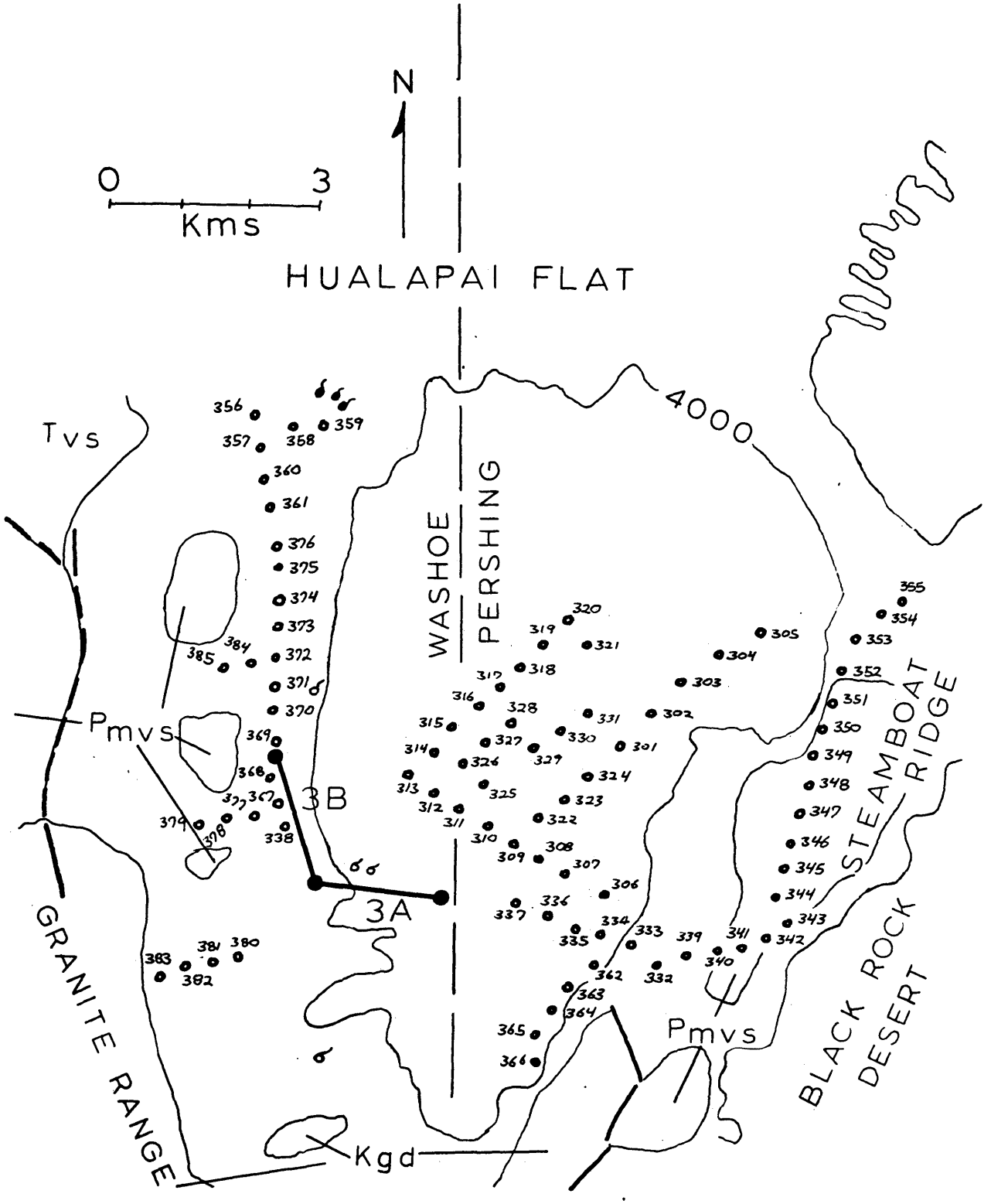

Figure 32. Location of sources 3A and 3B and receiver stations.

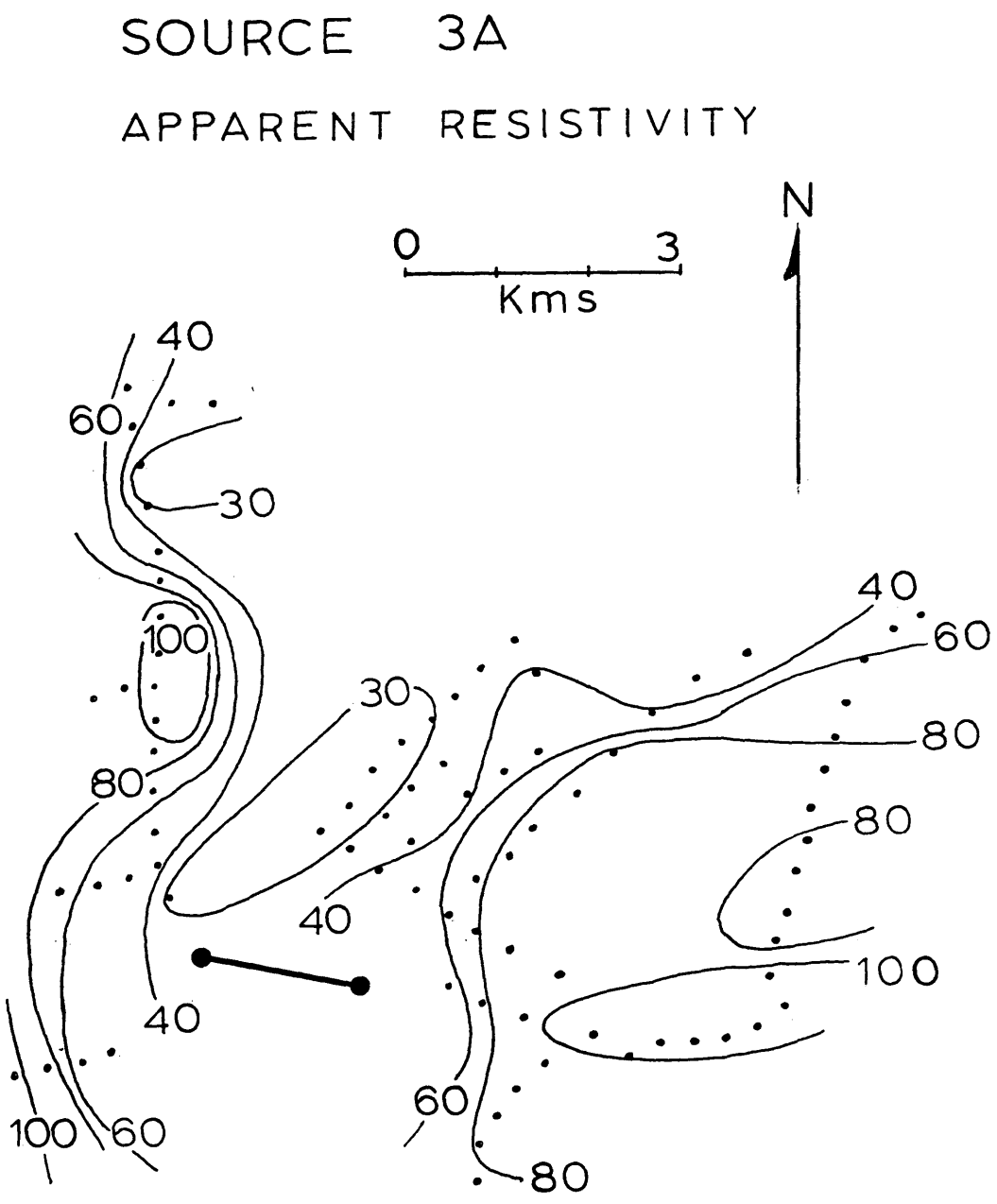

Figure 33. Apparent resistivities for source 3A.

assuming the resistivity of the alluvium is not much above 5 Ω-m . The closest receiver stations were about a kilometer from a source electrode or enough so that the high resistivities are an indication of resistive basement at shallow depth. It is also possible that these high apparent resistivities are due to the alluvium in this section of Hualapai having a higher resistivity due to a low water table and that resistive basement (if any) is not near the surface.

The apparent resistivities from source 3B are shown in figure 34. High resistivities are seen north of source 3A but because the source is now closer, the resistivities are usually less than 100 Ω-m . The stations in the Hualapai playa (301-331) form an equatorial (broadside) array with source 3B. Selecting stations so that they form a traverse perpendicular to source 3B, a plot of apparent resistivities versus spacing shows an increase with separation from the source, an effect of resistive basement. However, a north-south traverse parallel to the source will have lower resistivities in the northern end than in the southern part. This asymmetry suggests that the alluvium is thicker toward the north than in the south, supporting the conclusions drawn from the results of the second pair of sources.

The average resistivities (figure 35) confirm the single source interpretations. The metavolcanic outcrop north of the sources forms a resistivity high and the decrease in

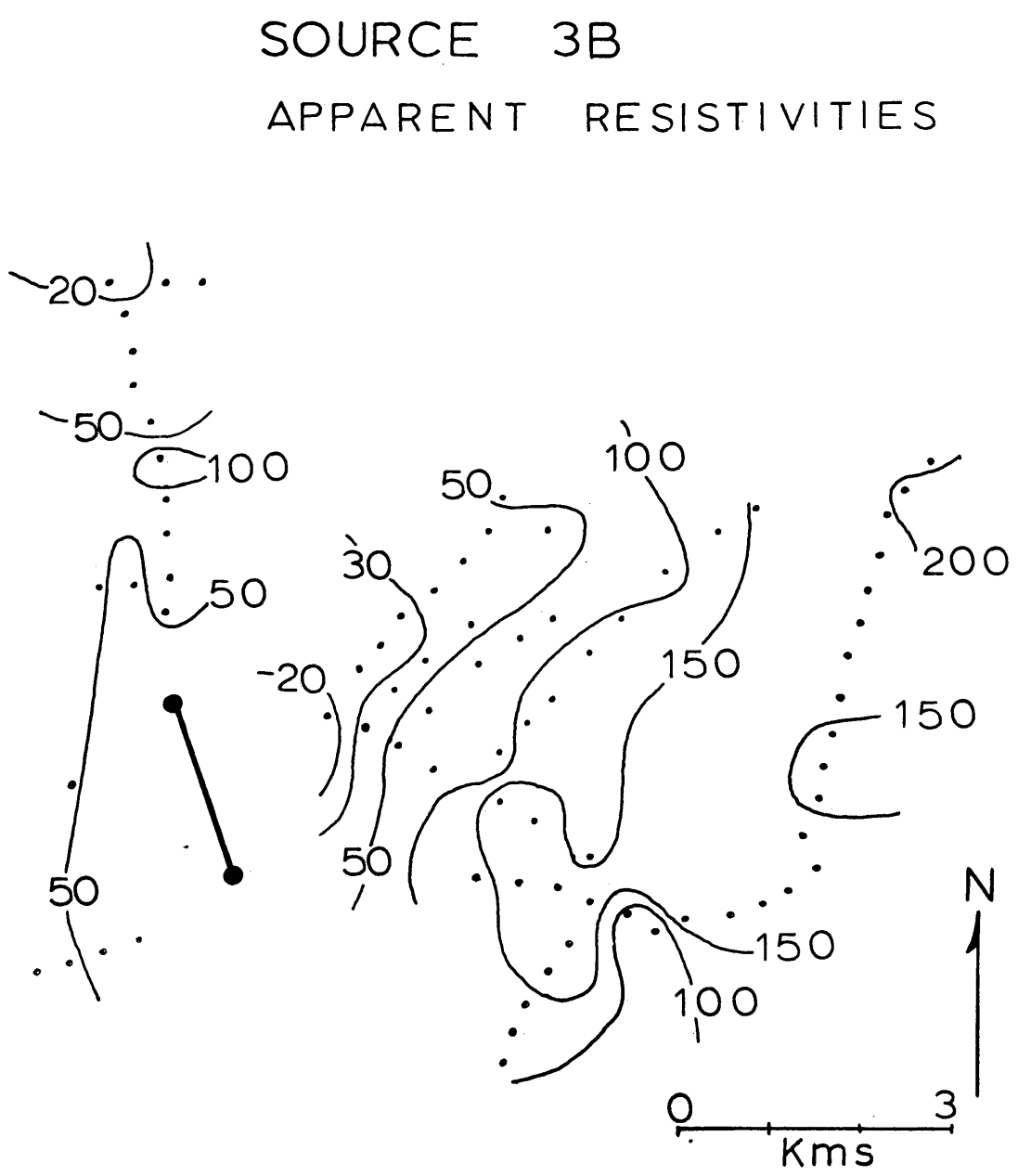

Figure 34. Apparent resistivities for source 3B.

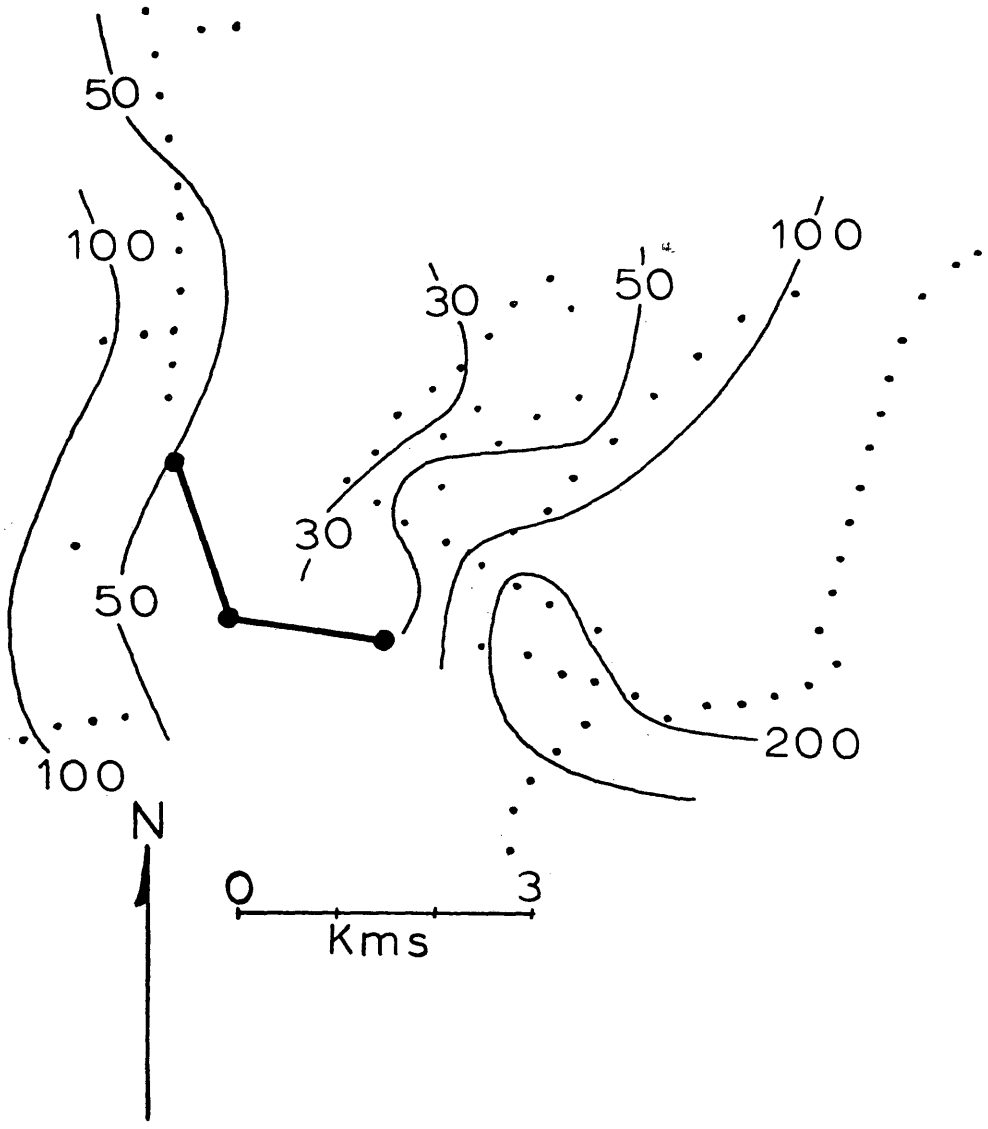

Figure 35. Average resistivities for sources 3A and 3B.

resistivities further to the north is not a false anomaly, but appears to be associated with the Fly Ranch hot springs. The northeast-southwest resistivity trends in Hualapai seem to be due to variations in the thickness of alluvium, the basement being closer to the surface in the southeast corner. Because of poor coverage, the eastern extent of the Permian metavolcanic outcrop cannot be determined, but it may extend a kilometer beyond Rt. 34 into Hualapai.

The resistivity ellipticities and bearing of ρ_{min} map (figure 36) indicates that the lateral resistivity changes (the Granite Range and the Steamboat ridge) do not show an appreciable effect. The bearings of ρ_{min} are generally toward the centroid of the sources, indicative that vertical resistivity variations are predominant. The stations along the Steamboat ridge also follow this pattern confirming the observation from the first pair of sources; that is, that they are in the Hualapai basin and not in the levee, geoelectrically.

The ellipticities also confirm the predominance of vertical resistivity changes over lateral effects. Generally, the values decrease with distance from the sources which was a feature of the two layer case but a trend present in the other models when there were no near lateral variations in resistivity. The ellipticity high (>3) that was noted in the Hualapai palya (figure 36) is similar to the ellipticity

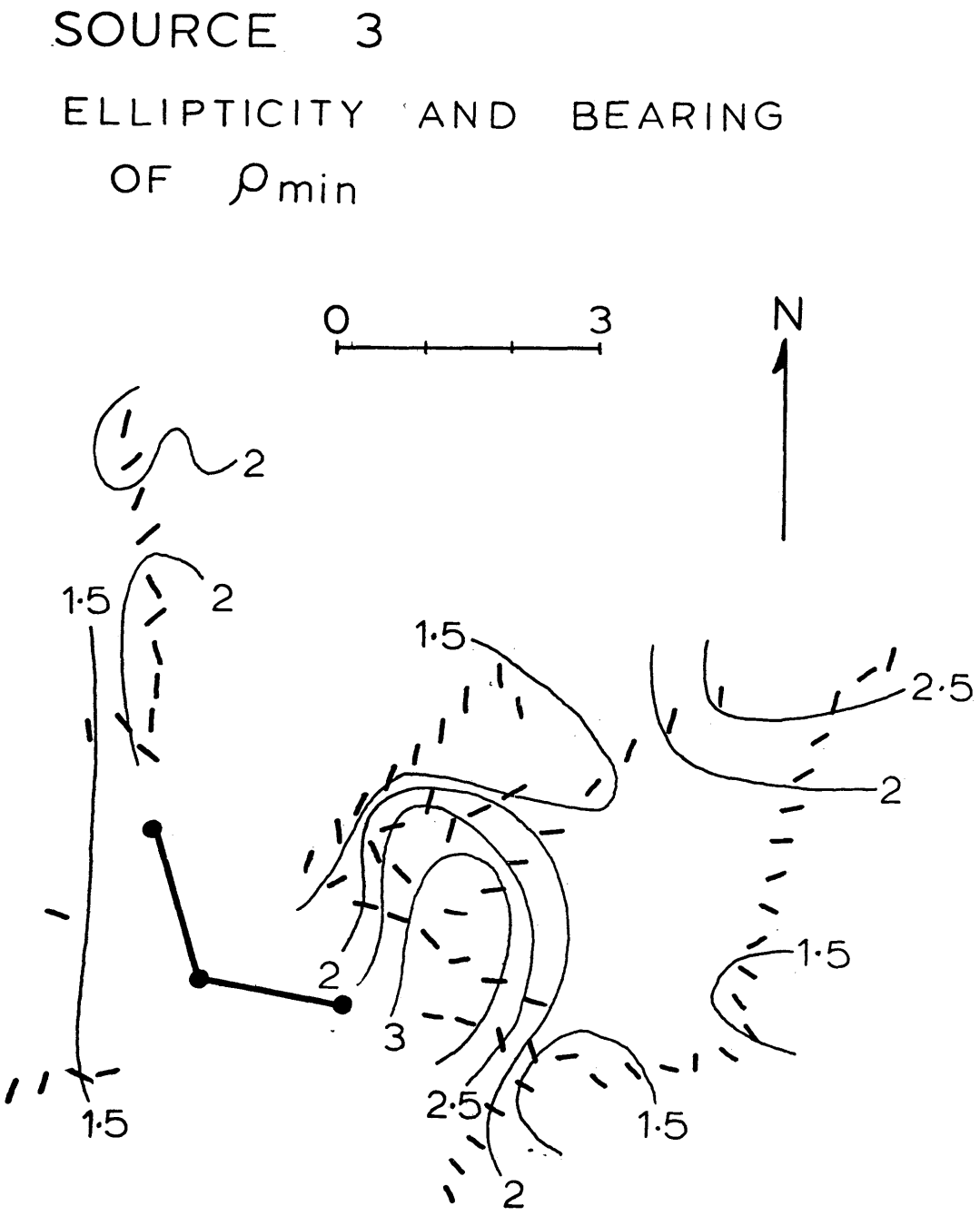

Figure 36. Ellipticities and bearings of ρ_{min} for sources 3A and 3B.

highs formed off the ends of the sources in the two layer case (figure 30), although resistive basement cannot be shown to be the unique cause. The Fly Ranch hot springs are not associated with anomalous resistivity ellipticity or bearing of ρ_{min} patterns although this could be because the geothermal system is deep (> 2 km) and could not be detected when the sources are this close.

SUMMARY AND CONCLUSIONS

The general trend of the basement surface was determined from the quadripole results. The alluvium in Hualapai Flat is thickest north of the Fly Ranch hot springs near sources 2A and 2B. Depths to basement of 3000 feet are possible, placing the basement elevation at 1100 feet. The alluvium thins to the south and southeast to thicknesses less than 1000 feet. The resistivities near the sources 3A and 3B indicated the effects of shallow basement and by comparing the results from the first pair of sources with the theoretical models, a depth of 1000 feet in the eastern edge of Hualapai near the levee was found to be a more likely answer. This would put the elevation of the basement in the southern part of Hualapai at 3100 feet above sea level.

There is a series of springs along the western side of Hualapai Flat that lie in a north-south trend about a kilometer east of Rt. 34. The Fly Ranch hot springs make up the northern end and cold springs, near the Holland Granite Creek Ranch make up the southern end. Between the extremes are the springs at Holland Fly Ranch and some seeps near the common electrode of sources 3A and 3B. The resistive outcrop of Permian metavolcanics, north of the third pair of sources, could be a fault block that is terminated sharply on its northern end near the Fly Ranch hot springs. If so, then this

linear trend of springs could represent the eastern margin of this fault block. However, because of the gap in stations between Hualapai and Rt. 34, the eastern margin cannot be located precisely. During a microseismicity survey (Carlson, 1975) there were no earthquakes recorded whose epicenters would lie along this trend.

The elevation of the basement surface and outlines of major subsurface structural trends are presented in figure 37 along with the previous geophysical data. Cross sections along lines indicated on this map are shown in figure 38. The faults shown in the cross sections are hypothetical, however, the sharp decrease in resistivities north of sources 3A and 3B and the thickening of alluvium to the north near sources 2A and 2B, suggest that block faulting in the basement is responsible. These cross sections should not be considered final and cannot be confirmed until soundings (TDEM or Schlumberger) or seismic reflection/refraction studies are made.

The existence of the low resistivities (10 Ω-m) around the second pair of sources contradicts Harrill's (1969) statement that the Hualapai alluvium is nowhere deeper than 1000 feet. The electrical data indicate that the depth to basement is much greater than 1000 feet in this portion of Hualapai and is closer to 3000 feet. The drillers' report of "basement" at 350 at Fly Ranch hot springs or 450 feet

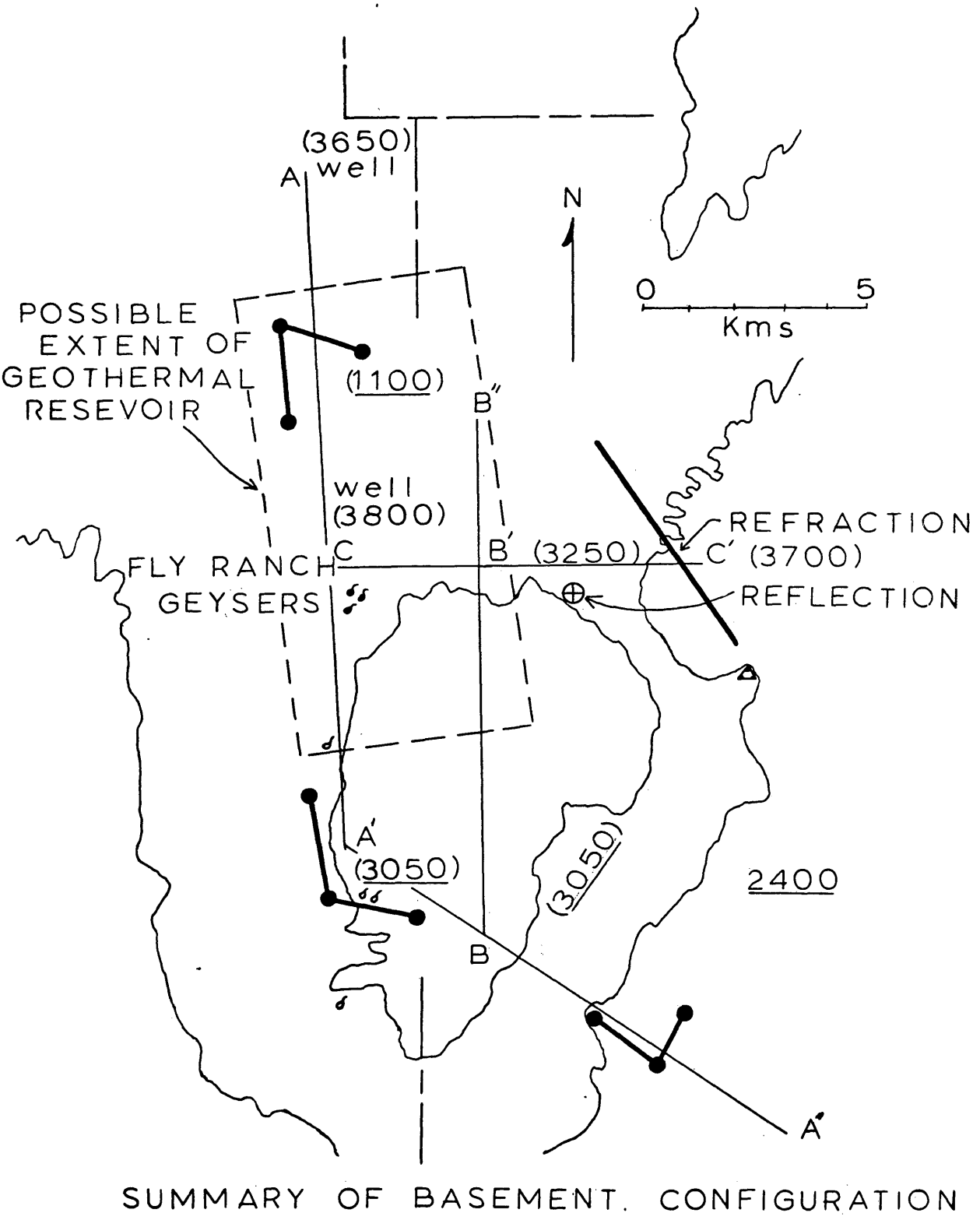

Figure 37. Location of previous seismic work and configuration of basement results.

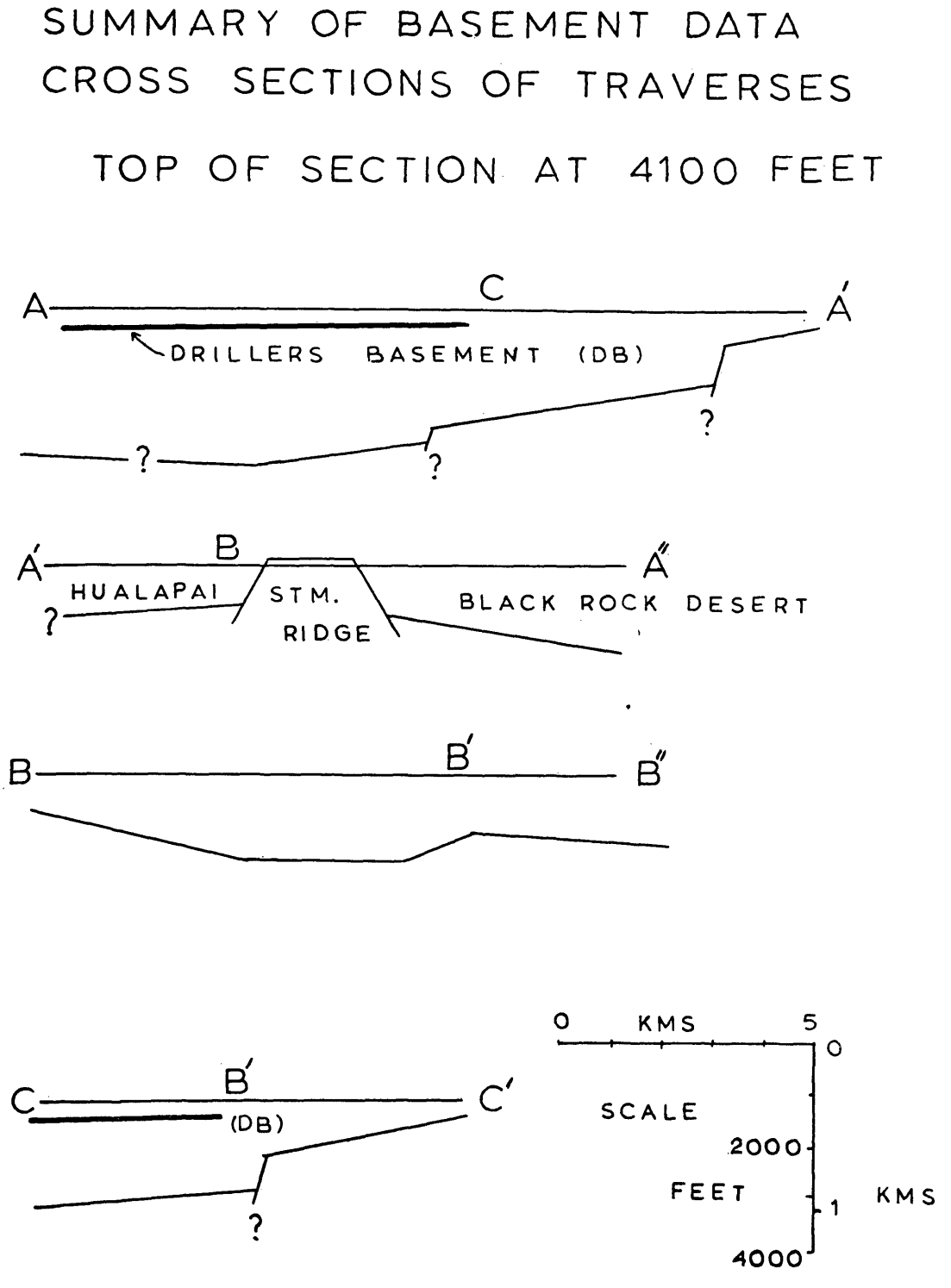

Figure 38. Cross sections of basement surface as determined from well data, previous seismic work and this study.

further north suggests that there is a caprock or impermeable layer that divides the alluvium. If this is the case then there could be two geohydrologic systems, an upper meteoric fresh water system and a lower system which may be thermal and saline. This hypothesis is supported by the difference in the chemistry of water from deep wells and shallow wells. The shallow wells and warm seeps do not form sinter or calcium carbonate deposits while the deeper wells have a tendency to precipitate these solids.

The anomaly in Hualapai Flat from source 1A is considered to be a false anomaly, but in light of the third pair of sources, there could be a small anomaly with a southeast trend of geothermal origin from the hot springs as the microseismicity and groundnoise studies indicate (Carlson, 1975). If the geothermal system is deep (> 2 km) then to see this, large separation between the source and receiver stations is necessary. This was the case with source 1A, when the conductive anomaly was six kilometers from the center of the source. Sources 3A and 3B got progressively closer to the anomaly and did not get enough depth penetration to see the anomaly, even though receiver stations were as far as 10 km from the centroid of the sources. For the case of a resistive basement, the resistivities should rise along a line of slope one when plotted on a log-log graph as a function of separation from the source. This was not the case for the

results from the third pair of sources, indicating that a possible conductive zone at depth will result in slower, if any, increases in resistivity with distance.

The nature of the basement rocks cannot be determined from the quadripole results. They may be Tertiary volcanics or Paleozoic metasediments and metavolcanics, but the results from the second pair of sources indicate that the basement rocks have resistivities over 100 Ω-m , so that they may also be Cretaceous granodiorite.

Even though the Fly Ranch hot springs are not associated with a large resistivity anomaly, the prospect should not be written off. Assuming an average alluvial thickness of 500 meters in an area 10 km by 5 km (figure 37), the colume of the geothermal system reservior is about 25 cubic kilometers, which would make the Fly Ranch prospect economically feasible if high (> 200°C) temperatures are present in the alluvium.

However if high temperatures are not present in the alluvium then it will be necessary to drill into the basement perhaps several kilometers. Besides being expensive, a geothermal system in granitic basement would only be possible if extensive fracturing to increase permeability is present.

In figure 39, the values of ρ_{ave} for all five pair of sources have been plotted and contoured. Some of the receiver stations were occupied for two or more pairs of sources, so the average of the average resistivities was used. The Black

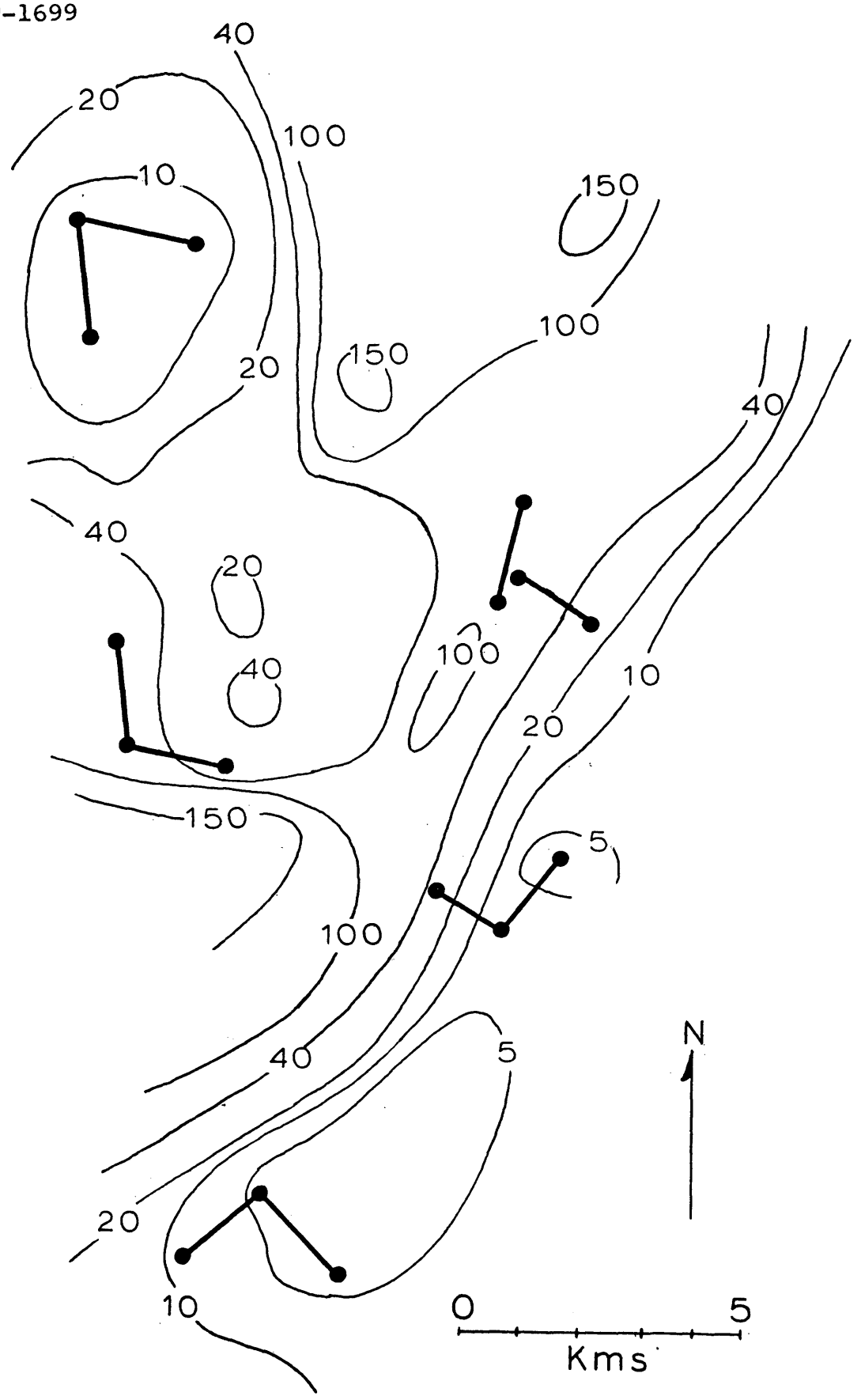

Figure 39. Compilation of average resistivity results from all five pairs of sources.

● GERLACH

Rock Desert is characterized by average resistivities under 10 Ω-m and these values decreased away from the Granite Range and Steamboat ridge. The lowest resistivities were observed in Hualapai Flat around the second pair of sources (10 Ω-m) with higher values being observed in all directions. The Granite Range and the Calico Mountains are represented by higher resistivities, as was the Steamboat ridge which separates the Black Rock Desert from Hualapai Flat. If coverage had been extneded beyond the second pair of sources to the north, the low resistivities of the northern part of Hualapai should end at the base of the foothills, making the Hualapai area a conductive anomaly in more resistive surrounding rocks.

Quadripole mapping offers significant improvements over conventional single source techniques. The ellipticities and bearings of ρ_{min} can help distinguish between vertical resistivity changes and lateral changes. Given some geologic control, it is possible to develop models that will match the field results. However, models with analytic expressions for the potential are simple and few which will necessitate the use of resistor network modelling (Pires, 1975) or finite difference methods to study regions of complex geology.

APPENDIX A

This appendix contains the resistivity data (single source and quadripole) from the three pair of sources that are used in this study.

STA	:	The station number whose location can be found in figures 12, 21, and 32.
ρ_1	:	The apparent resistivity measured from just the A source. (ohm-m)
ρ_2	:	The apparent resistivity measured from just the B source. (ohm-m)
ρ_{ave}	:	The average resistivity found by using both the A and B sources. (ohm-m)
r	:	Ellipticity of the resistivity ellipses.
θ_{min}	:	Bearing of the minor axis for each resistivity ellipse. (degrees)

STA	ρ_1	ρ_2	ρ_{ave}	ϵ_r	θ_{min}
101	4.47	3.92	4.16	1.1	35.
102	7.72	5.44	6.47	1.8	170.
103	8.44	9.43	12.56	3.4	140.
104	9.88	5.91	263.11	14.5	150.
105	15.98	7.48	17.58	4.8	175.
106	18.72	3.52	16.88	4.1	25.
107	11.07	3.58	4.61	6.7	170.
108	11.70	2.32	0.30	4.9	0.
109	6.24	1.17	4.17	3.0	20.
111	16.78	20.59	17.47	2.5	110.
112	73.58	24.03	47.73	2.4	60.
113	93.45	30.07	54.24	3.1	80.
114	71.34	37.65	51.55	2.4	90.
115	52.39	34.43	44.18	1.3	60.
116	55.60	33.65	42.85	2.3	85.
117	51.73	24.87	33.90	2.9	75.
118	35.74				
119	32.22				
120	32.67				
121	25.63				
122	33.49				
123	35.49				
124	38.47				
125	40.91				

STA	ρ_1	ρ_2	ρ_{ave}	ϵ_r	θ_{min}
127		23.53			
128	20.32	16.49	17.53	1.6	135.
129		19.83			
130		21.21			
131	30.97	24.09	27.84	1.3	160.
132	33.11				
133	29.45				
134	27.15				
137	69.85	15.49	45.29	2.9	55.
138	123.30	27.35	72.41	9.7	65.
139	99.70	19.91	55.51	3.6	30.
140	45.97	11.24	30.16	2.7	40.
141	62.73	21.75	38.80	2.1	50.
142	69.31	17.87	47.44	2.1	50.
143	44.27	25.80	38.00	2.2	80.
144	47.73	13.58	34.13	2.2	55.
145	41.57	17.65	33.39	2.1	70.
146	33.96	18.89	27.93	3.5	65.
147	55.33	29.51	40.52	4.2	75.
148	60.48				
149	45.81	74.89	66.95	1.4	150.
150	54.05				
151	84.93				
152	91.99	18.82	35.53	4.9	90.
153	90.20	33.25	62.11	2.6	115.

STA	ρ_1	ρ_2	ρ_{ave}	ϵ_r	θ_{min}
154	97.79	16.63	26.61	4.8	140.
155	114.28	27.71	62.77	3.5	135.
156	70.81	19.78	39.87	3.7	160.
157	68.42	32.38	44.37	2.5	145.
158	69.63	10.36	38.63	3.1	110.
159	51.65	13.19	32.11	2.0	125.
160	76.16	8.28	39.99	3.0	130.
161	83.51	12.99	46.26	2.7	130.
162	114.71	11.88	60.76	3.1	120.
163	127.60	11.24	66.83	3.7	90.
164	144.25	10.19	6.84	4.8	45.
165	106.06	24.06	64.20	2.2	145.
166	144.84	26.82	18.25	5.2	160.
167	120.93	47.22	69.69	2.5	175.
168	65.16	19.59	44.60	3.2	50.
169	43.67	12.06	22.36	5.2	65.
170	36.50	12.50	3.62	4.9	65.
171	98.34	20.05	47.33	3.5	155.
172	152.28	30.76	85.52	2.9	160.
173	122.41	25.80	64.95	4.2	170.
174	124.66	34.55	69.05	3.0	170.
175	10.78	1.36	12.45	4.2	10.
176	9.11	1.03	7.66	4.0	5.
177	6.12	0.91	4.05	2.9	10.

STA	ρ_1	ρ_2	ρ_{ave}	ϵ_r	θ_{min}
178	4.61	0.88	3.01	2.4	15.
179	2.42	1.44	2.13	1.9	75.
180	2.07	1.59	1.93	1.7	80.
181	2.18	2.02	2.06	2.1	90.
182	22.85	1.82	10.90	3.8	10.
183	24.69	2.22	15.40	3.6	10.
184	5.53	4.34	3.86	1.6	65.
185	4.21	8.25	6.14	2.0	95.
186	8.20	6.47	16.82	2.2	25.
187	4.97	1.76	3.77	1.8	30.
188	2.86	2.01	2.91	1.4	15.
189	4.03	1.41	3.18	2.1	165.
190	2.14	2.61	3.86	2.1	40.
191	2.44	1.74	3.19	1.8	5.
192	2.09	2.42	3.98	1.9	45.
193	1.75	2.05	3.52	2.1	25.
194	2.32	2.19	3.80	1.9	25.
195	2.17	4.07	6.81	2.3	45.
196	1.91	2.89	4.24	1.9	5.
197	1.59	2.74	3.52	1.9	175.

STA	ρ_1	ρ_2	ρ_{ave}	ϵ_r	θ_{min}
201	7.39	14.63	11.01	1.4	175.
202	5.33	17.42	11.37	1.8	5.
203	6.54	18.01	11.72	1.8	145.
204	8.90	22.36	15.85	1.6	175.
205	7.11	23.31	15.15	1.9	175.
206	4.27	32.66	18.48	2.9	5.
207	7.77	46.49	28.40	2.5	40.
208	9.35	31.23	20.23	1.9	5.
209	8.51	42.26	25.74	2.3	10.
210	10.88	53.78	32.50	2.4	10.
211	7.52	14.03	9.67	1.6	50.
212	8.14	14.64	9.77	1.8	60.
213	10.95	11.48	9.74	1.5	50.
214	9.05	9.68	8.03	1.6	70.
215	14.76	10.95	10.04	2.1	70.
216	15.44	10.62	10.62	1.9	60.
217	20.30	8.48	11.77	2.6	55.
218	7.14	8.81	5.78	1.9	70.
219	9.00	7.26	7.29	1.3	95.
220	9.34	5.03	11.50	2.0	110.
221	6.17	4.69	6.69	1.6	140.
222	6.49	3.52	9.53	2.2	140.
223	8.82	5.12	12.37	2.0	145.
224	7.80	5.89	11.14	1.7	130.

STA	ρ_1	ρ_2	ρ_{ave}	ϵ_r	θ_{min}
225	8.30	5.38	16.42	2.5	140.
226	8.34	18.15	14.55	2.0	165.
227	6.66	21.19	14.93	2.0	170.
228	6.71	25.31	17.37	2.2	175.
229	14.88	23.15	19.23	2.5	25.
230	11.11	39.75	27.50	2.9	10.
231	16.73	36.72	25.36	1.6	15.
232	15.68	51.50	32.49	6.0	25.
233	5.85	17.93	11.73	2.1	20.
234	6.74	16.18	11.65	1.6	160.
235	9.03	15.04	12.22	1.5	160.
236	9.43	16.85	13.53	1.6	145.
237	8.79	14.45	12.19	1.6	140.
238	9.91	12.55	11.92	1.6	135.
239	12.01	12.79	13.23	1.8	130.
240	13.47	12.20	14.10	1.8	140.
241	12.47	14.60	15.33	1.5	135.
242	15.07	12.85	15.92	1.8	140.
243	12.03	16.01	15.67	2.6	150.
244	15.30	9.33	14.23	1.5	175.
245	18.13	10.20	17.25	2.3	145.
246	24.04	16.09	24.31	1.6	125.
247	16.30	20.64	21.19	2.7	150.
248	11.23	10.06	14.15	1.4	40.

STA	ρ_1	ρ_2	ρ_{ave}	ϵ_r	θ_{min}
249	4.89	7.86	10.26	2.2	130.
250	8.03	7.76	16.00	1.9	15.
251	5.23	9.40	15.11	2.2	0.
252	5.13	11.09	14.70	2.2	170.
253	6.89	12.57	17.49	2.1	0.
254	9.91	14.99	21.16	2.0	15.
255	9.35	19.70	23.75	2.3	10.
256		12.50			
257	5.30	6.64	8.19	1.5	25.
258	5.67	9.69	8.43	1.5	10.
259	5.75	8.57	8.00	1.4	10.
260	5.23	8.17	7.13	1.4	10.
261	5.70	6.56	5.65	1.2	170.
262	6.17	10.08	8.77	1.4	25.
263	8.15	10.42	8.02	1.4	0.
264	9.15	11.00	8.50	1.6	10.
265	8.48	12.55	9.79	1.5	20.
266	13.64	15.89	14.23	1.4	25.
267	11.83	16.87	13.49	1.8	45.
268	14.77	20.92	16.54	2.1	50.
269	12.19	13.97	12.82	1.6	45.
270	13.48	14.20	13.50	1.7	50.
271	12.07	9.62	10.57	1.9	50.
272	10.74	12.90	9.79	2.2	25.

STA	ρ_1	ρ_2	ρ_{ave}	ϵ_r	θ_{min}
273	10.28	12.44	10.59	1.6	35.
274	7.31	10.86	6.75	2.2	25.
275	8.93	9.09	6.96	1.4	120.
276	6.20	7.66	6.44	1.3	0.
277	6.80	7.64	6.85	1.1	20.
279	8.90	8.23	8.33	1.5	50.
280	13.40	7.89	10.59	1.7	45.
281		7.76			
282	12.18	5.80	9.04	1.8	55.
283	11.92	5.14	8.72	1.6	45.
284	7.83	6.11	5.46	1.9	25.
285	9.06	10.55	9.44	1.1	80.
286	8.68	9.81	8.47	1.2	80.
287	11.26	11.50	11.64	1.0	135.
288	13.23	9.42	10.29	1.4	70.
289	17.25	4.38	11.26	2.1	90.
290	17.63	4.81	11.46	2.0	90.
291	18.99	4.56	11.81	2.1	90.
292	13.51	4.64	9.11	1.9	85.
293	12.77	5.53	8.77	1.7	100.
294	14.37	4.27	8.60	2.3	110.
295	7.43	6.51	1.97	4.7	85.
296	10.90	3.77	7.26	1.8	105.
297	17.31	4.75	10.80	2.0	105.

STA	ρ_1	ρ_2	ρ_{ave}	ϵ_r	θ_{min}
298	19.73	4.89	12.25	2.0	95.
299	18.77	5.13	11.90	1.9	100.
2100	16.11	5.03	9.49	2.5	110.
2101	14.17	7.54	2.37	4.7	50.
2102	21.33	13.52	16.35	2.6	10.
2103	12.70	9.33	11.27	1.6	120.
2104	13.48	8.32	11.12	2.0	110.
2105	11.05	9.14	10.23	1.4	120.

STA	ρ_1	ρ_2	ρ_{ave}	ϵ_r	θ_{min}
301	71.10	108.29	81.70	1.6	70.
302	92.38	109.61	106.86	1.1	35.
303	29.25	73.20	59.74	1.8	10.
304	31.03	106.23	79.31	2.0	10.
305	31.35	165.05	109.06	2.9	0.
306	80.71	145.80	147.03	2.0	100.
307	76.25	154.83	206.56	2.6	100.
308	73.53	155.79	304.44	4.6	95.
309	53.77	116.00	126.77	6.5	110.
310	48.89	83.49	89.38	3.6	105.
311	43.72	56.99	45.30	1.5	100.
312	35.74	44.55	32.77	1.5	75.
313	20.33	17.29	15.81	1.3	30.
314	25.08	22.17	29.58	1.5	170.
315	25.63	22.76	21.17	1.5	60.
316	27.89	24.54	17.73	1.9	40.
317	27.57	34.17	25.89	1.4	15.
318	33.67	40.23	33.34	1.2	5.
319	39.39	44.52	39.54	1.1	5.
320	34.19	54.29	43.63	1.3	170.
321	58.47	31.56	42.86	1.5	155.
322	64.33	99.46	88.80	4.1	95.
323	78.26	147.41	140.26	2.8	85.
324	57.16	128.36	109.88	2.5	70.

STA	ρ_1	ρ_2	ρ_{ave}	ϵ_r	θ_{min}
325	55.08	48.64		6.6	135.
326	35.14	36.05	109.65	2.3	140.
327	36.64	40.77	20.05	5.8	55.
328	36.90	46.51	29.90	2.0	40.
329	35.04	58.59	98.93	2.9	30.
330	46.22	65.95	37.26	2.8	65.
331	43.72	53.73	41.54	1.4	50.
332	61.73	76.49	88.33	1.4	120.
333	98.16	67.22	96.64	1.5	80.
334	139.89	197.14	167.36	1.6	135.
335	92.28	249.18	200.03	3.5	135.
336	49.98	187.40	240.91	3.2	105.
337	44.13	134.19	191.84	3.1	120.
338	24.47				
339	86.66	121.22	130.72	1.4	140.
340	145.15	170.22	238.11	1.6	105.
341	80.98	147.16	101.97	2.5	170.
342	95.95	202.54	215.34	1.9	120.
343	121.20	185.33	174.39	1.5	130.
344	132.92	189.46	156.36	1.4	140.
345	58.18	73.27	65.54	1.2	120.
346	61.17	113.15	140.38	2.2	65.
347	53.77	135.96	123.61	1.9	95.
348	75.64	170.57	168.85	1.9	65.

STA	ρ_1	ρ_2	ρ_{ave}	ϵ_r	θ_{min}
349	97.64	203.68	174.92	1.6	85.
350	92.63	169.41	139.02	1.5	60.
351	57.38	299.75	224.43	2.7	40.
352	64.33	182.85	150.78	2.1	45.
353	67.62	243.24	183.56	2.3	20.
354	49.12	279.37	185.93	2.6	40.
355	44.39	175.77	118.10	3.1	25.
356	56.92	20.20	46.34	2.2	15.
357	46.11	24.38	58.76	3.4	30.
358	28.46	29.73	36.60	1.3	25.
359	33.57	30.14	47.56	2.9	45.
360	18.44	25.58	32.28	1.6	20.
361	20.80	28.04	44.17	2.8	35.
362	68.76	201.97	221.63	2.4	130.
363	95.97	208.89	246.36	2.1	135.
364	119.66	108.70	181.03	2.1	110.
365	83.75	107.86	127.70	1.6	145.
366	64.98	134.59	129.77	1.8	160.
367	45.17				
368	45.44				
369	66.58				
370	83.12				
371	102.48	84.51	86.01	1.7	130.
372	112.89	71.68	149.35	1.9	0.

STA	ρ_1	ρ_2	ρ_{ave}	ϵ_r	θ_{min}
373	120.80	91.20	119.31	1.5	0.
374	109.92	95.84	101.27	1.2	170.
375	47.94	113.19	95.07	2.7	40.
376	31.38	26.31	43.04	1.6	140.
377	45.87				
378	48.91				
379	75.04	86.96	78.71	1.2	100.
380	43.68	36.27	65.57	1.6	75.
381	49.42	45.68	71.59	1.5	115.
382	81.74	111.87	98.85	1.3	25.
383	120.45	151.65	132.63	1.2	15.
384	56.35	24.44	54.91	2.6	140.
385	77.98	73.56	103.64	1.4	165.

REFERENCES

Alpin, L. M., 1966, The Theory of Dipole Sounding, in Dipole Methods for Measuring Earth Conductivity: Consultants Bureau, N.Y., N.Y., p.1-60.

Bibby, H. M., and Risk, G. F., 1973, Interpretation of Dipole-dipole Resistivity Surveys Using a Hemisperoidal Model: Geophysics, vol. 38, no. 4, p.719-736.

Bonham, H. F., 1969, Geology and Mineral Deposits of Washoe and Storey Counties: Bulletin 70, Nevada Bureau of Mines, Reno, Nevada.

Carlson, K., 1975, Microseismicity and Ground Noise Studies in Hualapai Flat, northwest Nevada: M. Sc. Thesis, Colorado School of Mines, Golden, Colorado.

Crewdson, R., 1975, Written Communication.

Furgerson, R. B., 1970, A Controlled Source Telluric Current Technique and its Application to Structural Investigations: M. Sc. Thesis T-1313, Colorado School of Mines, Golden, Colorado.

Furgerson, R. B., and Keller, G. V., 1974, Computed Dipole Resistivity Effects for an Earth Model with Vertical and Lateral Contrasts in Resistivity: Technical Report to the Office of Naval Research, 12 March, 194 pp.

Furgerson, R. B., 1975, The Rotating Dipole Method: Ph. D. Thesis, Colordao School of Mines, Golden, Colorado.

Harrill, J. R., 1969, Hydrologic Response to Irrigation Pumping in Hualapai Flat, Washoe, Pershing and Humboldt Counties, Nevada, 1960-1967: Water Resources Bulletin No. 37, Division of Water Resources, Nevada Dept. of Conservation and Natural Resources, Reno, Nevada.

Jordan, J. M., 1974, Geothermal Investigations in the San Luis Valley, South-Central Colorado: M. Sc. Thesis T-1478, Colorado School of Mines, Golden, Colorado.

Keller, G. V., 1966a, Dipole Method for Deep Resistivity Studies: Geophysics, vol. 31, no. 6, p.1088-1104.

Keller, G. V., 1966b, Electrical Properties of Rocks and Minerals: in Handbook of Physical Constants, edited by S. P. Clark, Memoir 97, Geological Society of America, Boulder, Colorado.

Keller, G. V., and Frischknecht, F. C., 1966, Electrical Methods in Geophysical Prospecting, Pergamon Press, New York.

Keller, G. V., Furgerson, R. B., Lee, C. Y., Harthill, N., and Jacobson, J. J., 1975, The Dipole Mapping Method: Geophysics, in press.

Lee, C. Y., 1973, The Dipping Layer Problem in Resistivity: M. Sc. Thesis T-1610, Colorado School of Mines, Golden, Colorado.

McGinnis, L. D., and Dudley, W. W., 1964, Seismic Studies of Three Areas in Northern Nevada, in Geophysical Studies in Nevada Relating to Hydrology: Technical Report No. 2, Desert Research Institute, University of Nevada, Reno, Nevada, p.31-33.

Ofrey, O., 1975, Time Domain Electromagnetic Soundings in the Black Rock Desert, Northwest Nevada: M. Sc. Thesis, Colorado School of Mines, Golden, Colorado.

Pires, A. C., 1975, Resistor Network Modelling of Dipole Mapping Surveys: Ph. D. Thesis, Colorado School of Mines, Golden, Colorado.

Risk, G. F., Macdonald, W., and Dawson, G., 1970, D. C. Resistivity Surveys of the Broadlands Geothermal Region, New Zealand: Geothermics, Special Issue 2, vol. 2, part 1.

Stanley, W. D., Jackson, D. B., and Hearn, B. C., 1973, Preliminary results of Geoelectrical Investigations near Clear Lake, California: U.S. Geological Survey open file report.

Tasci, M. Tahsin, 1975, Geophysical Exploration in a Geothermal Prospect Lualualei, Oahu, Hawaii: M. Sc. Thesis, Colorado School of Mines, Golden, Colorado.

Tatlock, D. B., 1971, Preliminary Geologic Map of Pershing County: U.S. Geological Survey open file report.

Van Nostrand, R. G., and Cook, K. L., 1966, Interpretation of Resistivity Data: U.S. Geological Survey Prof. Paper 499.

Vedrintsev, G. A., 1966, Problems in Conducting and Interpreting Electrical Sounding Surveys in an Area Where There is Sharp Relief in the Basement Surface, in Dipole Methods for Measuring Earth Conductivity: Consultants Bureau, N.Y., N.Y., p.147-173.